

David Nilssen

Corrosion Problem on Stainless Steel Alloy 1.4317 in Water Turbines

Master's thesis in Materials Science and Engineering

Supervisor: Roy Johnsen

June 2023



NTNU

Norwegian University of
Science and Technology



Statkraft

David Nilssen

Corrosion Problem on Stainless Steel Alloy 1.4317 in Water Turbines

Master's thesis in Materials Science and Engineering
Supervisor: Roy Johnsen
June 2023

Norwegian University of Science and Technology
Faculty of Engineering
Department of Mechanical and Industrial Engineering

Preface

This master's thesis was written at the Norwegian University of Science and Technology, Faculty of Engineering, Department of Mechanical and Industrial Engineering in the spring of 2023, in cooperation with Statkraft.

It is assumed that the reader has a general background in the fields of electrochemistry and corrosion.

I would like to thank my supervisor Roy Johnsen for his limitless support through this project with matters technical and practical, and I also would like to thank our laboratory engineer Dong Wang for his patience and helpfulness whenever I needed it.

11.06.2023

Trondheim

A handwritten signature in black ink, reading "David Nilssen", is written over a horizontal line. The signature is fluid and cursive, with a long, sweeping underline that extends to the right.

David Nilssen

Nomenclature

Ag AgCl / ref.	-	Saturated Silver Silver chloride reference electrode
Biofilm	-	Bacterially developed aqueous film
E_{rep}	-	Repassivation potential
E_{pit}	-	Pitting corrosion potential
E_{crev}	-	Crevice corrosion potential
E_{corr} / OCP	-	Corrosion potential / Open circuit potential
E_{bd}	-	Passive film breakdown corrosion potential
i_{pass}	-	Passive current density
AISI	-	American Iron and Steel Institute
ASTM	-	American Society of Testing and Materials
EN	-	European Standard
ISO	-	International Organization for Standardization
UNS	-	Unified Numbering System
1.4317	-	EN 1.4317 Stainless Steel
1.4470	-	EN 1.4470 / GX2CrNiMoN22-5-3 Stainless Steel
304L	-	AISI 304L Stainless Steel
316L	-	AISI 316L Stainless Steel
904L	-	UNS N08904 Stainless Steel
22Cr / DSS	-	UNS S32205 Duplex Stainless Steel
25Cr / SDSS	-	UNS S32750 Super Duplex Stainless Steel
MnS	-	Manganese Sulfide
Cr	-	Chromium
Fe	-	Iron
Ni	-	Nickel
Mo	-	Molybdenum

Sammendrag

Formålet med dette M.Sc. prosjektet er å undersøke korrosjonsegenskapene til utvalgte rustfrie stål i ferskvann med ulike mengder salt. Flere ulike typer tester er gjennomført: i) syklisk polarisering, ii) potensiostatisk polarisering, iii) fri eksponering av prøver i et kraftanlegg, og iv) fri eksponering av prøver ved 7°C i laboratoriet.

Vi har kjørt potensiodynamiske eksperimenter for å undersøke spaltkorrosjonspotensialet, passivstrømmen og det frie korrosjonspotensialet til forskjellige legeringer med mål om å prøve å bevise eller motbevise den log-lineære sammenhengen mellom det kritiske kloridinnholdet og spaltpotensialet til legeringene. Dataene vi samlet inn har gitt oss en indikator om at sammenhengen gjelder, men en konkret konklusjon krever flere datapunkter.

Vi har også gjort felteksperimenter for å kartlegge den reelle responsen til de forskjellige legeringene ved utvikling av en bakteriell biofilm på overflaten ved eksponering i ferskvann. Dette ble gjort for å kunne sammenlikne den originale problemstillingen gitt ut fra analysen gjort fra Moglice-anlegget med kontrollert feltdata. Vi endte opp med å få korrosjonsinitiering på legeringen vi har satt fokus på når den ble satt ut med spaltformere, som gjensker og bekrefter det originale problemet. Initiering skjedde også ved lav temperatur i laboratoriet, noe som videre underbygger konklusjonen vår.

I tillegg til å kjøre eksperimenter i felten med en aktiv biofilm, ble et sett med eksperimenter kjørt i laboratoriet hvor prøvene ble utsatt for gitte kloridinnhold og polarisert til et fast potensial på +300 mV vs. Ag | AgCl for å etterlikne den faktiske potensialutviklingen som skjer på legeringer med biofilm. Felteksperimentene bekreftet det eksperimentelle grunnlaget for denne verdien, og vi endte opp med å få initiering på legeringen vi satte søkelys på. Parallelt har vi hentet ut strømtetthetsverdier for de andre legeringene som kan undersøkes senere.

Avslutningsvis fant vi at legeringen som er undersøkt ikke er korrosjonsresistent selv under mer beskyttende betingelser enn de originale parameterne. Problemet er forventet å vedvare for alle instanser av prosessnedstenging inntil delene som består av denne legeringen blir byttet ut med en mer korrosjonsresistent legering.

Abstract

The purpose of this M.Sc. project was to examine the corrosion capabilities of a select group of stainless steel alloys exposed to fresh water of varying chloride contents. Several different tests were performed: i) cyclic polarization, ii) potentiostatic polarization, iii) open circuit exposure of samples in a power station, and iv) an open circuit corrosion experiment at 7°C in the laboratory.

We have run potentiodynamic experiments in order to examine the open circuit potential, the crevice corrosion potential, and the passive current of several different alloys with the purpose of attempting to prove or disprove the log-linear relationship between the critical chloride content and the crevice corrosion potential of the alloys. The data we have collected indicates that the relationship holds, but additional data is required to make a concrete verdict.

Field experiments have also been conducted to collect the real response of our different alloys to the evolution of a bacterial biofilm on their surface on exposure to fresh water. This was done in order to compare the originally recorded problem taken from the analysis performed at the Moglice facility with controlled field data. The result was corrosion initiation on the relevant alloy when it was deployed to the field location with a crevice former, which recreates and confirms the original problem. Initiation was also found for the low-temperature experiment performed in the laboratory, which further reaffirms our conclusion.

In addition to performing field experiments with an active biofilm, a set of experiments was run in the laboratory wherein our samples were placed in electrolytes with specific chloride contents and polarized to a potential of +300 mV vs. Ag | AgCl to mimic the real potential development that happens on alloys with an adhered biofilm. Our field experiments confirmed the experimental basis for this value, and the result was both the 1.4317 alloy initiating as well as passive current density values for the other alloys that can be used in later experiments.

In conclusion, we found that the investigated alloy is not corrosion resistant even under more protective conditions than the originally reported parameters, and the problem is expected to last and worsen for all instances of process shutdown until the parts that this alloy is made of are replaced by those of a more corrosion resistant alloy.

Table of Contents

Preface	i
Nomenclature.....	ii
Sammendrag	iii
Abstract.....	iv
Section 1 Introduction.....	1
Section 2 Theory	2
Section 2.1 Production	5
Section 2.2 Passivity	8
Section 2.3 Welding	11
Section 2.4 Corrosion.....	14
Section 2.5 Biofilm development.....	21
Section 2.6 Effect of flow	25
Section 2.7 Testing methods and standards.....	26
Section 3 Experimental	30
Section 4 Results.....	35
Section 5 Discussion	51
Section 6 Conclusions.....	60
Section 7 Further Work	62
References.....	63
Appendix A Tables and Graphs.....	69
Appendix B Risk assessment	96

Section 1 Introduction

Stainless steels of different grades have different alloying elements and are therefore used for different purposes. Structural steels focus on mechanical properties and therefore require alloying elements of other types and in other quantities than for example heat exchanger parts, which need a higher resistance to corrosion and a focus on higher heat transfer coefficients. In this thesis, stainless steels with a focus on corrosion resistant properties will be the focus, and extra emphasis will be placed on the steel EN 1.4317. This steel type was used for a water turbine wheel at Statkraft's power station in Moglice, Albania, and it was found that during maintenance or operation standstill, the water turbine was surrounded by stagnant water, and after remaining in this state for merely a few days, corrosion was later found to have initiated on the surface of the part. The reason for this was deemed unclear, and a corrosion expert was hired to examine the issue. After examination, the reason was expected to be either chloride induced pitting or crevice corrosion, or bacterial activity, and the project work was initiated. Pitting and crevice corrosion attacks are generally accepted to happen by chloride induced breakdown of the stainless steel. Chlorides are found in all waters across the globe. They account for many of the corrosion attacks happening globally, which are estimated to cost in excess of 1.8 trillion USD every year. This in mind, it is the corrosion engineer's job to mitigate this cost at all turns, to improve structures and coatings that will extend the lifetime of every part exposed to humidity.

The original purpose of the problem this thesis is based on was to examine the corrosion properties of alloy EN 1.4317, and then later attempt to recreate the conditions that led to the corrosion initiation observed in the field. For this reason, a literature review was done, and introductory experiments were run on a potentiostat at varying chloride levels to examine the basic corrosion-related electrochemical attributes of the alloy such as crevice corrosion potential (E_{crev}), repassivation potential (E_{rep}), and the corrosion potential / Open Circuit Potential (E_{corr} / OCP). It was later decided to expand this analysis to stainless steels of other grades for the purpose of comparison. The result of this is the core problem of this thesis, the independent confirmation or invalidation of the log-linear relationship between the critical chloride content of an electrolyte and the corresponding crevice corrosion potential of a stainless steel.

Section 2 Theory

In building any structure, it needs to support its own weight as well as exhibit any necessary auxiliary properties required. For structural purposes, steel is one of the most preferred materials of choice worldwide, especially in combination with concrete. Steel is a broad term that covers any base-iron alloy containing carefully selected impurities such as chromium, nickel, vanadium, and several others. The alloying elements all impact the mechanical, chemical, and material attributes of the steel in various ways. Strength (1), impact toughness, and ductility (2) are but some of the properties a metallurgist may seek to improve by adding alloying elements to iron. Metals are, however, multivariable systems, and as such changing one property may also affect another. Achieving the requested balance between the necessary elements of the steel's intended usage is the main challenge with steelmaking.

In combining any metal with different alloying elements of varying amounts, thermodynamics predict the existence of different phases with different crystal structures for the minimization of free energy within the material, see Figure 1. Some phases of high industrial importance for ferrous alloys are the ferrite (α), austenite (γ), martensite (α'), sigma (σ), and cementite (Fe_3C) phases. The various crystal structures in the phases give them dissimilar properties.

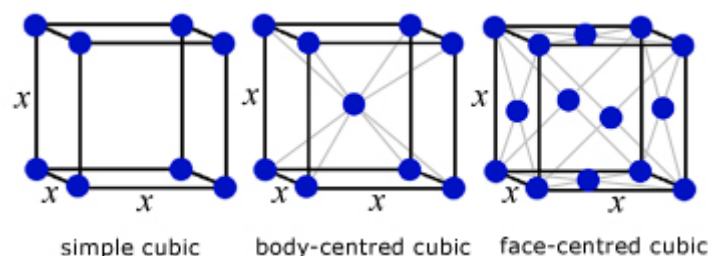


Figure 1: Typical simple crystal structures. Taken from <https://www.a-levelphysicstutor.com/matter-types-solid.php> on 06/04/2023.

Martensite is a very hard and brittle phase of steel manufactured by quenching smaller profiles of carbon-bearing steel in the austenite phase very quickly, with the time required for transformation to be possible dependent on specific alloying elements. It is a nonequilibrium or metastable phase, meaning that given infinite time, it will cease to exist. The reason is that in regular steels, specifically in the ferrite phase, carbon is too big to fit well as an interstitial impurity, putting strain on the matrix and creating a driving force towards conglomeration

and precipitation, resulting in the creation of carbides, and eventually, graphite. These carbides will be Fe_3C , or cementite, in pure iron-carbon alloys at room temperature.

In creating martensite, quenching the carbon-rich austenite will lead to a displacive, non-diffusional transformation where the carbon will stay interstitial and displace the unit cell in one direction by physical forces (3). This transformation leaves the material with a high amount of internal stress that can either be exploited for the benefit of the user or pose a large problem in certain circumstances. Nearly no martensitic steels are used in an as-quenched condition, they are almost always tempered. The process of tempering steel may be slightly different for different alloys, but the basics are the same, see Figure 2 below. After quenching the steel, it is raised to a temperature below the eutectoid temperature to precipitate specific carbides throughout the metal. It is important that the carbides are finely distributed throughout the alloy, and that their size is large enough to slow down dislocation lines, but small enough to allow for the dislocations to cut them. This way, maximum strength is achieved for the steel.

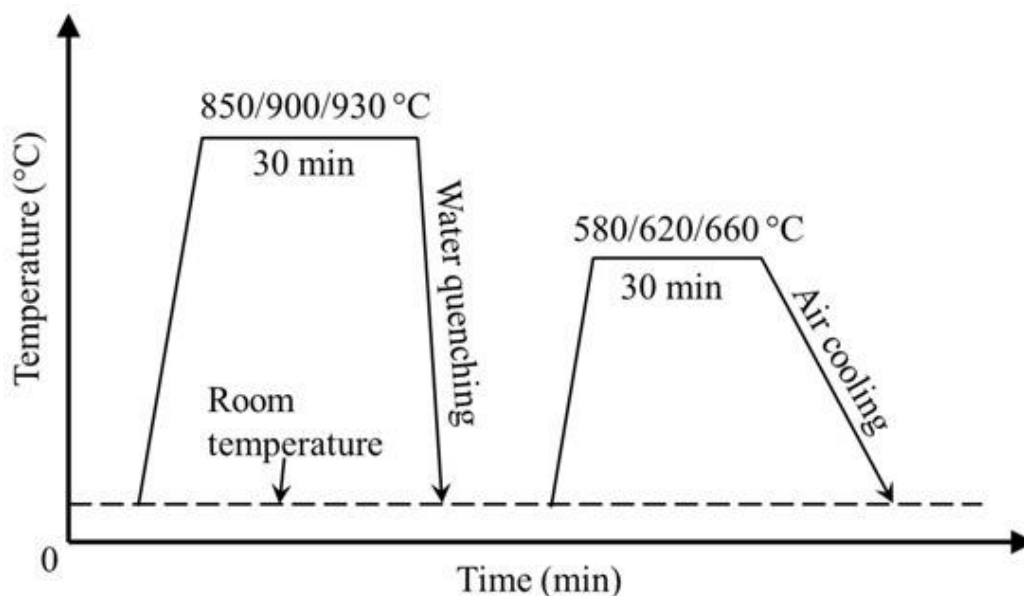


Figure 2: A typical quenching and tempering process. Taken from <https://www.mdpi.com/2075-4701/12/6/914> on 07/04/2023.

For heat treatment, the carbide precipitation often sensitizes the grain boundaries by drawing out nearby metal. The resulting carbide is primarily M_{23}C_6 carbides in more highly alloyed steels. This means it is a mixed carbide of different available metals. However, the carbides that this process produces can be a problem at the surface of the matrix, as the surroundings around the carbides are preferentially attacked during both crevice and pitting corrosion but

also generally, as the chromium content may fall below the critical minimum to protect the metal (4). The $M_{23}C_6$ carbides, being the most common carbides present in higher alloyed steels, deplete the areas around them of chromium during their formation, which for the surface of the alloy can be especially dangerous if it is stainless, as it removes the protective capabilities of the chromium. This reaction is called intergranular corrosion sensitization, or just sensitization for short, and happens on grain boundaries by reaching a temperature where the carbides are insoluble in the bulk matrix, which leads to their precipitation, see Figure 3. They then grow quite quickly by absorbing nearby metal, preferentially chromium because it forms the most stable carbide as well as molybdenum (5), and in a short time the damage has already been done. The structure is now vulnerable to intergranular corrosion and will stay so until the carbides are redissolved into the structure through heat treatment (6).

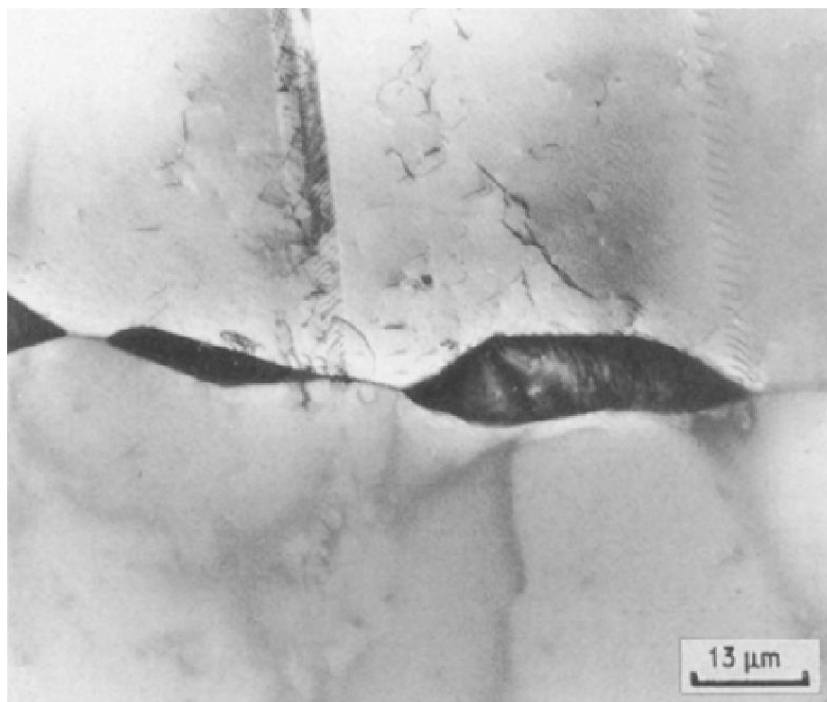


Figure 3: Precipitation of $M_{23}C_6$ on grain boundary. Taken from <https://link.springer.com/article/10.1007/BF01130196>, 09/04/2023.

Further exploring the concept, steel is a general term that in simple terms describes an alloy of iron and carbon, in general with greater mechanical properties than other simple iron alloys. It generally contains interstitial and substitutional alloying elements, which also exhibit a secondary property; they either promote the formation of ferrite in a wider range of alloying contents, cooling rates and temperatures, or they widen or open the austenite area in the phase diagram, possibly also to ambient conditions. These elements are called ferrite and

austenite formers, respectively (7). See Table 1 below for an overview of important corrosion-related elements of the two categories. Knowledge and understanding of these effects are crucial in the production of different grades of steel, the basis of which is centered around the phases in that steel and its specific alloying contents. The addition of specific elements thus promotes certain attributes in the steel, allowing for a high level of control in tailoring the properties of the steel needed for its purpose. This can be seen in by example the addition of approximately 11 % chromium to a steel leading to a protective oxide layer on the surface, and molybdenum improving the resistance of this oxide layer to local attacks. In our thesis, a selection of alloys of different grades have been chosen to map the properties of, to establish or disprove a connection between the critical chloride content of an electrolyte and the steel's alloying content. For this purpose, a table of the alloys used, and their most critical alloying elements are found in Table 2.

Table 1: Austenite and ferrite formers, ranked by potency.

Formers:	Increasing potency from left to right				
Ferrite	Cr	Al	Mo	V	P
Austenite	Cu	Ni	Mn	N	C

Table 2: Relevant approximate alloying content of alloys used in this thesis. All but alloy EN 1.4317 have been taken from <https://secure.outokumpu.com/steelfinder/properties/>. All values given are in weight percent.

Alloys / Content	C	N	Cr	Ni	Mo
EN 1.4317	0.06		13	4	< 0.7
AISI 304L	0.02		18.1	8.1	
AISI 316L	0.02		17.2	10.1	2.1
UNS N08904	0.01		19.8	24.2	4.3
UNS S32205	0.02	0.17	22.4	5.7	3.1
UNS S32705	0.02	0.27	25.0	7.0	4.0
EN 1.4470	0.02	0.17	22.3	5.8	3.1

Section 2.1 Production

Adding different elements to the steel will make it more difficult to obtain the desired properties during the process of producing and refining the steel. Production of steel takes

two main forms; casting, and forging- in addition to rolling, which all the alloys used in this thesis are made by barring EN 1.4317 and EN 1.4470. To cast steel, a pre-produced form of the base alloy, or potentially scrap metal of the same or similar grade, is heated to a temperature above its melting temperature before any additional scrap or alloying content is added. When the melt is homogenous, it is either further treated by for example oxygen lancing or cast into a mold that either comprises the shape of the part itself, or a shape that is intended to allow for later deformation and refinement to its intended final shape. This mold is designed to remove the heat of the molten metal while allowing the metal to retain the shape of the object as well as possible. This is done through both mold material choice, active heat removal and the use of risers, or molten metal reservoirs, to compensate for material shrinkage during cooling, see Figure 4 below. Cast alloys are in general cheaper and easier to manufacture than forged alloys, as the entire shaping process is very simple, and the use of displacive mechanical force is at a minimum. Cast products can also have a much larger size and more complex geometry than forged components.

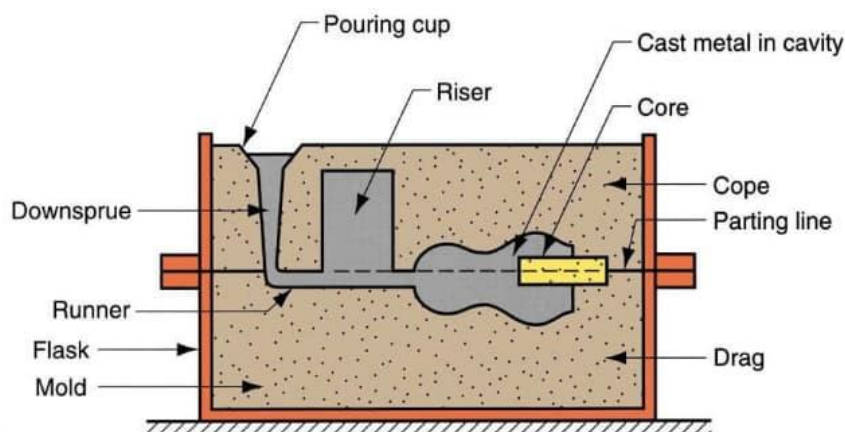


Figure 4: A standard sand mold casting process. Taken from <https://www.rapiddirect.com/blog/different-types-of-casting-process/> on 01/06/2023.

There are however problems with this type of manufacturing method. Segregation of alloying elements is an unfortunate problem that needs to be handled post-casting, wherein the movement of the solidifying front in the melt causes the first solidifying section of the part to have a different solute concentration than the rest of the melt (8). This continues with the solidification process, and the concentration varies throughout. Depending on the extent of segregation, it may be prudent to anneal the part at a temperature of higher diffusivity to homogenize the alloy, or, if the segregation is too large, the casting process itself must be modified to allow for mixing of the melt during solidification using for example

electromagnetic stirring methods. Casting can also generally leave the microstructure quite coarse, with large grains and precipitated microconstituents as well as unwanted carbides or phases like sigma (9). This can leave them vulnerable to corrosion attacks, by virtue of potentially large inclusions that can serve as initiation sites. To remedy these faults, many components may be processed further through forging.

Forging is a manufacturing process of steel that begins after casting. Billets or other intermediate steel products are produced and moved to the forge as in Figure 5 below. Here, depending on the alloy and its intended final use, it is cold, warm, or hot forged. This means that it is mechanically deformed at either ambient temperatures, temperatures where oxidation is undesirable and therefore unlikely, or temperatures closer to the melting temperature of the alloy. The mechanical deformation serves to change the shape of the part while providing either work hardening or recrystallization for cold and hot forging respectively. Work hardening is the permanent deformation of a metal or alloy with the purpose of reducing the average grain size of the part as well as introducing dislocations for increasing its strength. Recrystallization is the process of heating a part that contains a specific phase into a different area of the phase diagram to transform it, and subsequent rapid cooling to ensure a fine microstructure. This leads to a more desirable dispersion of alloying elements as well as higher strength and toughness. Through this, we can avoid the susceptibility towards corrosion that cast products have, but the forging process itself may introduce impurities into the surface in the event of residual matter on the forging equipment, which may once again serve as initiation sites for later corrosion. A point to take note of here is that in order to achieve higher formability and enhance the mechanical properties by virtue of nitrogen solubility increase, manganese is often added to many steels (10). This element has been ubiquitous in classical metallurgy due to its mechanical effects on steel but has some rather unfortunate effects on the corrosion resistance that will be addressed later.

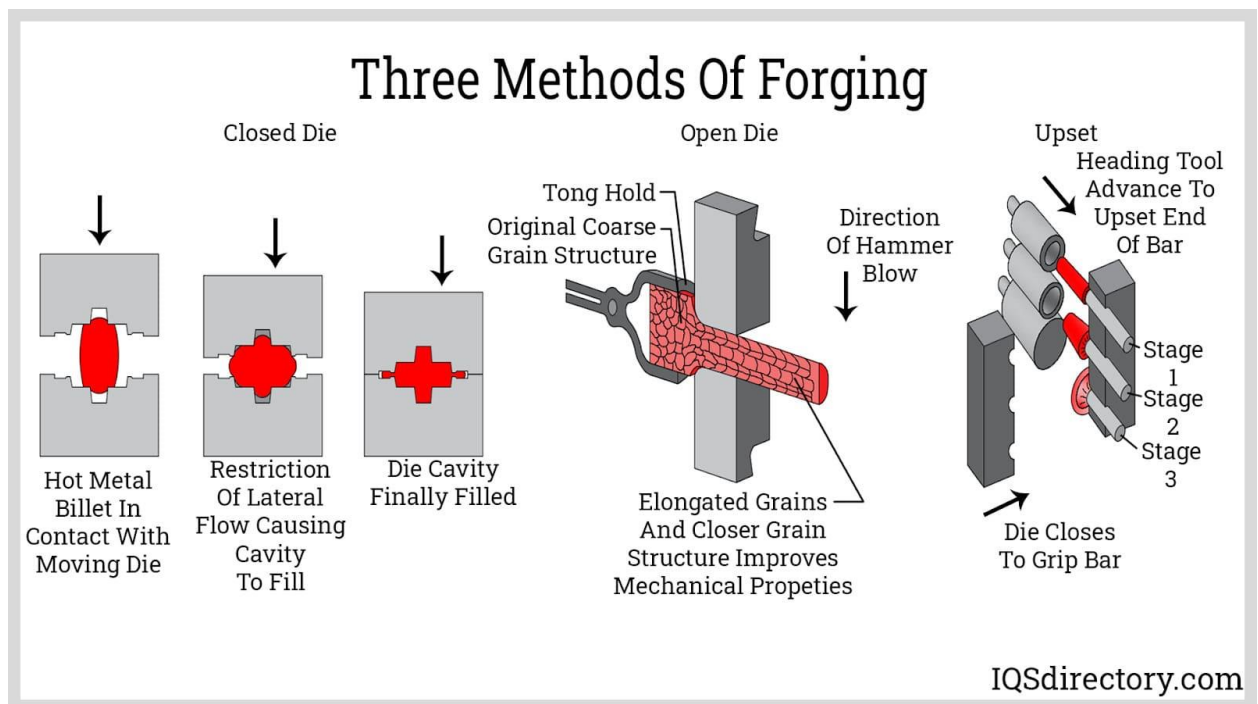


Figure 5: Forging methods, taken from <https://www.iqsdirectory.com/articles/forging.html> on 27/05/2023.

Section 2.2 Passivity

What makes a stainless steel stainless is the thin (5-10 nm), protective oxide layer on its surface. This consists mainly of chromium oxide and iron oxide, and potentially molybdenum oxide, should the alloy contain this element, and the parent phase allow for it. Studies show that the passive films on austenitic (11) and ferritic (12),(13) stainless steels are different in their composition. It is known that the passive film on the surface of the metal is adaptive, changing its composition and structure based on changes in local environmental factors like anion content or potential (14), and the passive film in general is seen to enrich in both iron and chromium oxides and hydroxides (15), which matches data from for example Wang, Seyeux and Marcus (16). The first of these sources states that the enrichment of chromium is implied to be caused by the dissolution of iron. Should the removal of iron from the passive film make it more resistant, the difference in aquatic capabilities of stainless and non-stainless steels is only further emphasized. See Figure 6 for data on the corrosion rates of carbon and stainless steel in microbiologically active and inactive environments.

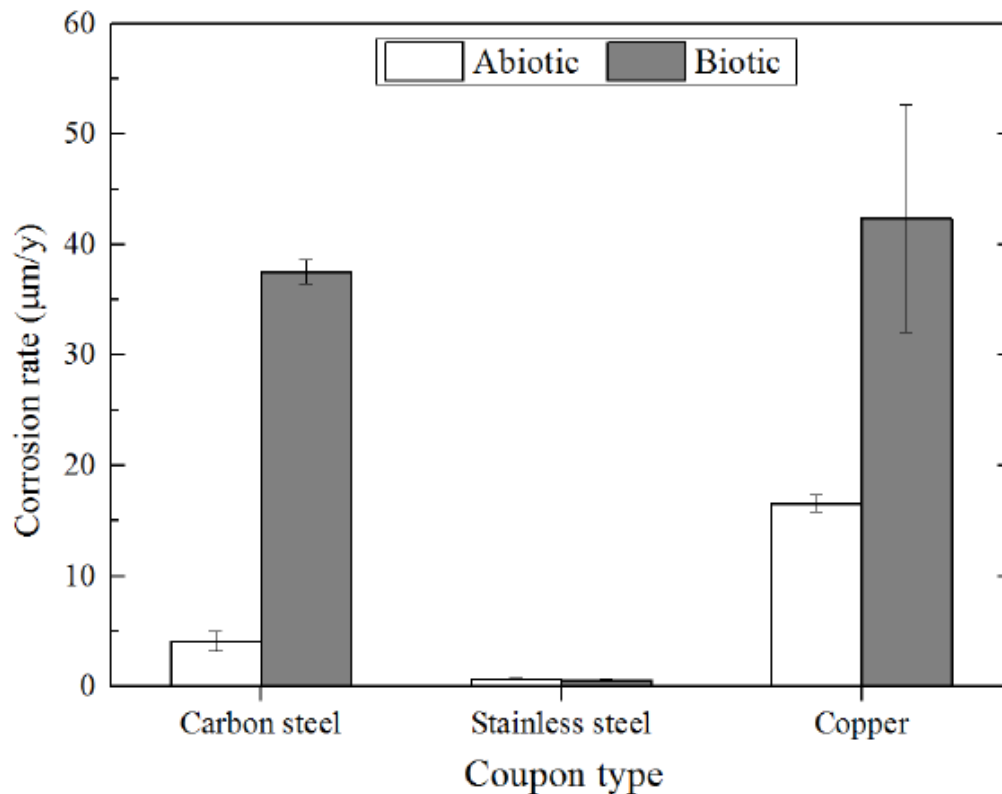


Figure 6: Corrosion rates of carbon and stainless steels in microbially active and inactive aqueous environments. Taken from <https://www.researchgate.net/publication/284179251> on 01/06/2023.

The source also confirms the data about enrichment of nickel in the metal/film interface, suggesting that the role of nickel is important to the corrosion resistance of a metal, but not directly in the passive film itself. It was shown that Ni promotes the formation of a thinner, more resistant passive film due to increasing nickel content leading to a decrease in acicular crystal size in the oxide layer (17), which may be due to the Cr/Fe-ratio being higher for alloys with higher amounts of nickel present. This indicates that the more resistant passive films contain more chromium and less iron, which is in complete agreement with theory and experience. A less obvious, more impactful observation is the fact that the nickel content promotes the preference of chromium oxide in the passive film. As the paper states: “The presence of Ni in the alloy appears to hinder the access of Fe to the passive films ...”, and “Moreover, the thickness of the air formed passive layers decreases when Ni amount in the alloy composition increases”. Austenitic stainless steels also enrich in metallic Ni underneath the passive film, which hinders the transport of Cr to the oxide layer, which is also seen in Maurice, Yang, & Marcus (18). A depiction of the passive film and near substrate can be seen in Figure 7 below.

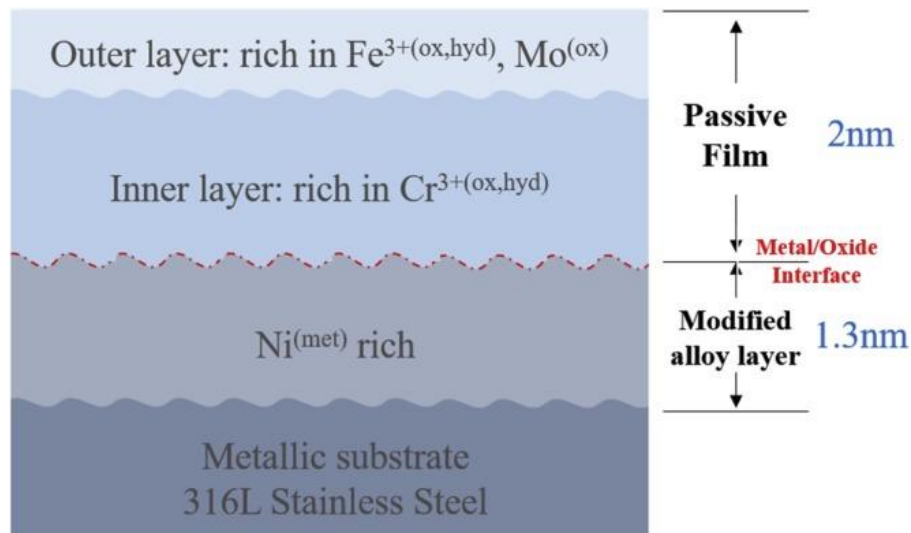


Figure 7: Illustration of a passive film on AISI 316L stainless steel, from (16).

A more recent addition to the corrosion engineer's toolbox is the duplex stainless steel. This type of steel has a nominal 50/50 phase distribution of ferrite and austenite and a generally higher alloying content. This gives the steel, having both mechanical strength as well as corrosion resistance, an advantage over pure austenitic and ferritic steels. Duplex stainless steels are engineered to have increased resistance to corrosion in addition to higher strength compared to the austenitic stainless steel alloys, and were specifically developed to resist intergranular corrosion in the 1930's. This corrosion resistance is partly due to high levels of alloying contents when compared to, for example, lower grade steels such as 316L. It is the preferred steel type for use in particularly harsh conditions (19). Due to the alloying elements' tendency towards changing the phase balance between austenite and ferrite, great care is taken with respect to the choice of elements, as an intention of improving the strength of the alloy may force a reduction or addition of another element, changing the properties further. Find an image of a duplex microstructure below in Figure 8.

A recognized issue with duplex steels however, is that, despite their resistance to solidification cracking, due to their high chromium content and ferrite phase content they are quite susceptible to the precipitation of intermetallic phases like the previously mentioned sigma phase during welding or other heat treatment methods (20). These phases like sigma and chi are quite brittle and therefore will have a highly deleterious effect on the mechanical properties of the structure. In addition to this, the phase absorbs alloying elements critical to the corrosion resistance of the alloy like Mo and Cr (21). Through understanding this issue, a common cure is to solution heat treat the steel afterwards, heating it into the range of

approximately 1070 to 1200°C and holding it at this temperature for roughly 30 minutes before quenching to ensure no precipitation upon cooling. This way, the steel remains both mechanically sound and corrosion resistant.

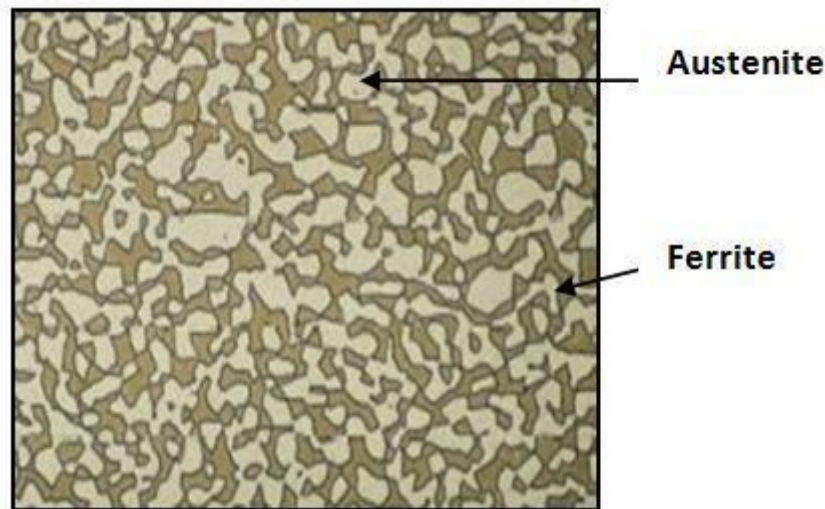


Figure 8: Duplex microstructure, showing regions of austenite and ferrite. Taken from <https://www.researchgate.net/publication/316537256> on 01/06/2023.

Section 2.3 Welding

Welding is a process in which two metals are joined together by a melted contact layer either autogenously, meaning by itself, or using a filler metal. It is widely used because it is quick, simple, relatively inexpensive, and versatile. Very often, it is inefficient, impossible, or very expensive to create whole parts for use in industrial settings. To remedy this, welding is the most efficient solution, often requiring little material and conditions that are available even in the field. In order to safely and efficiently weld parts, there are a number of procedures that need to be followed, given by for example ISO 3834 (22). The general procedure to follow is usually preheating followed by welding and then post-weld heat treatment, depending on the alloy and the welding method. Preheating the weld can reduce fatigue crack growth (23), as well as hot and cold cracking by slowing down the cooling rate of the weld. Welding without preheating may lead to residual stresses (24) and potential hydrogen concentrations within the material that can lead to further problems down the line. The reason for this is that after the welding is finished, the process of cooling down the weld is usually done in air, which will cause it to solidify quite quickly. This rapid solidification may result in shrinkage and internal tensile stresses, and it may lead to hydrogen generated from moisture during welding in the air not being able to diffuse out of the metal. If the hydrogen that has entered the metal is not

dealt with, it may very well lead to hydrogen cracking in many cases, which is a problem wherein tensile stress is applied to a structural part of an alloy of susceptible composition, meaning one of high strength, containing hydrogen. This can lead to brittle fracture of a part that otherwise would be ductile in nature due to hydrogen within the material applying pressure to micropores. If the weldment is preheated however, the retained heat will assist in the diffusion of hydrogen out of the weld (25).

After the welding has been completed, the microstructure of the weld is improperly distributed and requires correction. As an example, duplex stainless steel welds have large amounts of ferrite that is more susceptible to attack than the austenite phase (26) and as such, it is usually subjected to post-weld heat treatment, depending on for instance carbon content and microstructural considerations. The microstructure of the weld is often unusable in its as-welded condition, see Figure 9 below for reference, and as such, must be treated to maintain the soundness of the weldment.

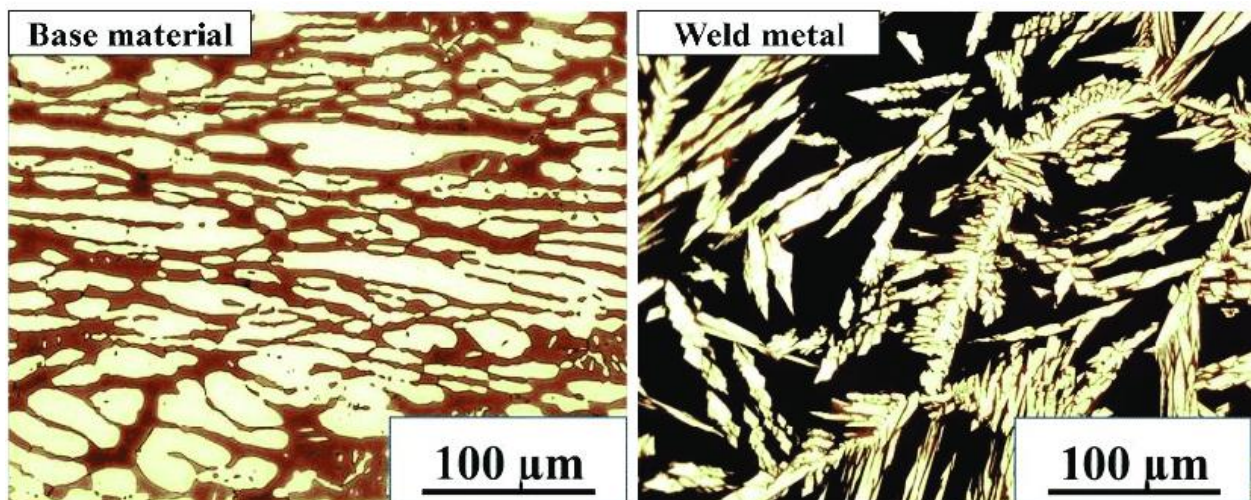


Figure 9: Microstructure of duplex stainless steel, unwelded (left) and welded (right). Taken from <https://www.researchgate.net/publication/327552719> on 27/05/2023.

The different phases in stainless steels have different weldabilities. For many ferritic stainless steels that are high in ferrite-promoting alloying elements, the ferrite phase may exist all the way down to room temperature. This means that delta-ferrite will be the equilibrium phase all the way from the liquid phase, and these types of steel are considered non-hardenable partly due to their low carbon content, but some success has been achieved on this front using novel methods (27). Austenitic stainless steel is similarly non-hardenable and is considered more easily weldable partly due to no required preheating. From more precise control over both the

phase balance and alloying contents, as well as improvements in welding technology, welding of duplex is considered to be more applicable than it once was (28). Due to segregation within the weld, the filler metal used is often not of the same type as the base metal, similar, but it can be richer in other elements to make up for losses to oxidation or internal diffusion during welding (7).



Figure 10: Weld scale. Note the color difference on the surface of the weld as well as the surrounding metal. Taken from <https://www.bottlegases.co.uk/what-is-the-difference-between-tig-mig-welding/> on 04/06/2023.

Cleaning of the surface of the weld is important both before and after welding. Impurities that may get into the weld during the process will severely affect the properties of the steel afterwards, especially with respect to the corrosion resistance. There are several methods for cleaning the surface like grinding or polishing, or grit blasting amongst others. A method often used for this purpose is called pickling, wherein the surface of the part is treated with a solution, most commonly containing an acid such as sulfuric or hydrochloric acid, and usually by submersion. This solution serves to remove impurities from the surface of the metal by chemical reaction and is for example used to remove the oxide layer called scale that forms on a part after hot rolling or welding. This oxide layer is brittle and flakes off quite easily and will cause problems with coating adhesion if not removed. Figure 11 shows the critical pitting temperature of a welded alloy containing 22 % chromium.

This weld scale, the layer of compromised material on the surface of a weld, is also known to be an issue in the context of corrosion resistance (29), and so its removal or modification is critical for the integrity of the weld when used in environments where corrosion is an issue. See an example of weld scale in Figure 10 above. As stated, improper welding of stainless steel parts with substantial chromium and carbon content will very often result in the precipitation of carbides like $M_{23}C_6$. As a purpose of this thesis is to explore the limits of the alloy 1.4317 and its strengths and weaknesses in connection to corrosion, it is important to understand the mechanics and reasons behind the damage that may occur in aqueous environments, and this also includes damages that may happen post-production of the part from the supplier. It is common for pitting corrosion attacks to happen in weldments (30), (31), and so it is of utmost interest to examine why this happens and how to avoid it.

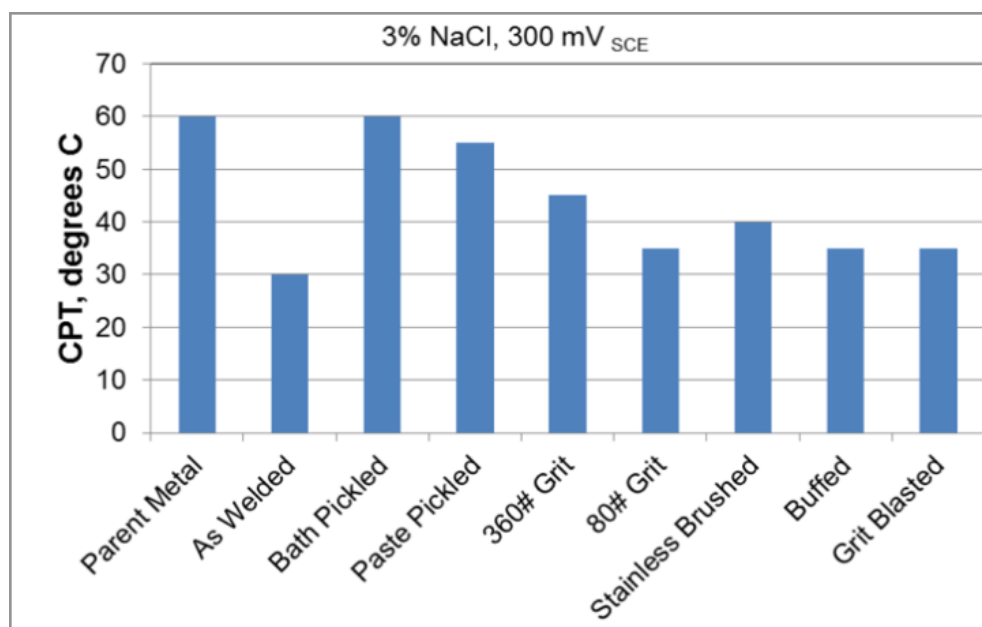


Figure 11: Critical Pitting Temperature (CPT) on an alloy containing 22% Cr, polarized to 300 mV versus SCE, as a function of surface treatment methods. Taken from SOURCE on 10/06/2023.

Section 2.4 Corrosion

Corrosion will in this thesis be defined as the preferential dissolution of a metal or alloy into an aqueous solution by chemical or electrochemical reactions. In other words, this means that corrosion is a net mass loss of structural metal over time, necessitating protection or replacement of parts, substructures, or the entire structure exposed to the environment. In simple carbon steels, direct contact with neutral water is enough to initiate corrosion, as seen from the free energy of formation of its aqueous species. This means that the direct

dissolution of iron metal is thermodynamically favored in non-alkaline pH, see the Pourbaix diagram in Figure 12.

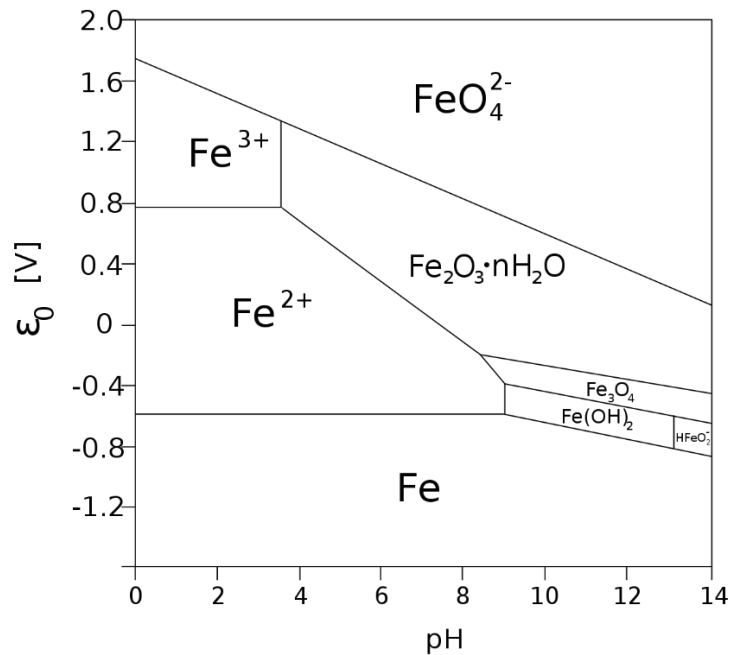


Figure 12: Pourbaix diagram showing the predominant species of iron in water at different pH. Taken from https://en.wikipedia.org/wiki/Pourbaix_diagram on 12/04/2023.

Corrosion appears in many forms, but some exceptionally dangerous variants are known under the designation of localized corrosion. Hereunder some factor present will result in a part of the metal becoming a permanent or semi-permanent cathode or anode, meaning that a corrosion reaction will happen on a larger scale with higher current densities than those in the passive regime. This may be the product of galvanic corrosion, where two dissimilar metals are in electric contact, and one is notably nobler than the other on the galvanic series, an example of which is shown in Figure 13. It may come from inclusions in the metal, where impurities are either more or less noble than the substrate metal. In the first case, the impurity will enable reactions to dissolve the metal around it, and in the second case, the impurity itself will dissolve. This process is called pitting corrosion and will be discussed shortly. It is even more likely that the process does not stop with the complete dissolution of the inclusion in the event that it contains corrosion-catalyzing species such as Fe²⁺ (32) or manganese species like MnS.

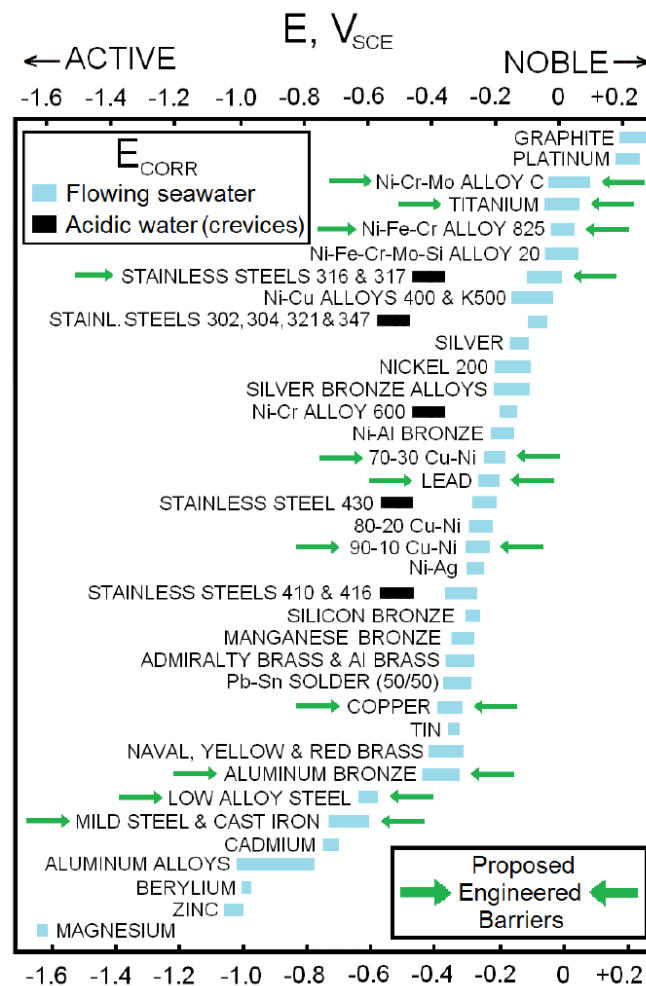


Figure 13: Galvanic series containing many industrially relevant alloys in flowing seawater. Taken from <https://www.researchgate.net/publication/339183036> on 04/06/2023.

For structures made of stainless steel placed in or near water, the most important aggressor is chloride ions. As discussed, the passive layer on industrially produced stainless steel is not perfect and will naturally have inclusions and defects that act as initiation points for local breakdown in all but the most well controlled cases of metal part manufacturing. Chloride ions are the key to breaking down the passive layer on stainless steel, for both pitting and crevice corrosion. The chloride ion's effect is complex, leading both to the active breakdown of certain types of inclusions (33), to the buildup of diffusion gradients into crevices and pits, and to the dissolution of iron through the passive layer (34). The level of chloride ions also plays a role in determining the potential at which localized corrosion takes place, see for example (35). This source also notes the competitive nature of the chloride ion, being displaced locally on the surface of the metal by other anions. An increase in other anions was reported to result in more noble potential values, quoted directly as "sufficient concentrations

of which act as pitting inhibitors.”. They also note the connection between the critical potential and the electrolyte temperature, pointing out lower temperatures give lower probability for corrosion to occur. See Figure 14 below for an illustration on electrolytic ion flow in relation to pitting corrosion.

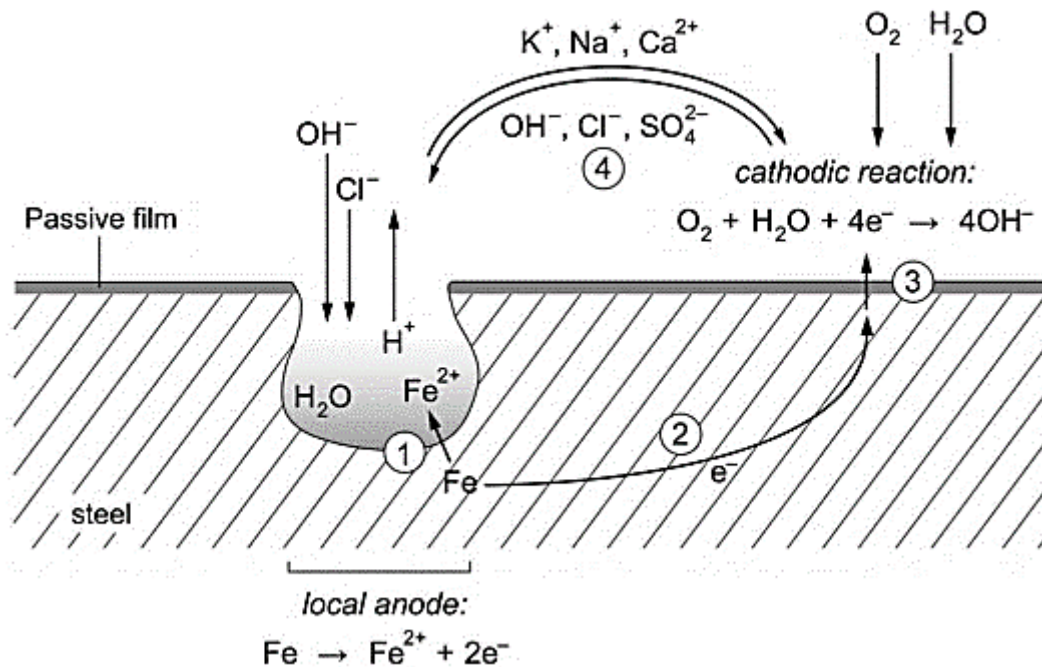


Figure 14: An illustration of pitting corrosion and related electrolyte ion flow. Taken from <https://www.researchgate.net/publication/335976531> on 04/06/2023.

A highly common source of pitting corrosion is the dissolution of sulfide inclusions, as mentioned. After an inclusions in the passive layer has been exploited and an initial pit has been established, the pit will need to go through a metastable growth phase where the geometry of the pit and its products determine whether it will stabilize (36). The local pH inside the pit reduces with the dissolution of metal ions into the pit anolyte, and this continues until the passive film is so weakened by the local pH that it starts to dissolve. At what point this happens can be seen from the metal's Pourbaix diagram. As this occurs, the corrosion products will migrate to the entrance of the pit and settle, forming a growing cover that limits the exchange of ions, thereby keeping the pit acidic and the chloride concentration high. During this time, the state of the pit is called metastable, and stable pitting only occurs when the entrance cover becomes unnecessary for the maintenance of the diffusion barrier. Hong and Nagumo (37) confirmed that the pitting or crevice corrosion potential of a stainless steel decreases linearly with the logarithm of the chloride concentration. The initiation and survival of metastable pits, pits which start to corrode, but are stopped by some force like

electrolyte mixing from agitation or the collapse of the pit cover before a critical depth has been achieved, is also shown to have a similarly log-linear relation.

Due to its high abundance in seawater and its presence in freshwater, it is impossible to find a natural environment on the earth today that is free of chlorides. It is of utmost importance to corrosion and marine engineering specifically because of its deleterious effects on all steel-bearing structures situated in marine environments. Chloride ions adhere to the surface of the steel and are especially attracted to faults in the surface layer, like chips, pits, and grain boundaries (38). It can bind directly to metal and make complex ions like FeCl_2^{2+} , or it can attack the oxide layer directly and break apart the oxides present as in with the reaction $\text{Al}_2\text{O}_3 + 8\text{Cl}^- + 6\text{H}_3\text{O}^+ \rightarrow 2\text{AlCl}_4^- + 9\text{H}_2\text{O}$ (39). It is therefore seen as doubly important that when combining steel and other metals with materials or environments where chlorides are not considered an issue or worse, when chlorides are considered a positive influence as in concrete, special care must be taken to protect the metal.

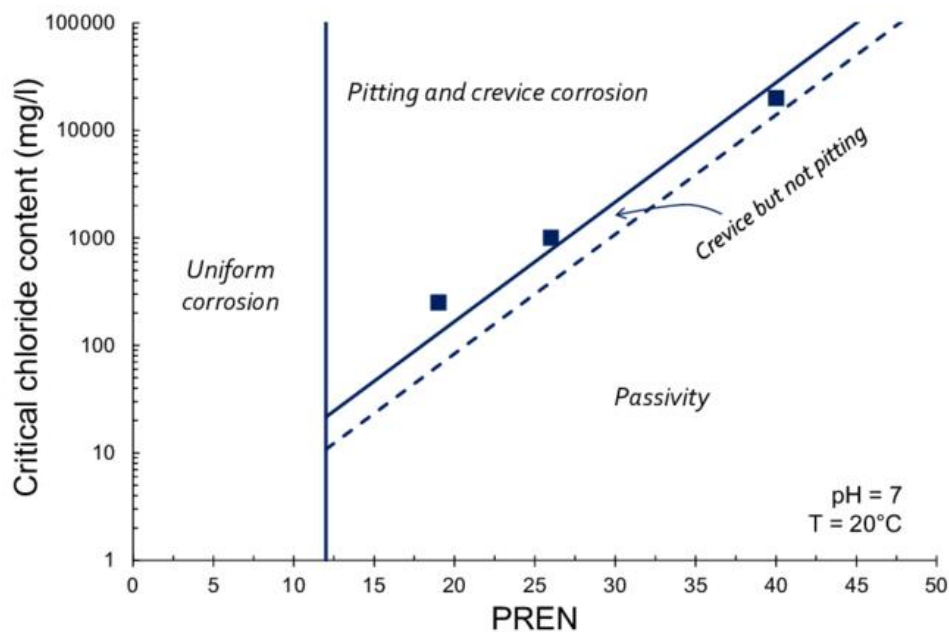


Figure 15: An illustration of the correlation between the critical chloride content and PREN. Taken from <https://www.researchgate.net/publication/281279714> on 04/06/2023.

A natural protective mechanism against localized corrosion is the aforementioned passive layer, the breakdown of which is illustrated below in Figure 16. It acts as a barrier between the substrate and the solution, and a measure of the protective capabilities of this layer is the Pitting Resistance Equivalent Number, or PREN for short. Its value is calculated from the content of a few relevant alloying elements, ($\text{PREN} = \% \text{Cr} + 3.3 \% \text{Mo} + 16 \% \text{N}$) and Figure

15. This graph shows the transition between uniform corrosion and passive / active behavior. The equation also has a term for wolfram / tungsten content, but as this is not common in the specific alloys used in this thesis, we have chosen to omit it for simplification. The equation does not take into account certain elements that have a profound effect on the pitting resistance like nickel, whose effect is previously examined, and manganese, an element that is essentially ubiquitous in steels yet whose presence seems to severely affect the resistance of the alloy to localized corrosion as seen in (40). This source says PREN is not an absolute determinator and is best used to roughly estimate the grade of resistance of steels to localized corrosion to evaluate and exclude the usage of certain steels in certain environments. Of the alloying elements commonly added to stainless, nitrogen and molybdenum are experimentally shown to reduce the tendency towards pitting corrosion (41). This is the experimental basis for the equation, with the chief effect of chromium increasing the more general resistance against corrosion.

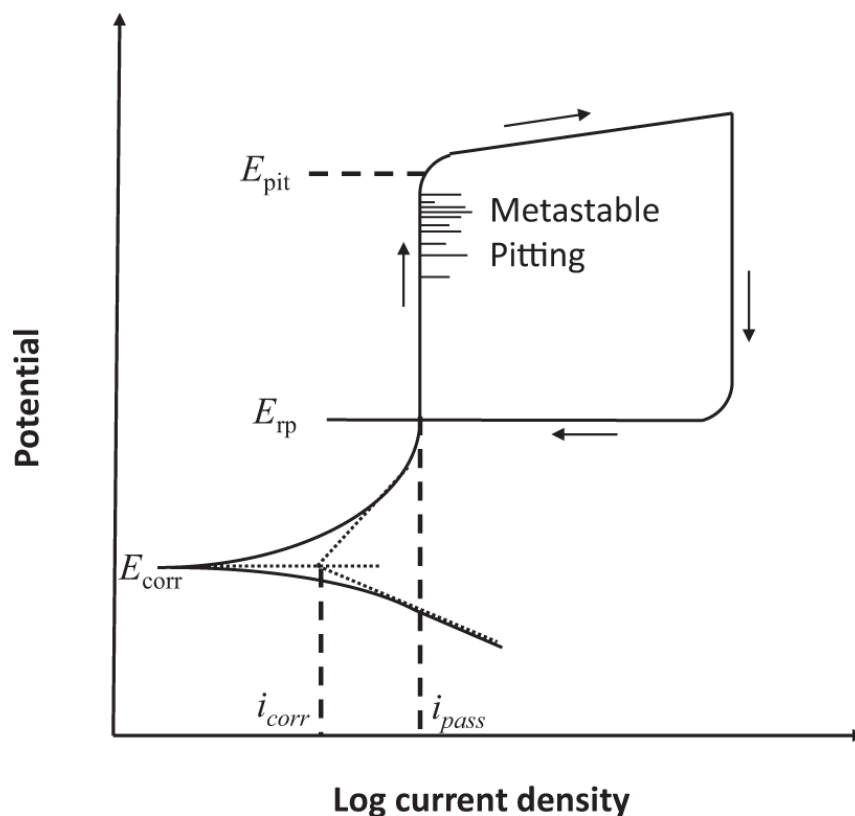


Figure 16: Evans diagram depicting a hysteresis curve typical for pitting initiation and repassivation during potentiodynamic experiments, showing both the open circuit potential, pitting potential and repassivation potential. Taken from <https://www.researchgate.net/publication/349235791> on 04/06/2023.

A special subset of localized corrosion is called crevice corrosion. It occurs when there exists a space between two objects, at least one of which is a metal, with an electrolyte in between.

Within this crevice, cathodic reactions can deplete the oxygen content very rapidly, leading to a shift in the cathodic reaction of self-corrosion from the inside to the outside of the crevice. There can be considered to be two main models for crevice corrosion initiation on stainless steels in use today (42), (43): 1) Passive dissolution and subsequent acidification of the local environment leading to breakdown of the passive layer, and 2) crevice or surface profile geometry inducing an IR drop that forces the metal into an actively corroding state, (44), (45). The following paragraphs will explore these two models.

The passive dissolution or critical crevice solution model: Given a preexisting crevice or other secluded area, the anodic dissolution and cathodic reduction reactions will initially occur uniformly over the surface of the material. Reactions of special note here are the hydrolysis of metal ions and the reduction of hydronium with oxygen to produce water. These are the most likely reactions to take place on the surface of the metal in neutral and acidic solutions regardless of passivity or alloy. Given an area on the surface of the metal that is sufficiently protected from agitation occurring on the surface of the rest of the metal, the oxygen reduction reaction within the crevice or pit will eventually exhaust the supply of available oxygen. Subsequently, the reduction reaction shifts to the entrance of the pit or crevice where oxygen is readily available, and the metal ions within the crevice will react with water and form complexes, acidifying the pit electrolyte. This pushes the local critical potential for the breakdown of the passive layer to a more active state, and eventually leads to a runaway reaction and causes the metal to start actively corroding.

IR drop model: As a crevice is filled with an electrolyte and the crevice geometry permits, there exists a resistance within the electrolyte. Given a sufficiently narrow crevice gap entrance, the ionic flow will be stemmed by the increased solution resistance (45), leading to an increase in dissolution current. An illustration of the IR-drop mechanism is shown in Figure 17. Close to the entrance of this crevice, no corrosion takes place, as the potential difference between the mouth and the edges is not high enough to push the potential from the passive region into the active region. Far into the crevice, corrosion is also not observed, as one enters the boundary of the limiting value for the mixed potential according to mixed potential theory. In between these regions, there exists a space of possible and probable corrosion, where the metal dissolution reaches a maximum value and crevice corrosion will initiate and propagate.

Stainless steel in freshwater containing microbes is more exposed to attacks of pitting corrosion, often of a very high rate. This can happen even in waters containing under 200 ppm chlorides, near the limit of potability. It was experimentally determined on several occasions that failure can happen even on stainless steel grades 316L as well as on 304L under these conditions. Common detections of local microbiological activity in these conditions include iron- and manganese-oxidizing bacteria, and so a recent proposition for the damage on these grades is by the ennoblement of the open circuit potential by the formation or presence of manganese oxides. The bacteria seem to be the source of this ennoblement and this seems to contribute to the initiation of pitting or crevice corrosion when coupled with other ennobling effects such those of sulfate-reducing or iron-oxidizing bacterial activity. Suleiman et al (50), suggested that “pitting on stainless steel in potable water is enabled by the pit-stabilizing effect of the iron-based deposits generated by IOB.”, which could pose a problem for lower grade steels or steels with a higher proportion of metallic iron in the oxide layer.

In order for a biofilm to form on the surface of a stainless steel, it must be able to adsorb onto that surface. In this regard, the roughness profile of the steel may influence the kinetics of adhesion. A source (51) shows exactly this, noting that biofilm formation on smooth surfaces produced thinner, clear biofilms, while the samples with the rougher surfaces produced darker, thicker, more uneven biofilms. The structures formed on the latter biofilms were stated to be associated with the initiation of pitting and crevice corrosion. Another paper (52) adds a more detailed description of the adhesion process, stating that the process goes from reversible to irreversible due to acidic polymers bridging the cell and the substrate metal, ensuring more difficult removal. It also says amongst other factors that the micro-roughness plays a role in the formation and growth of the biofilm, suggesting that surface treatment of structures to finer roughness profiles enable less frequent and less damaging biofilms. (53) gives the same result, showing thicker biofilms on the rougher heat exchanger surfaces and stating, “The results suggest that the finish (...) is critical for improving energy efficiency and avoiding biofilm adhesion”. Their illustration is found in Figure 18.

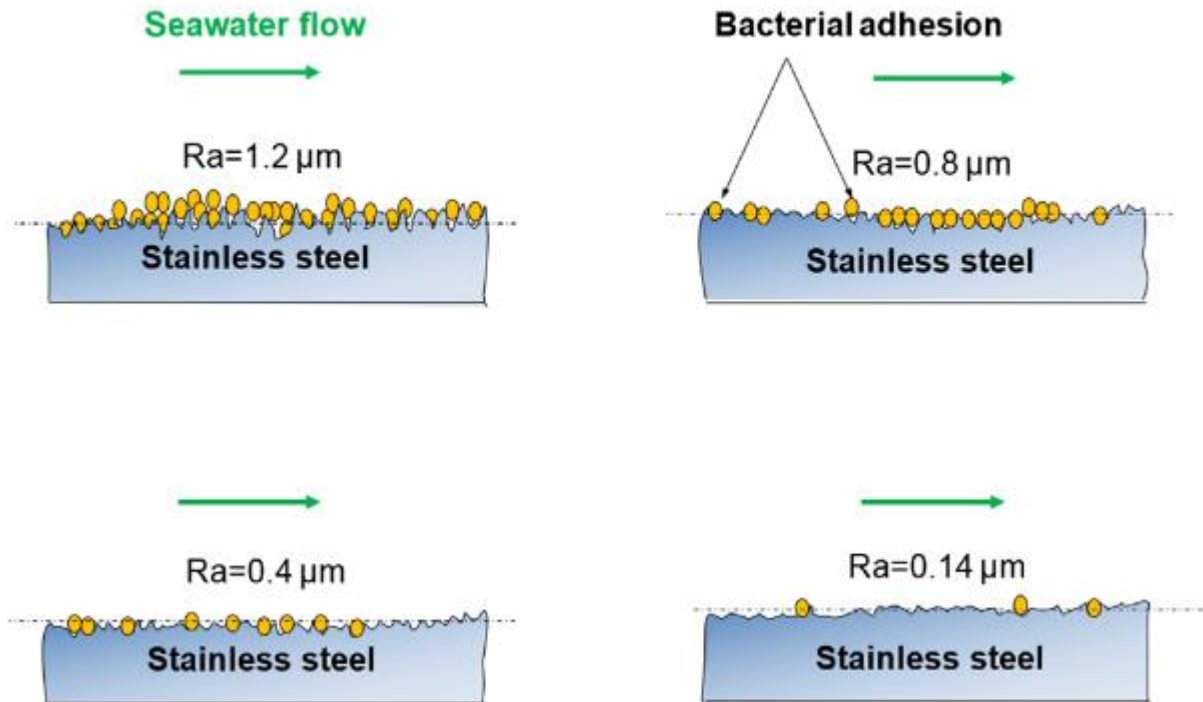


Figure 18: Initial biofilm adhesion on stainless steel with different surface roughness values. Taken from <https://www.tandfonline.com/doi/full/10.1080/08927014.2016.1241875> on 29/05/23.

Characklis (54) and Kwok et al. (55) both found that an increase in shear stress sharply increases the biofilm density, meaning that an increase in flow speed will lead to a denser biofilm. Melo and Vieira (56) showed that even in turbulent flow conditions, the biofilm density increases with increasing flow velocity. A result of the biofilm adhesion and propagation is the increase of the corrosion potential of the alloy or ennoblement, see Figure 19 featuring alloy EN 1.4401 (316). Also note the D2 sample, showing later pitting initiation and repassivation event.

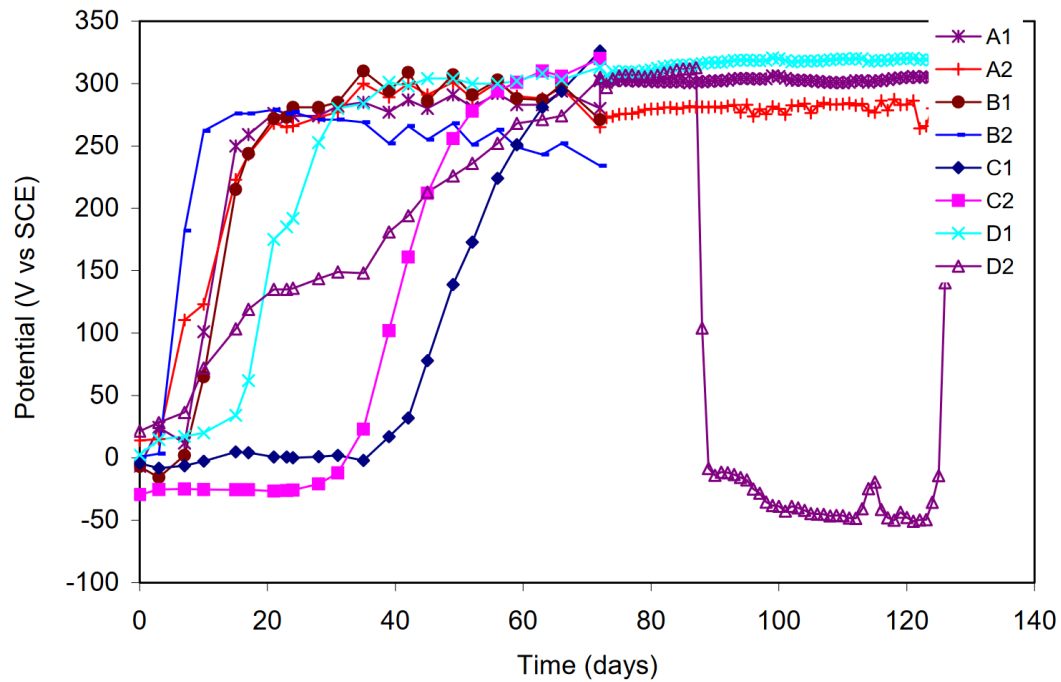


Figure 19: Potential development on alloy EN 1.4401 in stagnant water at four different locations (A,B,C,D). Taken from (57) on 10/06/2023.

Percival, Knapp, Wales and Edyvean (58) discovered that their samples of 304, given higher surface roughness profiles yet at the same roughness designation as their other samples of 316, had higher colonization counts of bacteria than their 316 samples, regardless of water velocity. This is congruent with the results from both (51) and (53). Dry weight was not found to be significantly different between stainless steels, and here also higher water velocities was found to correlate with significantly higher biofilm viable cell counts. A comment was made on the fact that no corrosion was found to have taken place during the experiment despite heavy biofouling and assumedly, the chloride content was low due to its supposed potability. It was also noted that from measurement of the bacterial types before the initiation of the experiment, no significant difference in the colony types was found between the grades or finishes of stainless steel, which suggests that neither surface roughness nor surface composition plays a role in the composition of the biofilm. A note was also made on the difference in the mode of attachment between high and low fluid velocities, being created by different bacteria as well as adapting to the different environments. It was stated that “higher flow rates provide higher nutrient levels and consequently higher bacterial growth”, which explains the differing growth speeds and densities of the biofilm.

It was also theorized that these biofilms can compress under high pressures and resist higher shear rates, matching the data from Characklis and Kwok et al., quote “Turbulent flow, in addition to providing enhanced nutrient uptake conditions at the biofilm surface, enhances chemical nucleation leading to precipitation of compounds which contribute to biofouling.” Little, Lee and Ray (59) concluded through external sources that for ennoblement in fresh and brackish water, “the result of microbial deposition of manganese and localized corrosion of 300 series stainless steels has been related directly to the biomineralized deposits on the surface”. It is also evident through Washizu et al. (47) and Scotto et al. (60) that H_2O_2 may also play a role in the ennoblement of stainless steel, as well as loss of ennoblement using certain enzymes, suggesting that there is no one single source of ennoblement in biofilms, varied in specimens and mechanisms as they are. Graphs of ennoblement may be found in for example (61) for marine biofilms and (62) for freshwater biofilms in river water. The growth of the open circuit potential on stainless steels in chloride-containing solutions is thus dependent on the microbial activity as well as the chloride content, temperature and flow speed (60). Liao et al. (63) showed that the OCP is “greatly affected by both immersion depth and sunlight”, which can be different for different bacterial species.

Sulfur in stainless steel is usually found as manganese sulfide (MnS), which is introduced artificially for lubricating purposes under cutting, meaning that many austenitic stainless steels will contain more of these inclusions. Castle and Ke (64) note that MnS inclusions or MnS precipitates associated with other oxide inclusions are often the initiation sites for pitting corrosion, confirming what was previously stated. They are thermodynamically unstable under ambient conditions and will dissolve into the electrolyte, leaving behind a sulfide stain under which the local pH and chloride concentration may vary from the bulk in such a manner that pitting or crevice corrosion is more easily initiated, as shown by Williams, Mohiuddin and Zhu (65). Additionally, the source on manganic oxide biofouling shows that stainless steel coated with MnO_2 paste exhibits “nearly identical” electrochemical behavior as that of the ennobled samples.

Section 2.6 Effect of flow

Flow induced corrosion is a phenomenon wherein the increase of flow through a system will increase the corrosion rate of that system. This is found in metals that form oxy/hydroxides with low adhesion to the substrate and works by way of physically removing the surface layer of oxy/hydroxide, exposing the substrate beneath. Another possibility is that the flow speed

becomes so high that the oxide layer is forcefully disbanded, which happens above approximately 25 m/s for stainless steels. This allows further corrosion to take place. As an additional detail, an increase in flow speed will likely cause thin the oxygen diffusion layer, thereby increasing the rate of corrosion on a specimen.

Conversely, (66) created from literature a model of pitting probability containing a section on flow based protection against localized corrosion for stainless steels. This model takes in the PREN value of the steel, the flow rate of the system and the calculated pitting probability in stagnant conditions. From their model, they imply that the protective effect of the passive film due to alloying elements becomes more and more negligible in the metapassive state, as the flowing conditions compete with the regenerative capabilities of the oxide layer in guarding the substrate. They also say that in the case of crevice corrosion, the probability of corrosion initiation becomes independent of the flow state due to the local stagnant solution within the crevices.

Section 2.7 Testing methods and standards

To explore and categorize the properties of metallic materials in aqueous or humid environments, testing methods that simulate the situation under research are needed. In this case, to examine the crevice, pitting and repassivation potentials of the alloys used in this thesis, a standard method of cyclic voltammetry will be used. Potentiodynamic scans allow for the variation of a single variable at a time in a multivariable system such as the one to be simulated in this thesis. This allows us to identify and categorize the impact of significant factors on the passivity breakdown potential individually and apply this knowledge to better understand the combined system when incorporating the effect of the separate variables. To this end, there are established standards to be followed when executing these tests, and the one used in this thesis is the ASTM G61 standard for cyclic voltammetry. It has been modified to fit the testing capabilities of the corrosion laboratory at the MTP institute and to fit our timeframe, with the changes seen below.

- Polished with 500 grit paper instead of 600 grit due to availability,
- Ultrasonically degreased in ethanol and rinsed in deionized water and acetone,
- Artificial crevice with PTFE / Ceramic crevice former at 2Nm torque, see Figure 20,
- Run at differing chloride concentrations instead of 3.5 % NaCl,
- Run at room temperature instead of 25°C,
- Run in a single cell containing the reference, working and counter electrodes,

- Run in aerated conditions instead of purged with an inert gas,
- Submerged for 30 minutes instead of an hour before polarization start,
- Ended scan at approximately 1mA instead of 5mA ($33\mu\text{A}/\text{cm}^2$ and an approximate sample area of 34cm^2).

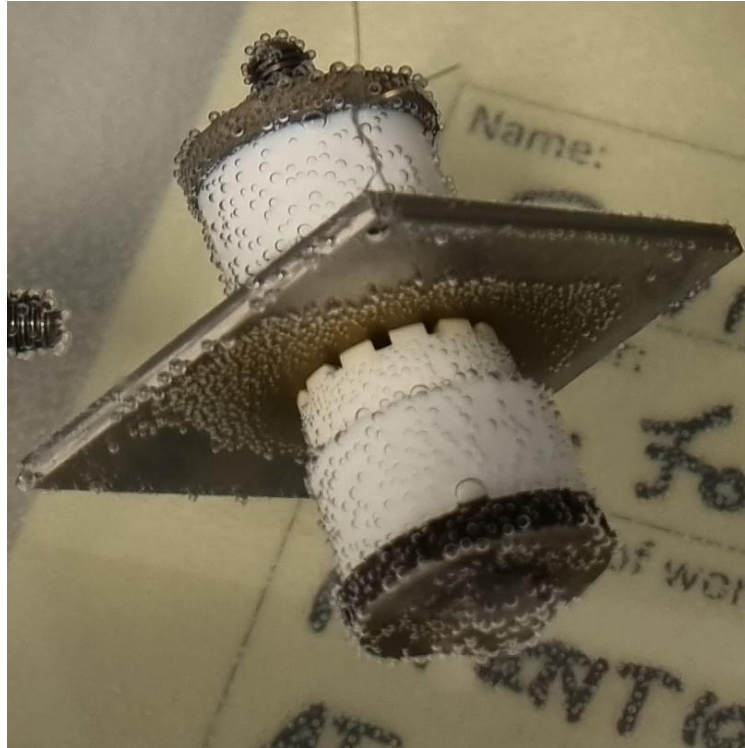


Figure 20: Ceramic crevice former in use on sample during potentiostatic experiment.

In addition to this, (67) gives a thorough explanation on how to interpret polarization curves that will be used in the discussion section. Below in Figure 21: Cyclic polarization curve showing passive current density, repassivation potential, pitting / crevice corrosion potential and transpassive corrosion potential with and without chloride ions. Figure 21 is an illustration of a typical anodic polarization curve on an alloy showing passive/active behavior. This means it has a passive layer that breaks down at a certain positive potential, and as the figure shows, the presence of Cl^- ions will significantly reduce the potential at which localized corrosion occurs, relative to the abundance of ions. Within the passive part of the polarization curve, the related passive current density can be seen. Its value can fluctuate, but in comparison to the rest of the curve, its value changes relatively little throughout the passive region. It can therefore be used to estimate the onset of corrosion, as a sudden increase in measured current density indicates a local breakdown of the passive layer.

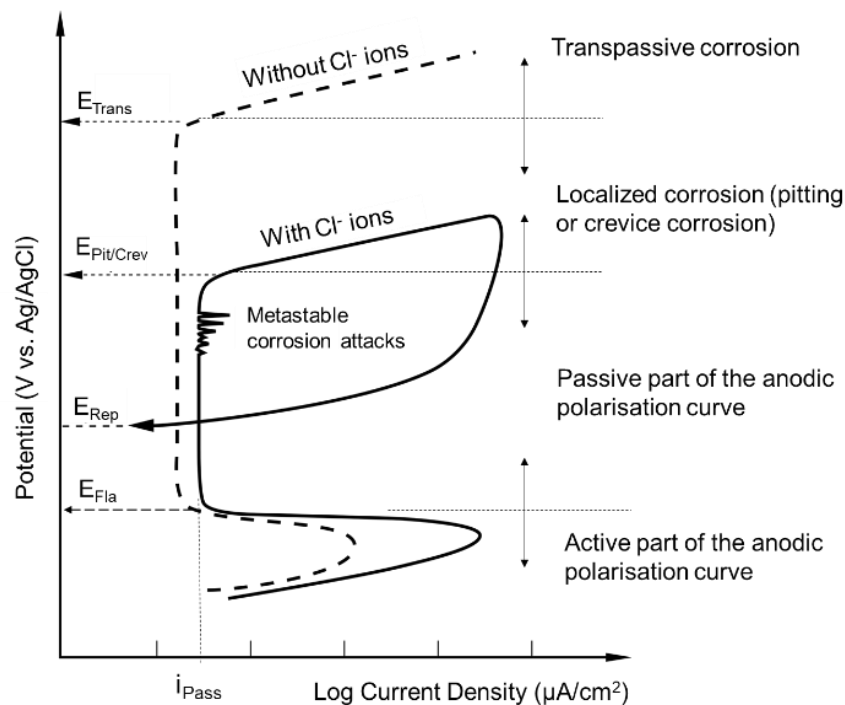


Figure 21: Cyclic polarization curve showing passive current density, repassivation potential, pitting / crevice corrosion potential and transpassive corrosion potential with and without chloride ions. Source unknown.

For our second set of experiments to be discussed later, sets of samples with and without artificial crevices were exposed at the upper Leirfossen power station for an extended period which is still ongoing as of the time of writing. By exposing samples freely in waters, in this case microbially active, one can observe the potential evolution over that sample as the sample adapts to the electrolyte and the microbes present in the water attach to and develop a biofilm on the surface of the sample. An example of this can be seen in Figure 19 and correspondingly, a potential drop is visible on the graph at one location, with a later increase back up to the previous value range. This potential drop is considered characteristic for the initiation of localized corrosion (68,69), and is known to correspond to the polarization resistance of the specimen. The polarization resistance is the specimen's resistance to oxidation under an externally applied potential, which can be understood as the sample's willingness to oxidize or corrode. This means we can often understand a potential drop when measuring the open circuit potential of an alloy as the initiation of corrosion on the sample, and this is the main source of information from this type of experiment.

Potentiostatic experiments are often done in order to test an alloy's resistance to corrosion at a static elevated potential. This may for example be because potentiodynamic experiments have been run and a potential pitting or crevice corrosion potential has been identified, and it

is of interest to explore if this is the case. The sample may then be suspended in a solution with parameters equal to that of the potentiodynamic scan, and then polarized to a potential near the previously recorded pitting or crevice corrosion potential to monitor its response.

Section 3 Experimental

Three types of experiments were run, one set of two parallels of potentiodynamic scans of current development on different alloys in solutions of varying chloride contents, one set of pitting and crevice corrosion potential measurements on different alloys in running river water at Upper Leirfossen power station as well as one with different chloride contents under low temperature, and one set of potentiostatic scans performed on different alloys at a potential mimicking ennoblement under specific chloride contents. A full table of each experiment type is shown in Table 3. X indicates that two parallels were run on this combination.

Table 3: Potentiodynamic scan experiment overview, chloride content and alloy combinations.

<i>Chloride Alloy</i>	<i>100 mg / l</i>	<i>250 mg / l</i>	<i>1000 mg / l</i>	<i>10000 mg / l</i>	<i>50000 mg / l</i>	<i>100000 mg / l</i>
EN 1.4317	X	X	X	-	-	-
304L	X	X	X	-	-	-
316L	X	X	X	X	X	-
904L	-	-	X	X	X	X
S32205	-	-	X	X	X	X
S32750	-	-	X	X	X	X

Experiment parameters for potentiodynamic scans:

- Stabilization time = 30 minutes
- $i_{\text{apex}} = 33 \mu\text{A} / \text{cm}^2$
- $E_{\text{apex}} = 1.2\text{V vs } E_{\text{ref}}$
- Forward and backward scan rate = $0.6 \text{ V} / \text{h}$
- Polish grade 500 grit (18 μm particle size)
- Ambient conditions (room temperature, no gas purging)

Instruments:

- Gamry Interface 1010e Potentiostat
- VWR CO-330 Portable TDS (Total Dissolved Solids) Meter
- Milli-DI Water Purification System for Deionized Water (measured to approximately 10 $\mu\text{S}/\text{cm}$)
- Wenking MP 87 Potentiostat
- Multimeter for verifying reference electrode potential
- Comet Systems MS6D Data logger
- Torque wrench for applying 2 Nm torque to samples
- Saturated Ag | AgCl reference electrode
- Platinum mesh counter electrode
- Alicona Infinitefocus Optical 3D microscope

For all experiments, all samples were wet ground and polished on all surfaces with 80 or 120 and 500 grit paper respectively, before being cleaned with deionized water and ethanol and stored for more than 24 hours in order to stabilize the passive layer on the surface. The average asperity height difference was tested on a few samples and found to adhere to the grit size ($\pm 18\mu\text{m}$).

The potentiodynamic scans were performed in a 2000 ml beaker filled to the label of 1800 ml with deionized water, then added chloride in the form of NaCl of nominal 100% purity in varying amounts. The samples were suspended by platinum wire to ensure an electrical connection and set against a platinum mesh counter electrode. A list of experiment critical parameters is shown above. All scans were done in accordance with a modified version of ASTM G61 (70), with parameters listed above. In addition to this, a short set of additional scans were done on the alloy 1.4470, received from Statkraft, with an increased i_{apex} of 1mA / cm to examine the alloy's behavior at more positive potentials. This was done due to the observed high passive current at lower maximum current densities. The setup is shown below in Figure 22.

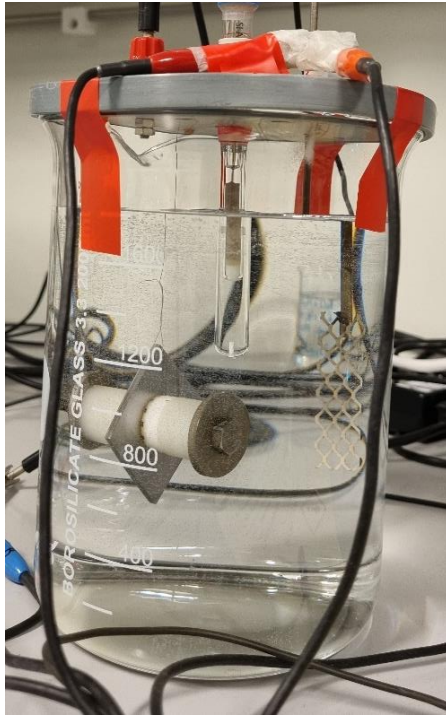


Figure 22: Potentiodynamic setup featuring submerged sample, reference electrode and counter-electrode in order from left to right.

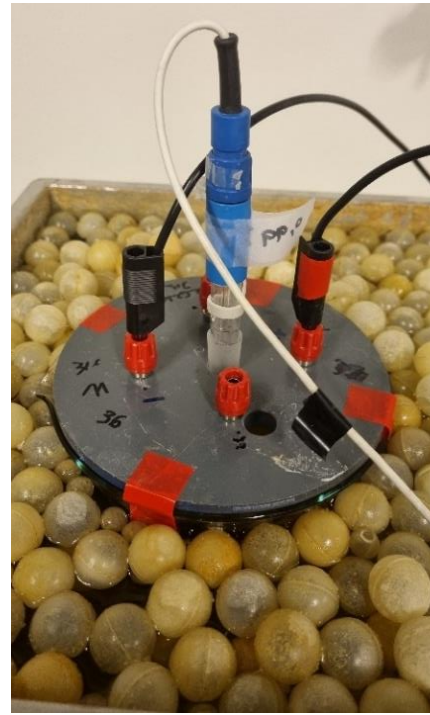


Figure 23: The low-temperature setup in use, submerged in 7°C water

The field experiment was deployed at the Upper Leirfossen power station using fresh water from the river that supplies continuous oxygen and slight water flow through the system. This was accomplished by making a setup with an input and an output at different heights and directions within the container, ensuring thorough exchange of oxygen and ions, see Figure 24 below. All samples were examined in comparison to Ag | AgCl. Four samples of alloy 1.4317 and two each of alloys 304L, 316L and 25Cr were used for this setup. The chloride content was tested during the project work and determined to be 19 mg/l NaCl using the VWR CO-330. The temperature was recorded and found to be in the range 5 – 8°C during the testing period using a thermocouple of possible type J. After two months of free exposure, two samples of type 1.4317, with and without artificial crevice formers, were removed from the setup, rinsed, and examined for possible corrosion initiation. A low temperature experiment run at 7°C to mimic the field setup was conducted in the laboratory, shown in Figure 23. This experiment featured a reference electrode and two samples, not shown in the figure as the experiment was running.

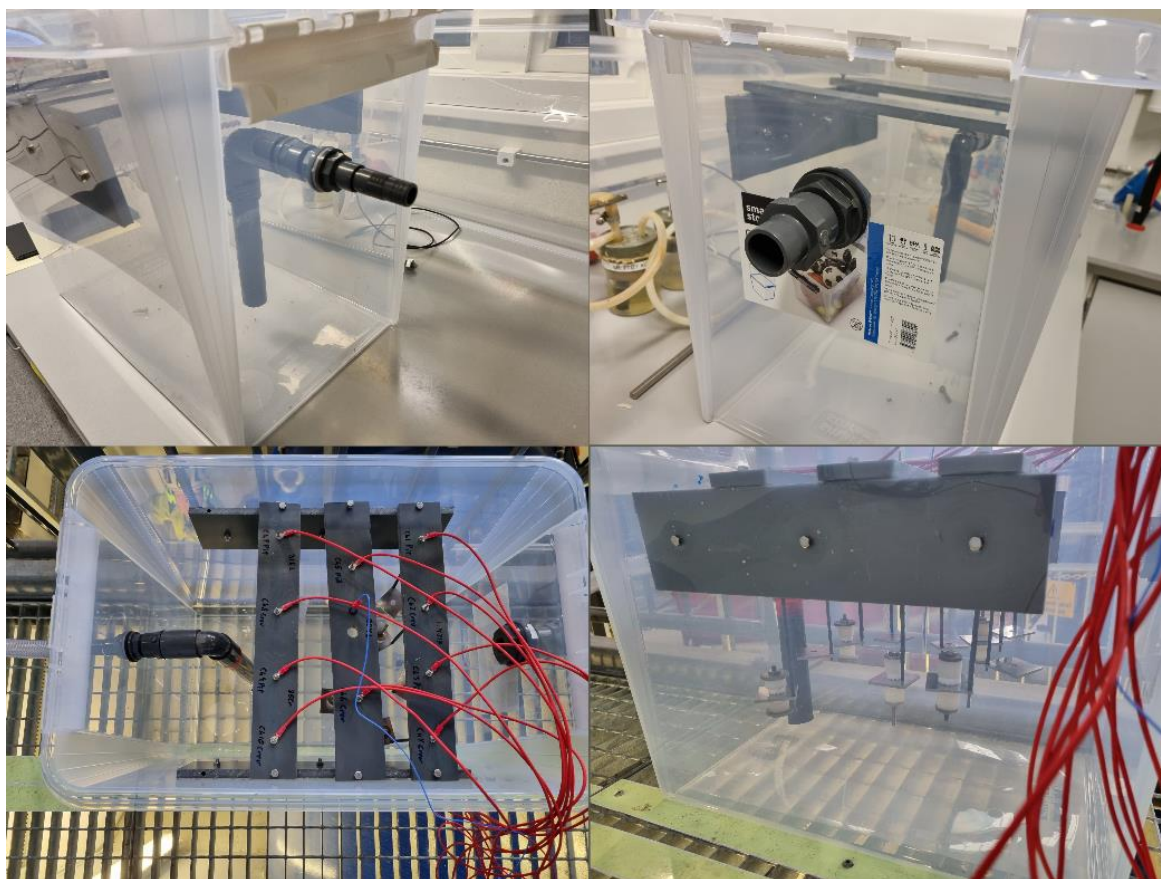


Figure 24: A field setup collage. Clockwise from the top left; i) Water inflow, ii) Water outflow, iii) Connected samples, half of which have artificial crevice formers, iv) Top view, electrical connection of the samples through wires.

Lastly, the potentiostatic experiments were done in deionized water added chlorides in the form of NaCl, to a potential of 300 mV vs. Ag | AgCl to simulate the ennobling effect of a biofilm that would be present in water containing bacteria. This was done in a 15-liter container added approximately 12 liters of deionized water supplied either 250 or 1000 mg/l chlorides. The data was gathered through the in-house data logging system, by measuring the difference between the potential impressed by the potentiostat on the samples against Ag | AgCl through a resistance of 1 ohm. This means the data we gather is the current that flows through the sample at any given time. For the first run at 1000 mg/l, two samples each of 1.4317, 316L and 1.4470 were used and two samples each of 1.4317 and 1.4470 were used for the second run. An image of the setup is shown below in Figure 25.

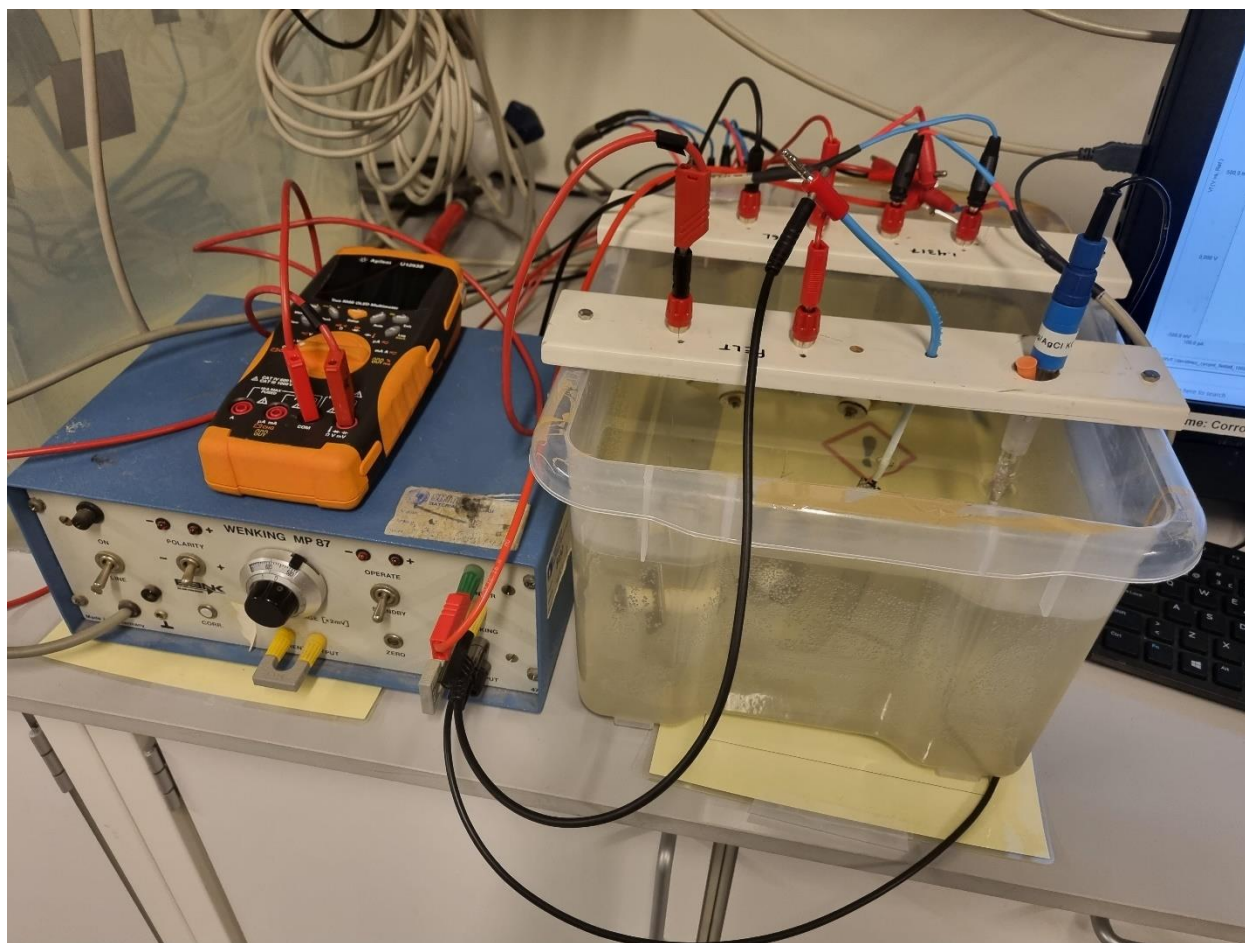


Figure 25: Potentiostatic experimental setup. Not shown is the connector located behind, ensuring equal and constant potential over our samples.

Section 4 Results

Figures 26 through 32 show the cyclic polarization experiment results. Here, only the first parallel is shown, with all chloride concentrations present. Of note is Figure 26, where the limiting current density was reached so fast that the samples could only be polarized to a few hundred millivolts above the OCP at the lowest chloride concentration. Samples of 304L and 316L shown below in figures 27 and 28 exhibit typical polarization behavior with passive regions, clear breakdown potentials and tendencies toward increasing current with increasing chloride content. Figure 29 shows the polarization graphs of 904L, which do not conform to the expected shape presented in the graphs for 304L and 316L, but they do more closely resemble the graphs for 22Cr and 25Cr, with the notable exception of a marked repassivation potential. The last graph in this set, Figure 32, shows the potential evolution on 1.4470, which is marked by a passive current over an order of magnitude higher than all other alloys tested, no visible transpassive region or oxygen evolution reaction and an oscillating current within the passive region.

Figures 33 through 38 show the potential development on all alloys exposed in the field experiment at Leirfossen. They all share some similarities in where their potentials increase and their open circuit potentials for the samples with artificial crevices are consistently higher than those without, save for those of alloy 1.4317. Here, the samples with the crevice formers are lower in potential from early on. Figure 38 shows the ongoing potential development of alloy 1.4470 as it was placed into the setup later than all the other alloys and does not have the same body of data. Figure 39 shows the temperature development in the water throughout the duration of the experiment.

Figures 40 and 41 show corrosion attacks, images obtained from the Alicona InfiniteFocus 3D Optical Microscope. Figure 40 shows the slight indication of crevice corrosion on the 316L sample after a week polarized at +300 mV vs Ag | AgCl in 1000 mg/l chlorides, and Figure 41 shows a 3D scan of the pit that had formed on alloy 1.4317 during 16 hours of OCP in 1000 mg/l chlorides.

Tables 4, 5, and 6 show obtained crevice and repassivation potentials as well as passive currents at initiation for alloys 304L, 316L, and 904L. These values could not be found for our alloys 1.4317, 22Cr, and 25Cr due to near instant initiation for the former alloy and no visible initiation for the latter two, showing that E_{crev} is higher than the oxygen reduction reaction within the parameters of these tests. As such, neither 1.4317, 22Cr, nor 25Cr were

possible to extract this information from. The red crosses denote the absence of a visible repassivation potential on the graph.

Graphs 42, 45, 46, and 47 show current development during potentiostatic experiments polarized to +300 mV vs. Ag | AgCl on alloys 1.4317 and 316L for the first two graphs and 1.4470 for the last two. Figure 42 shows the only alloy to corrode during the potentiostatic experiments. The reason the unit is measured in amperes here is because the datalogger system measures the potential difference between the anode and the reference electrode as run through a 1-ohm resistance, and use of Ohm's law gives a 1:1 conversion between volts and amperes. Note the higher oscillation in current on the samples of 1.4470 in the electrolyte with a higher level of chlorides, Figure 47 at 1000 mg/l versus Figure 46 at 250 mg/l.

Graphs 44, 45, and 47 all have a period of no data near the beginning of the graph, and it is unknown if this was caused by a power outage or if it was a planned shutdown.

Graphs 48, 49, 50, and 51 are semi-logarithmic graphs showing the potential-chloride content relation as it can be interpreted. Here, arbitrarily fitting dashed lines have been placed for comparison, in addition to a simple average of the two parallels of collected crevice corrosion potential values.

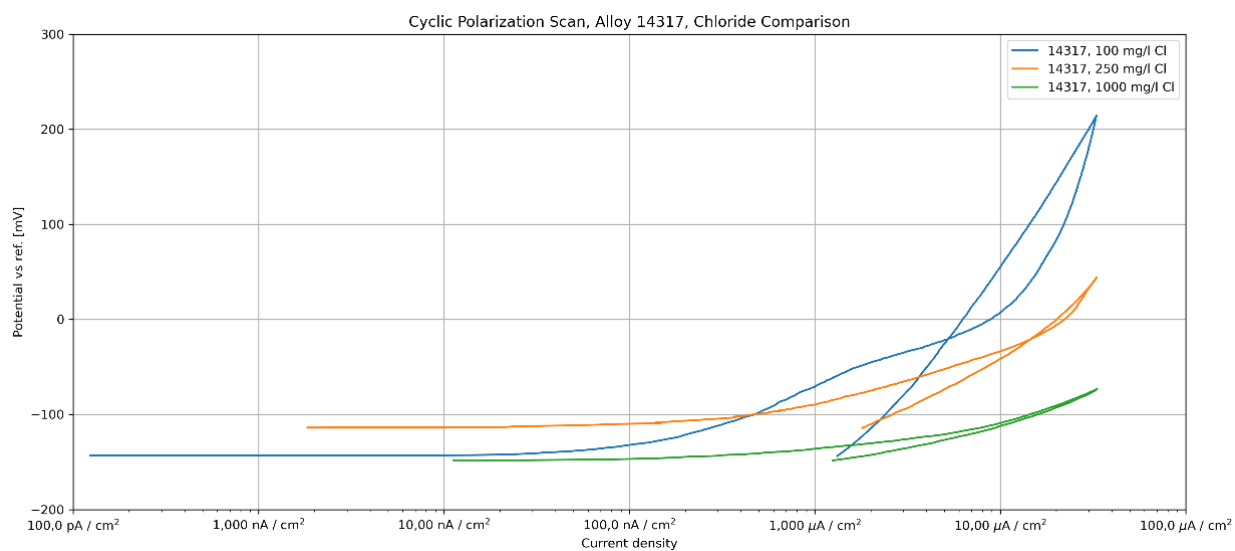


Figure 26: Cyclic polarization of alloy 1.4317 at various chloride concentrations, parallel 1.

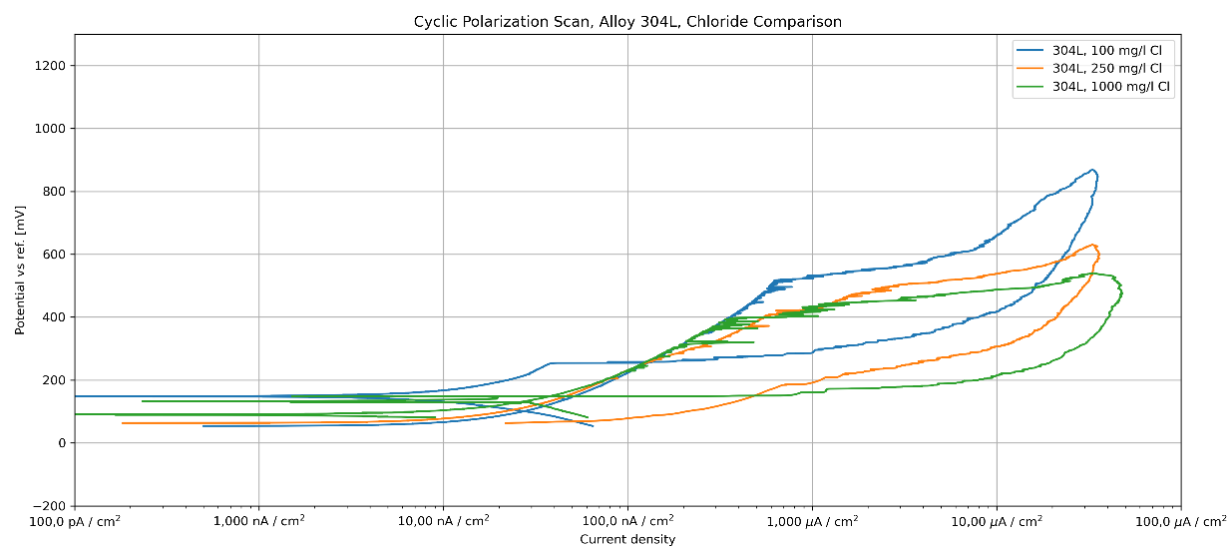


Figure 27: Cyclic polarization of alloy 304L at various chloride concentrations, parallel 1.

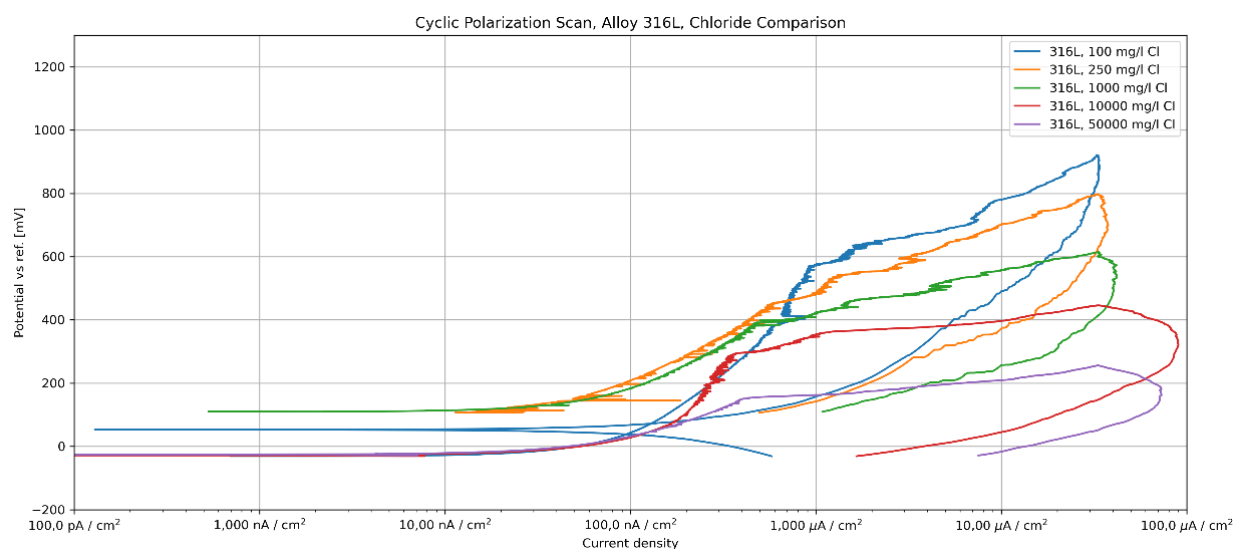


Figure 28: Cyclic polarization of alloy 316L at various chloride concentrations, parallel 1.

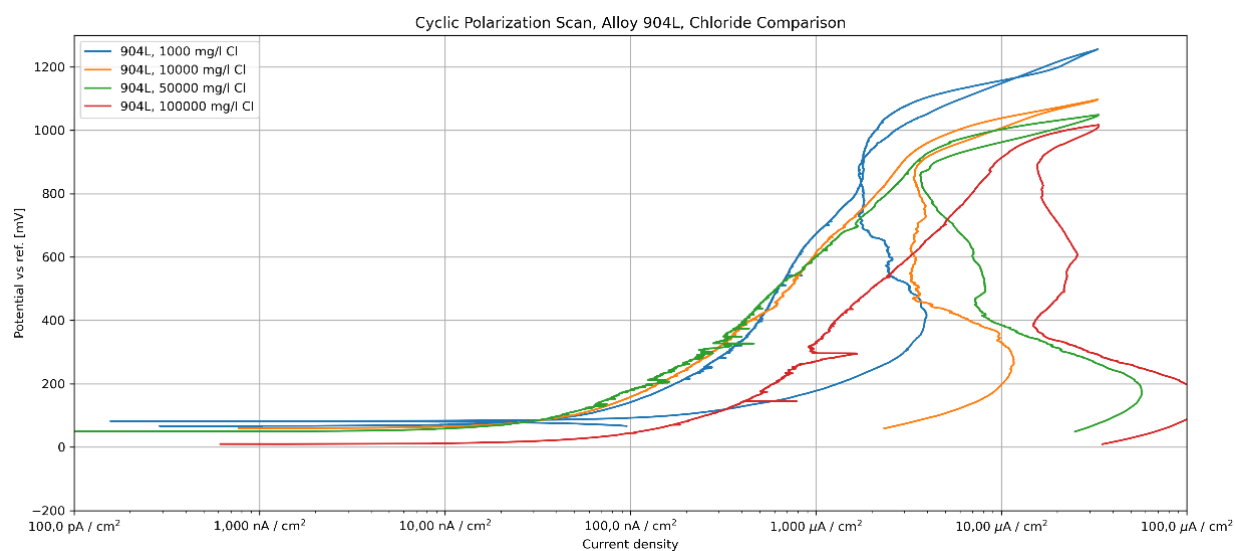


Figure 29: Cyclic polarization of alloy 904L at various chloride concentrations, parallel 1.

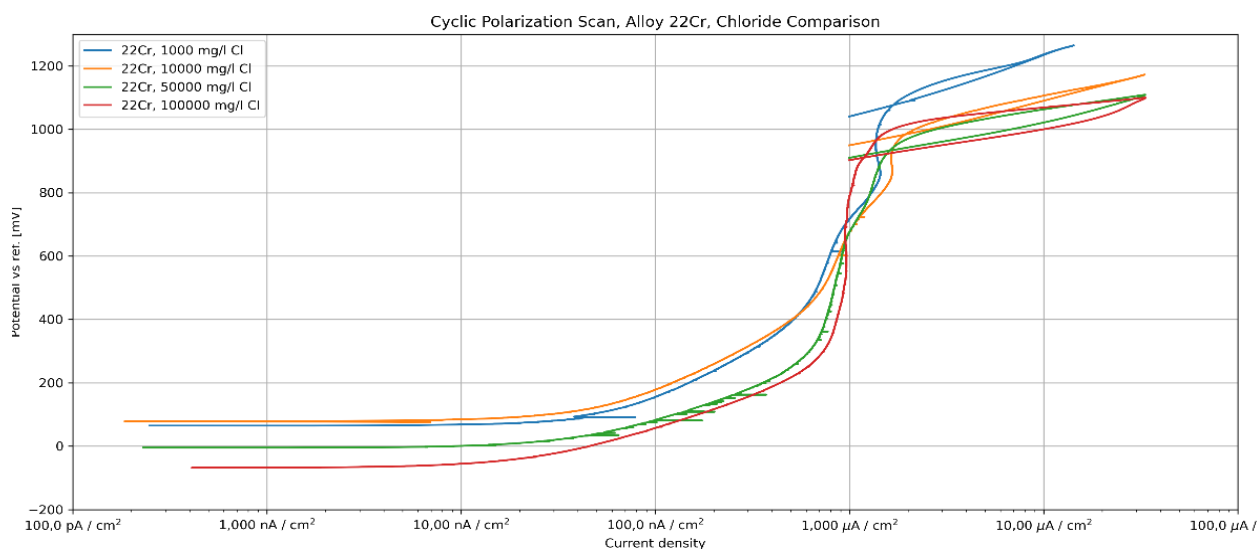


Figure 30: Cyclic polarization of duplex alloy S32205 at various chloride concentrations, parallel 1.

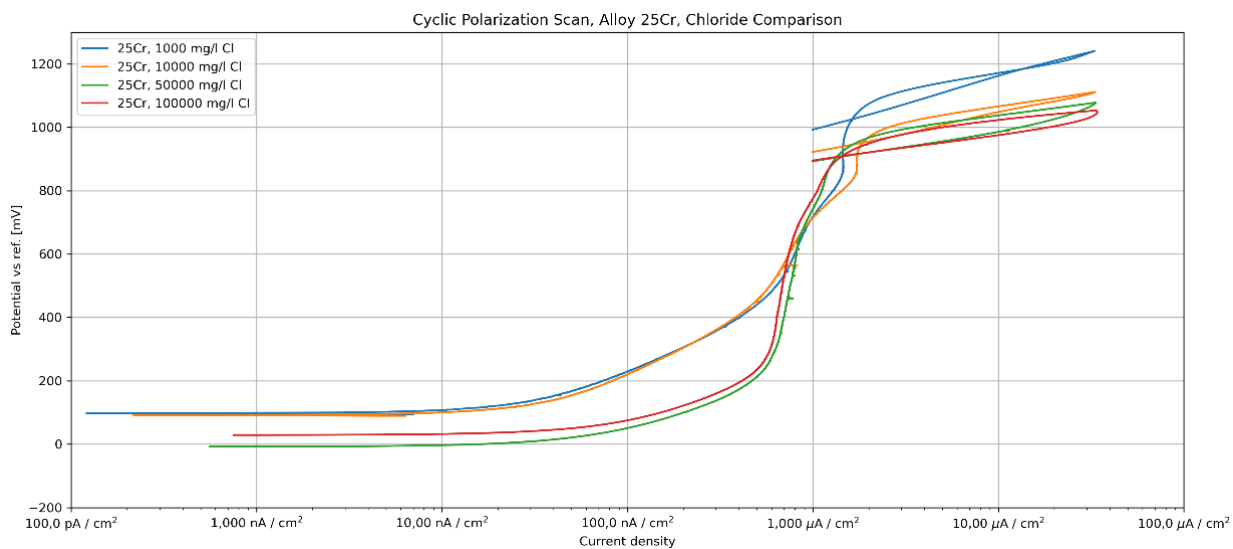


Figure 31: Cyclic polarization of super duplex alloy S32750 at various chloride concentrations, parallel 1.

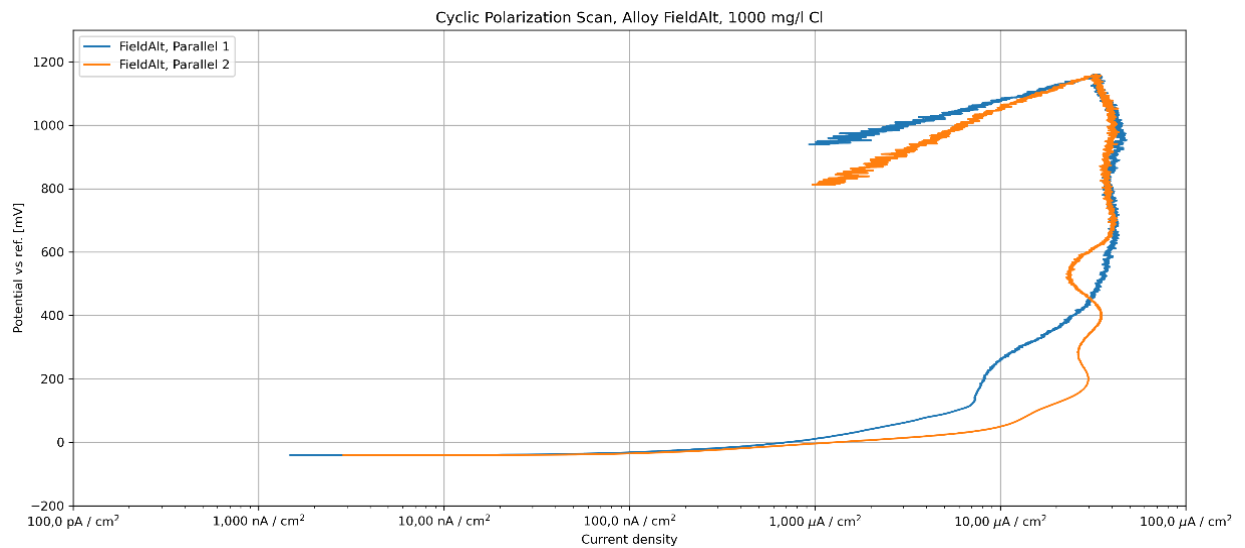


Figure 32: Cyclic polarization on the field alloy (EN 1.4470), maximum current density set to 1mA/cm2 in 1000 mg/l chloride solution.

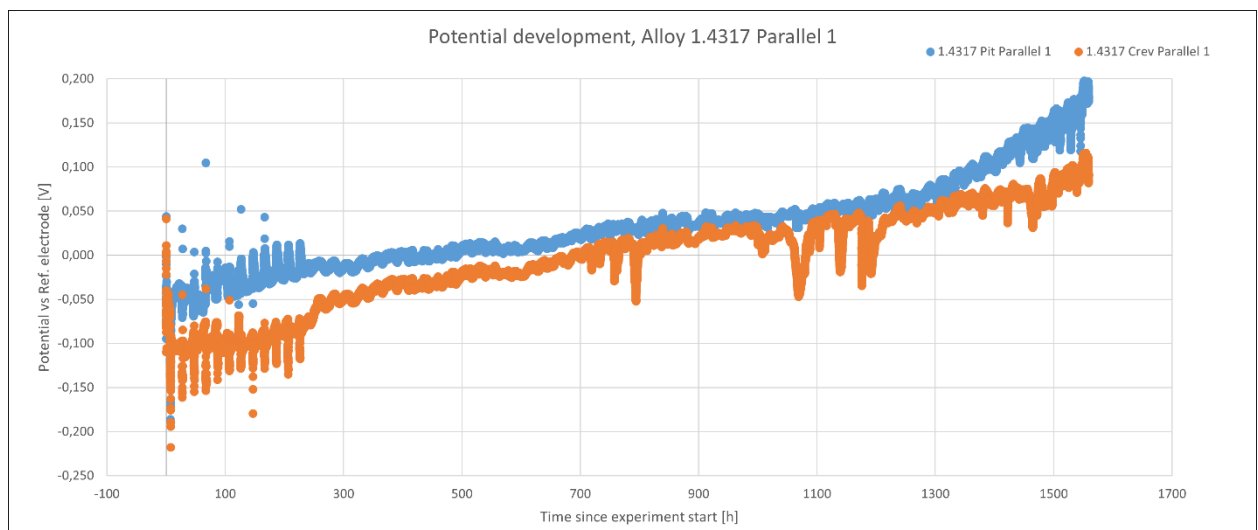


Figure 33: Potential development on EN 1.4317 exposed to continuous fresh river water at our field setup, parallel 1.

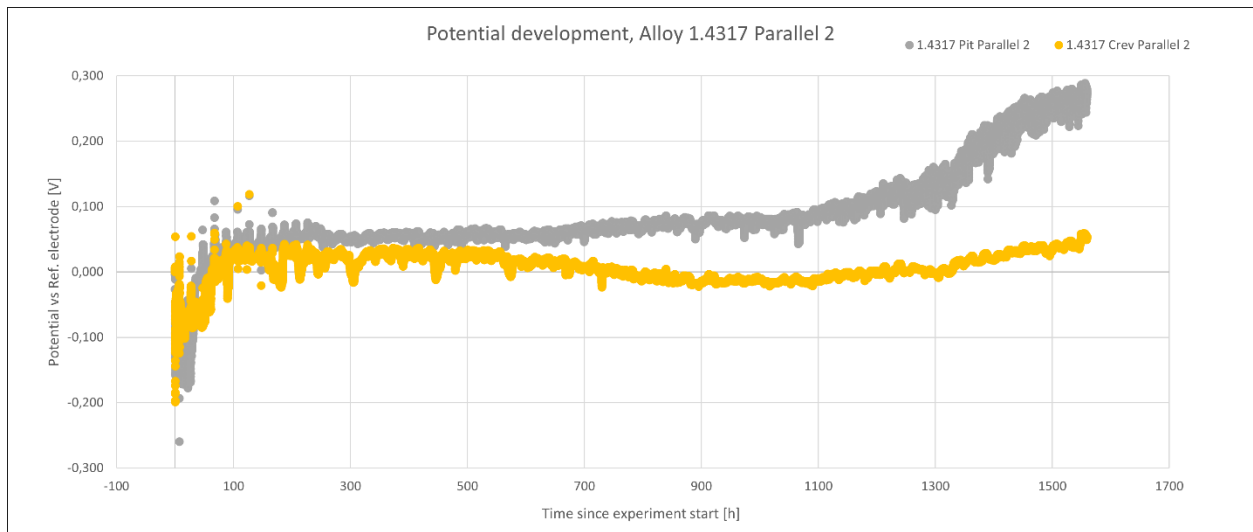


Figure 34: Potential development on EN 1.4317 exposed to continuous fresh river water at our field setup, parallel 2.

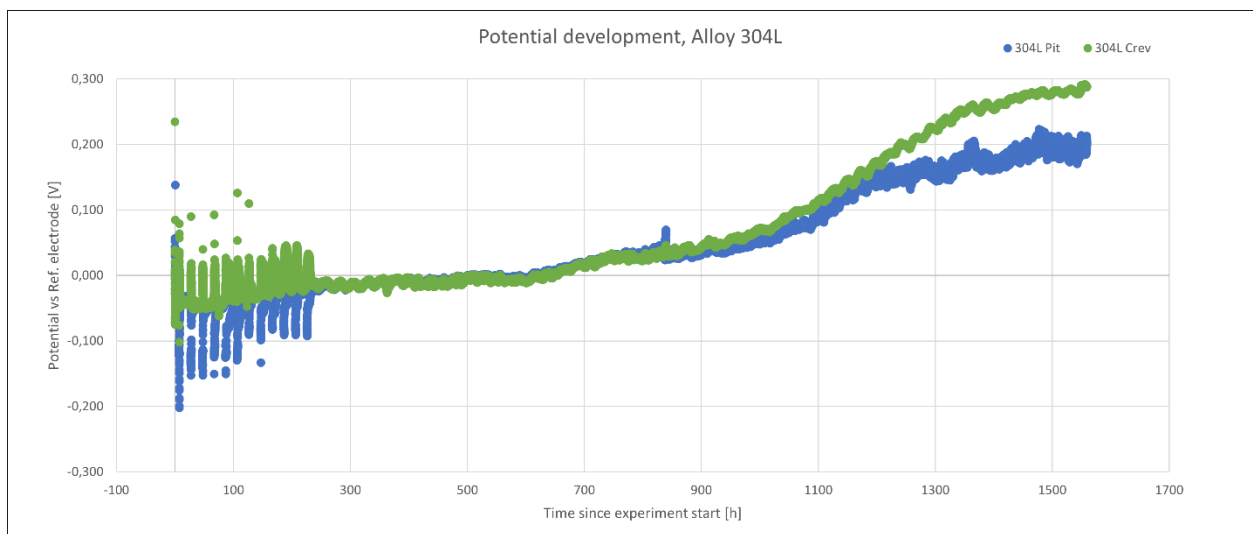


Figure 35: Potential development on AISI 304L exposed to continuous fresh river water at our field setup.

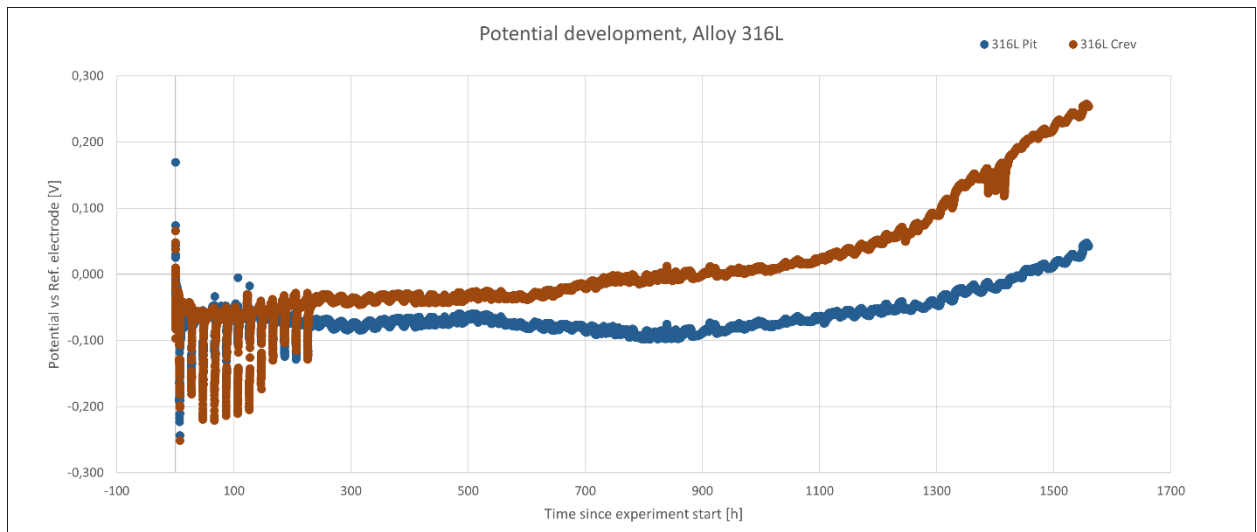


Figure 36: Potential development on AISI 316L exposed to continuous fresh river water at our field setup.

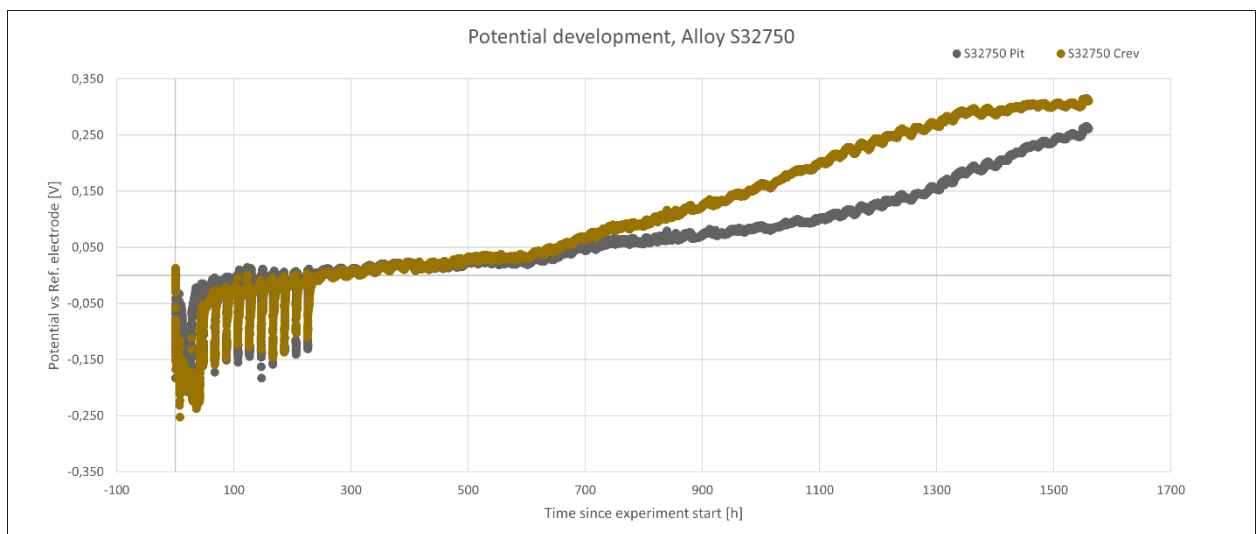


Figure 37: Potential development on super duplex S32750 exposed to continuous fresh river water at our field setup.

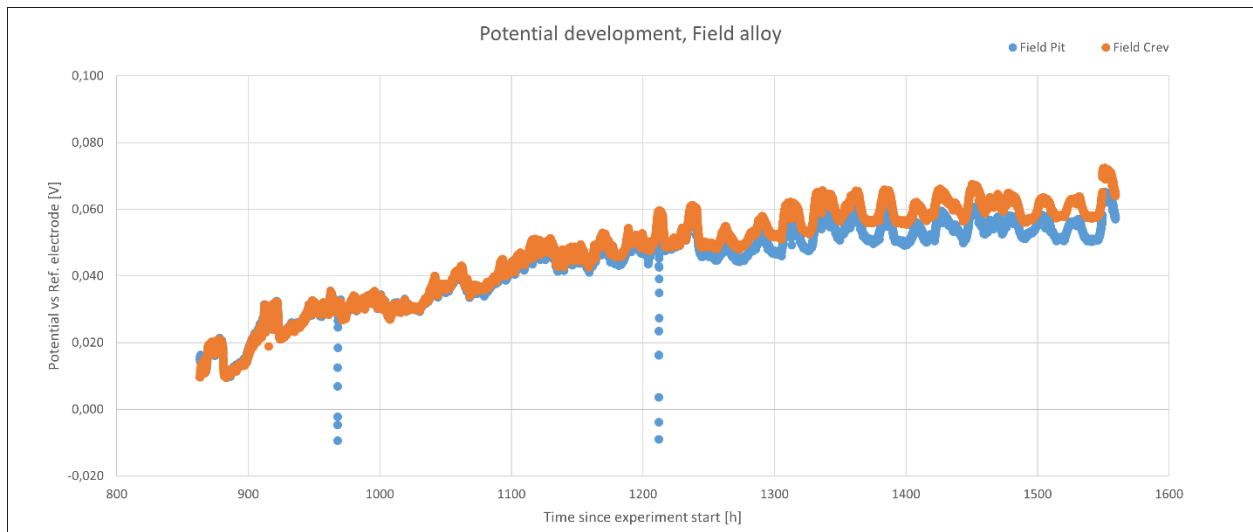


Figure 38: Potential development on the field alloy (EN 1.4470) exposed to continuous fresh river water at our field setup.

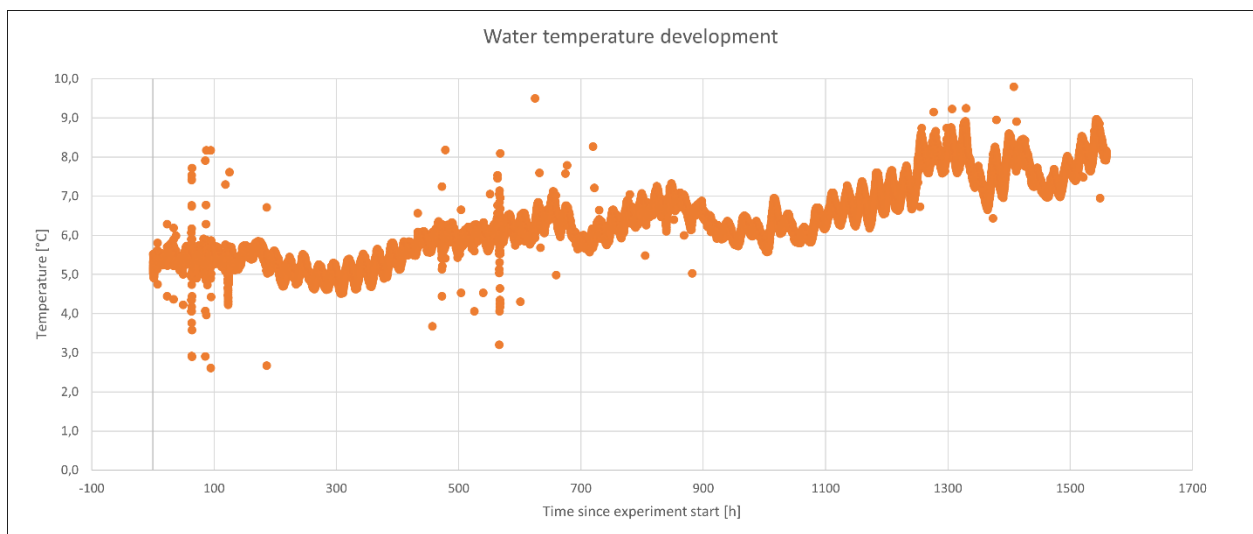


Figure 39: Temperature development in the water at the field experiment location.

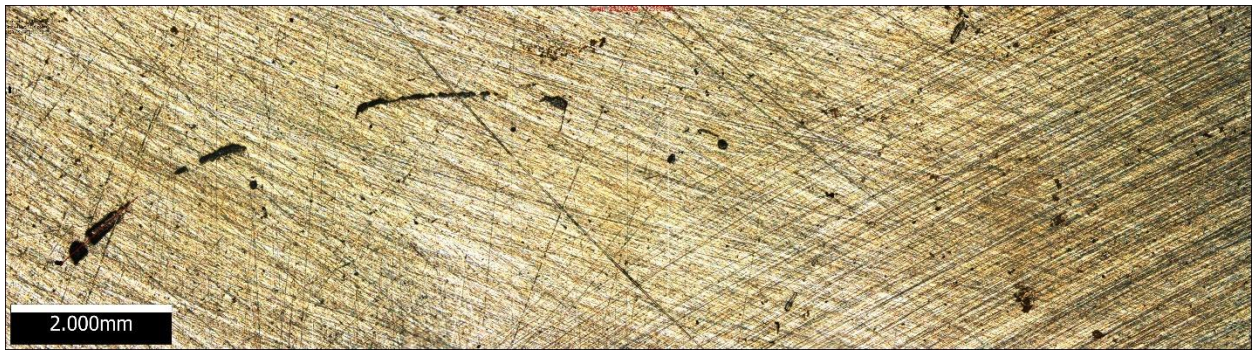


Figure 40: Surface of 316L after one week of polarization to 300mV vs Ag / AgCl. Crevices have started to form under the crevice formers.

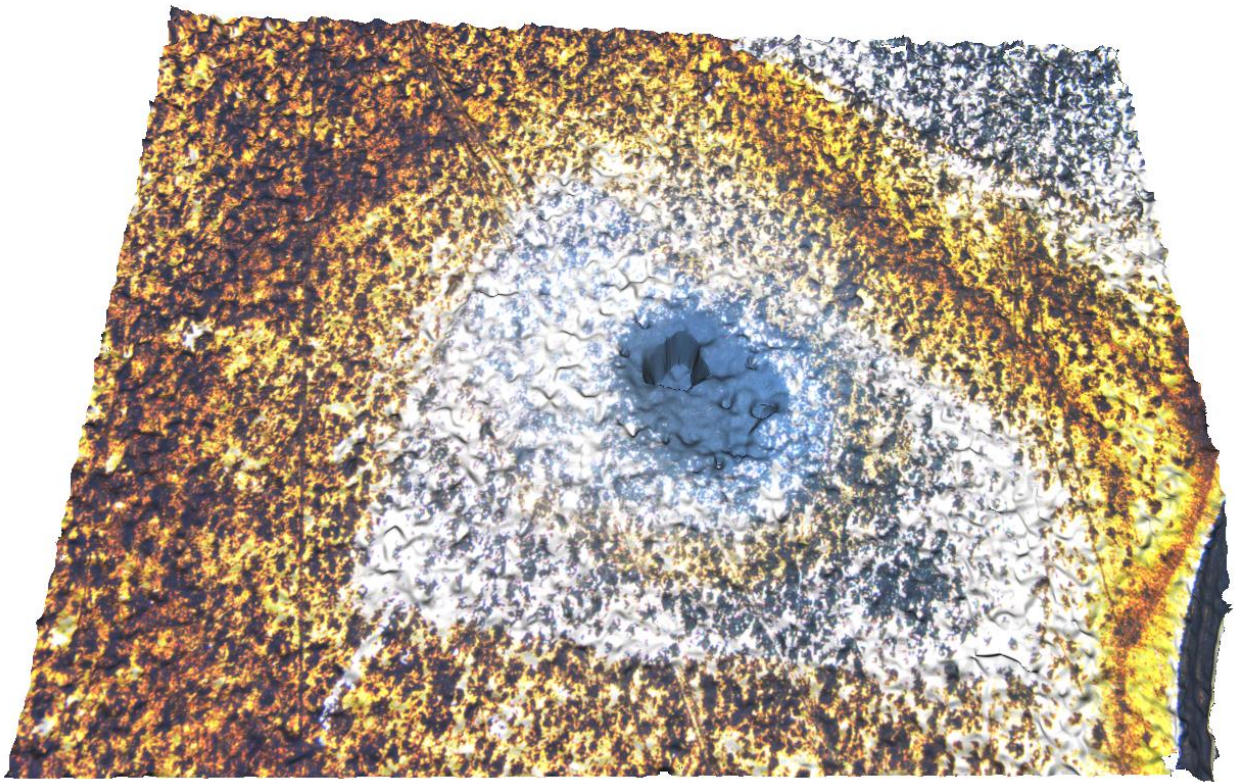


Figure 41: Pit initiated under crevice former of alloy EN 1.4317 under open circuit potential after approximately 16 hours, 3D image from Infinite Focus optical microscope.

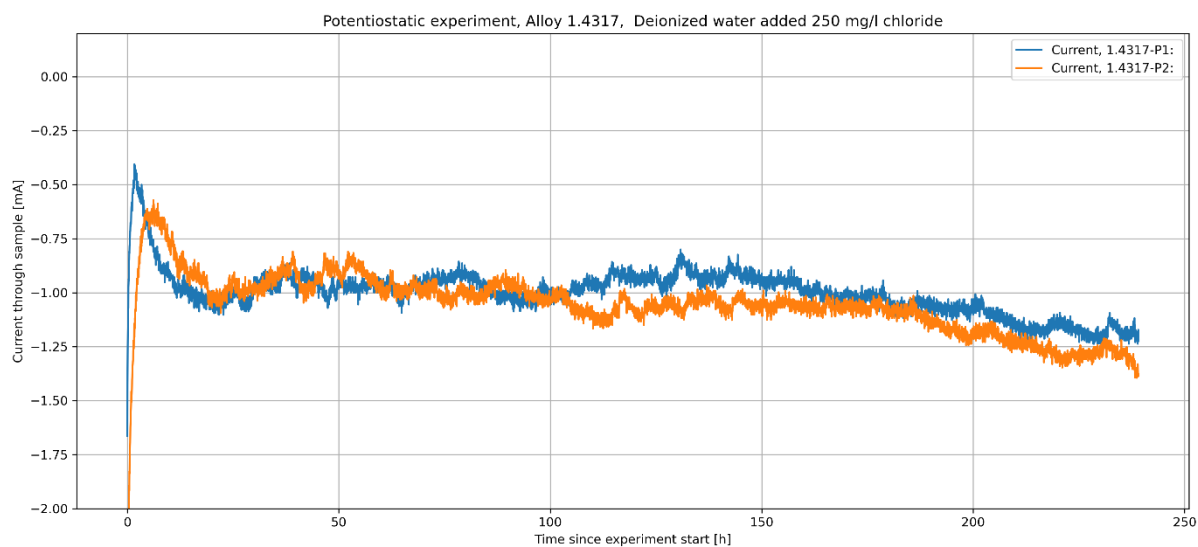


Figure 42: Current development on alloy 1.4317 during potentiostatic test at +300 mV vs Ag / AgCl in deionized water added 250 mg/l chlorides.

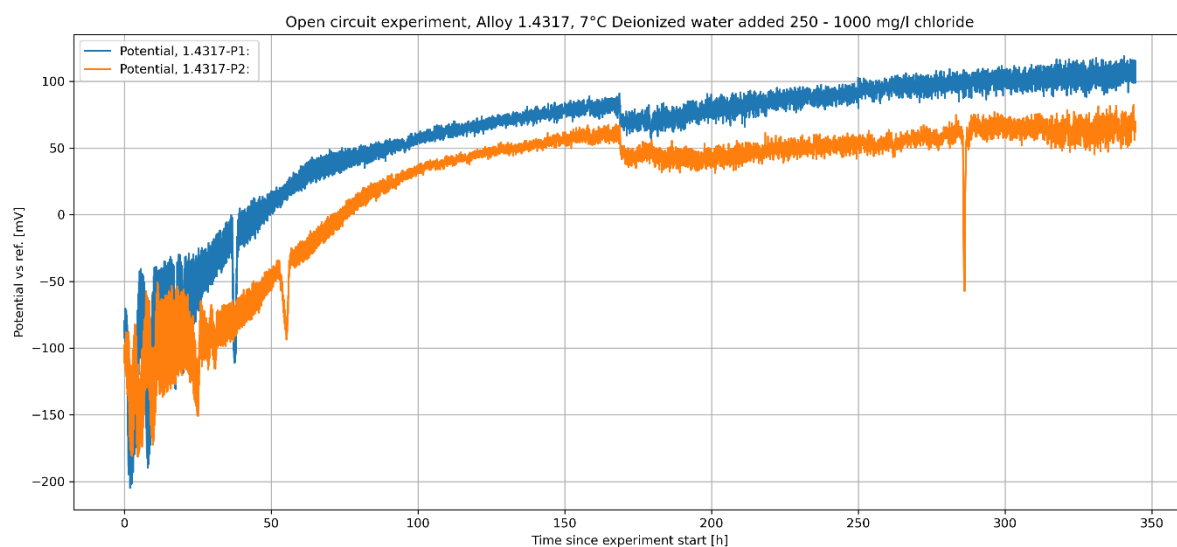


Figure 43: Potential development on alloy 1.4317 in deionized water added 250 mg/l chlorides at 7°C. Chloride content was increased to 1000 mg/l midway through the experiment, shown by the dip in potential.

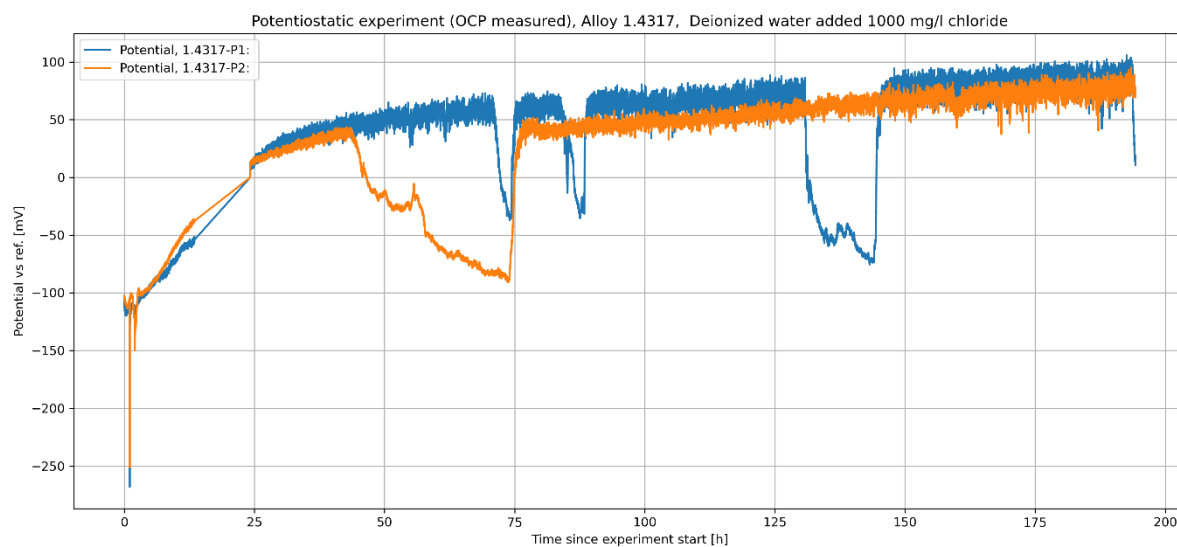


Figure 44: Potential development on alloy 1.4317 in deionized water added 1000 mg/l. Sample was intended to be polarized to 300 mV vs. Ag / AgCl., but it initiated before the experiment could be started. The OCP was therefore measured instead.

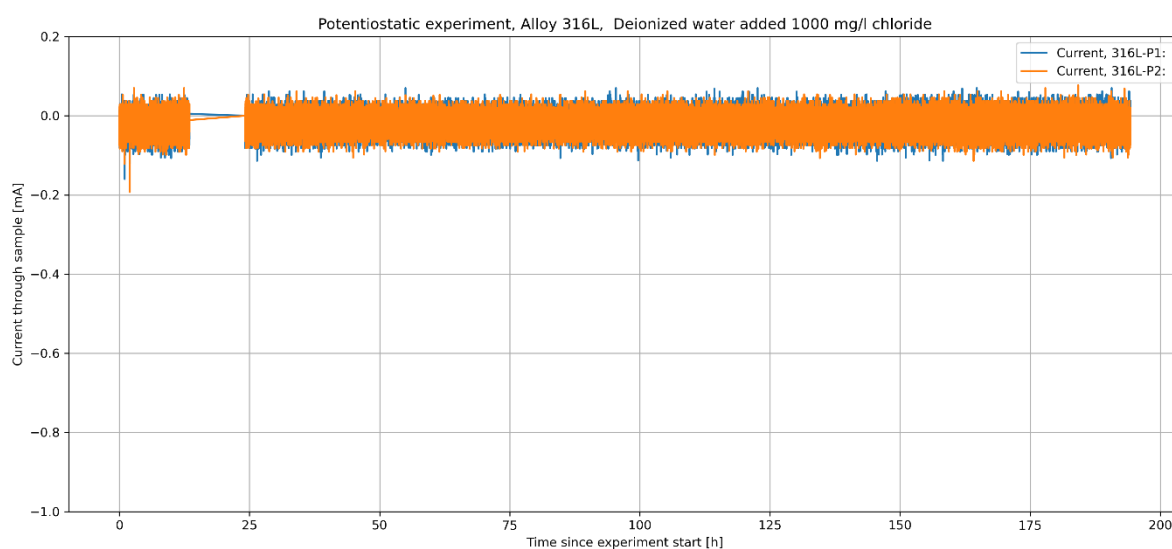


Figure 45: Current development on alloy 316L during potentiostatic test at +300 mV vs Ag / AgCl in deionized water added 1000 mg/l chlorides.

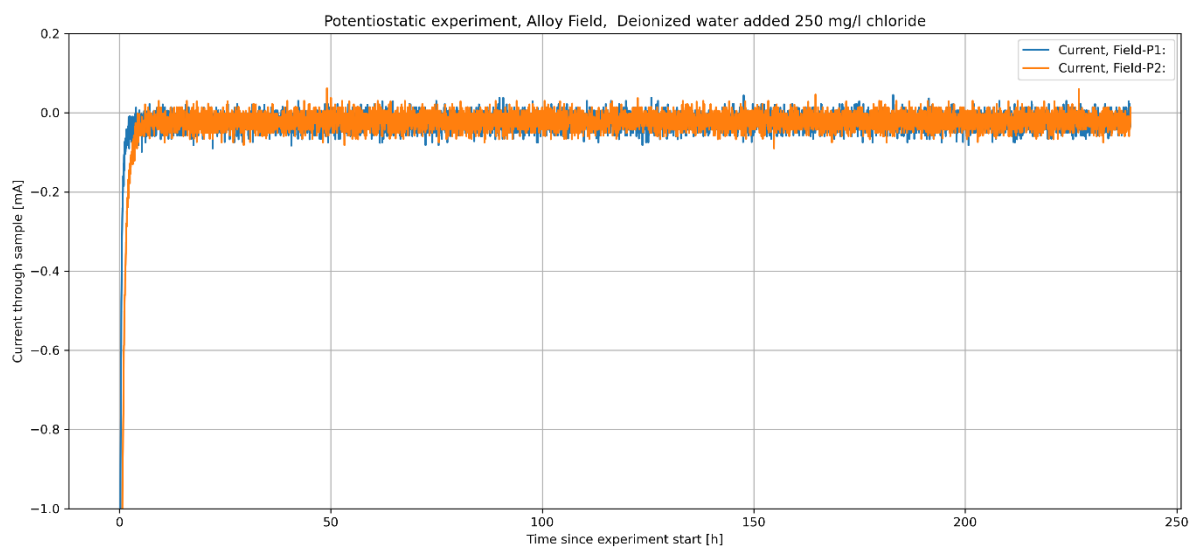


Figure 46:: Current development on alloy 1.4470 during potentiostatic test at +300 mV vs Ag / AgCl in deionized water added 250 mg/l chlorides.

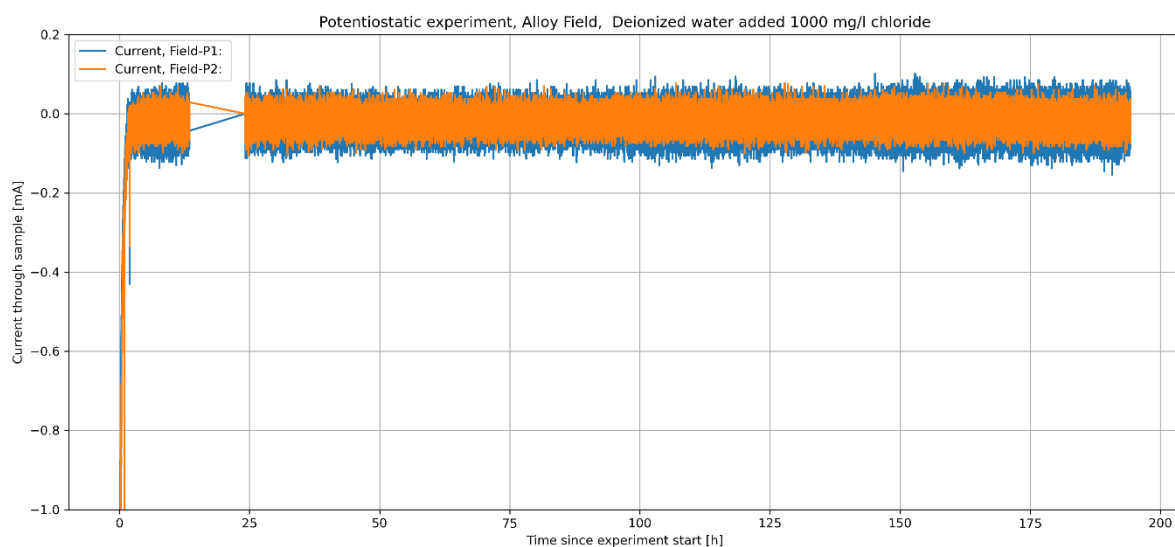


Figure 47: Current development on alloy 1.4470 during potentiostatic test at +300 mV vs Ag / AgCl in deionized water added 1000 mg/l chlorides.

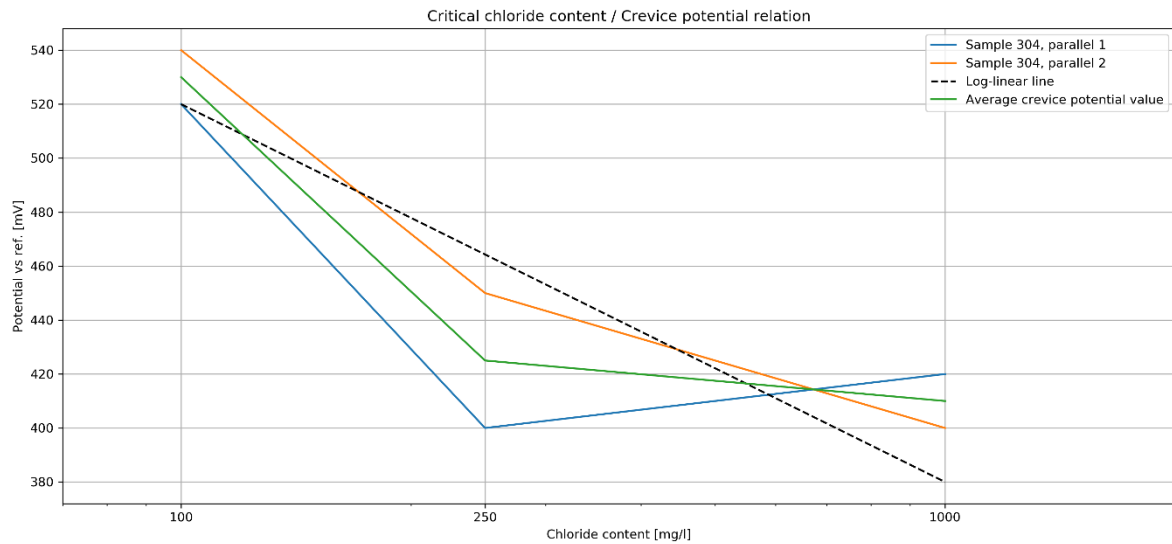


Figure 48: Critical chloride content / crevice corrosion potential log-linear graph, steel grade 304L.

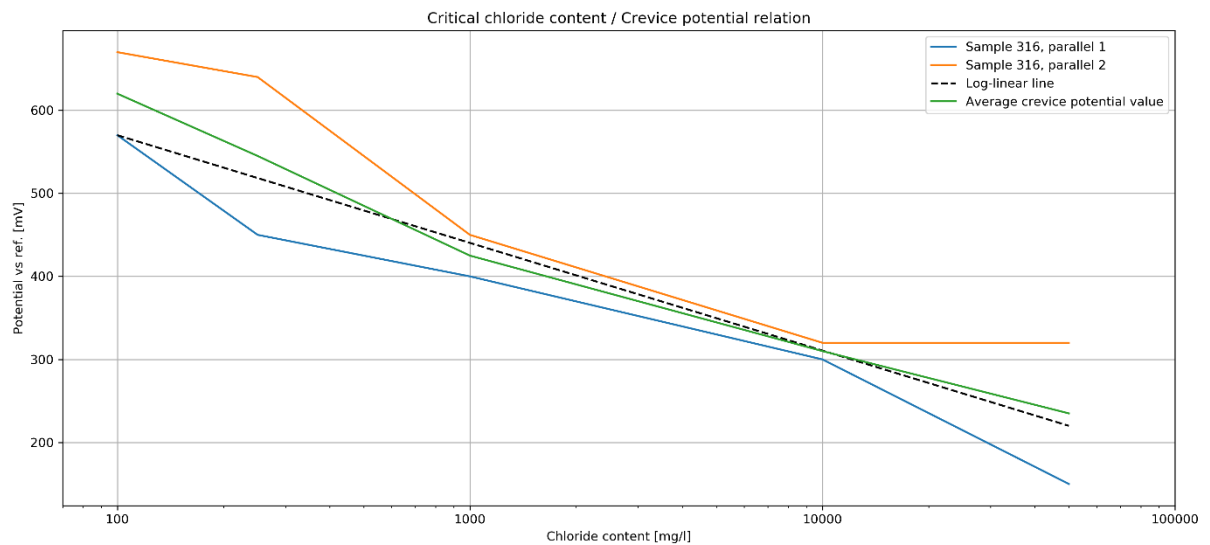


Figure 49: Critical chloride content / crevice corrosion potential log-linear graph, steel grade 316L.

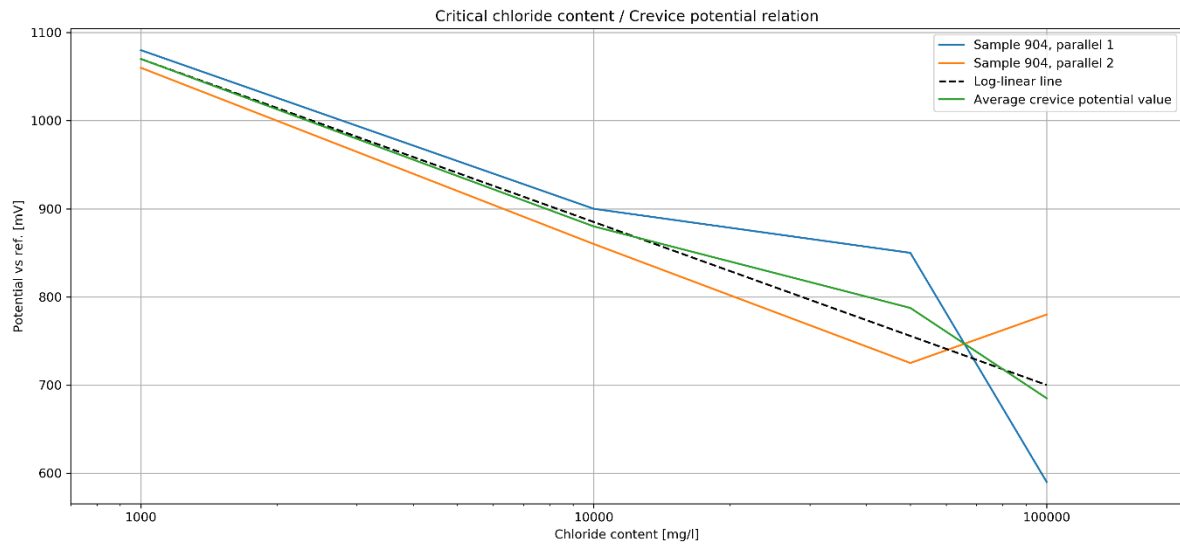


Figure 50: Critical chloride content / crevice corrosion potential log-linear graph, steel grade 904L.

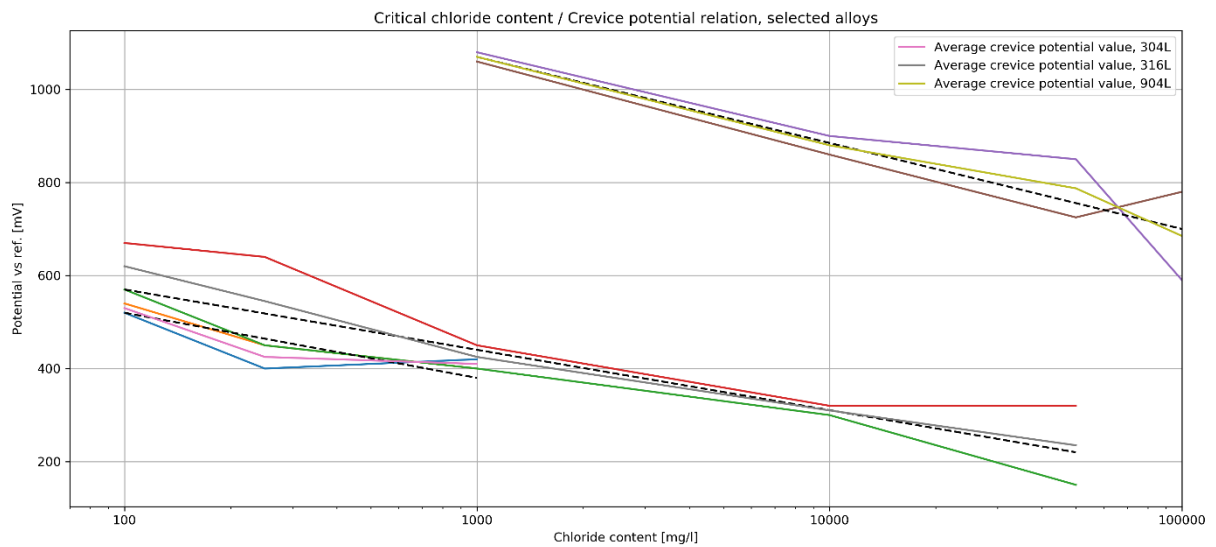


Figure 51: Critical chloride content / crevice corrosion potential log-linear graph, all available steel grades.

Table 4: Crevice corrosion potentials, repassivation potentials, and passive currents at initiation, alloy AISI 304L. All potentials with reference to Ag / AgCl. A red X indicates no clear repassivation potential was observed.

	Chloride content, Parallel 1 [mg/l]			Chloride content, Parallel 2 [mg/l]		
304L	100	250	1000	100	250	1000
E _{crev} [mV]	520	400	420	540	450	400
E _{rep} [mV]	260	X	150	80	100	X
i _{pass} [μA/cm ²]	0,6	0,6	0,4	0,8	0,5	0,6

Table 5: Crevice corrosion potentials, repassivation potentials, and passive currents at initiation, alloy AISI 316L. All potentials with reference to Ag / AgCl. A red X indicates no clear repassivation potential was observed.

	Chloride content, Parallel 1 [mg/l]					Chloride content, Parallel 2 [mg/l]				
316L	100	250	1000	10 000	50 000	100	250	1000	10 000	50 000
E _{crev} [mV]	570	450	400	300	150	670	640	450	320	320
E _{rep} [mV]	80	X	X	X	X	X	80	X	X	X
i _{pass} [μA/cm ²]	0,9	0,6	0,5	0,4	0,4	0,9	0,7	0,7	0,2	0,2

Table 6: Crevice corrosion potentials, repassivation potentials, and passive currents at initiation, alloy SAE 904L. All potentials with reference to Ag / AgCl. A red X indicates no clear repassivation potential was observed.

	Chloride content, Parallel 1 [mg/l]				Chloride content, Parallel 2 [mg/l]			
904L	1000	10 000	50 000	100 000	1000	10 000	50 000	100 000
E _{crev} [mV]	1080	900	850	590	1060	860	725	780
E _{rep} [mV]	1150	X	X	X	X	X	X	X
i _{pass} [μA/cm ²]	3	3	3	3	3	3	3	3

Section 5 Discussion

Firstly, the connection we sought to examine was that of the chloride content's effect on the critical crevice corrosion potential. From our results (Figure 26, Figure 27, Figure 28, Figure 29, Figure 30, and Figure 31), we can see that an increase in chloride content both increases the passive current before an eventual initiation and the alloy's critical crevice potentials decrease. This is in general agreement with the literature on this subject, as discussed in the theory section as well as (71–73).

The potentiodynamic experiments were performed in accordance with the standard that was set in the experimental section. Using (67) as a source, we will attempt to interpret our results in accordance with theory. Starting with 1.4317, from the curves shown in Figure 26, we can see that the limiting current density set by our experiment parameters was reached extremely quickly, reaching the maximum in the 1000 mg/l solution in a sweep of just ± 75 mV from the open circuit potential after 30 minutes of pre-exposure. Even for the lowest chloride content, it is evident that there is no critical chloride potential, and the alloy simply corrodes under a small potential increase. There is no visible passive region, as the alloy does not have a static current density under which the potential increases. This fits the data we have collected from the low-temperature experiments, as both the field experiment and the laboratory experiment led to corrosion initiation. For the field experiment the crevice sample was found to initiate in microbially active waters with chloride contents measured at 19 mg/l and temperatures around 7°C. In the lab test with microbe-free water, the alloy seems to have initiated at a chloride concentration of 250 mg/l in 7°C when freely exposed at the corrosion potential. Data therefore shows that the alloy in all likelihood would corrode from crevice and perhaps even pitting corrosion at slightly elevated temperatures and potable chloride concentrations.

From the 304L and 316L graphs (Figure 27, Figure 28), a clear indication of crevice corrosion potentials can be seen at every chloride concentration level. The curves show a transition from exhibiting protection potential, meaning a closed hysteresis loop, to showing no protection potential as the chloride content increases. This behavior is consistent across parallels and seems to be in good accordance with the theory presented in (67).

The 904L graph (Figure 29) is the most unique among our results. They have irregular shapes, initiate corrosion at lower chloride contents, and seemingly show no clear protection potential even for the very lowest concentrations. Due to the collected data showing a lack of a clear crevice corrosion potential, yet having visibly corroded after being removed from the

experimental setup, we've defined the crevice corrosion potential as a specific current density, which has precedent in literature (74). The value was agreed upon by internal discussion.

Lastly, both the 22Cr and 25Cr alloys both showed strong resistance against crevice corrosion for all chloride concentrations at room temperature used in this thesis, congruent with literature (75,76). Given the correct phase balance and avoidance of intermetallic and nitride/carbide formation, the resistance to localized corrosion is high enough to protect the metal until it breaks down by transpassive dissolution at room temperature. Our samples seemingly show only oxygen evolution and no marked attacks, with the sole visible evidence of experimentation being corrosion products even at chloride concentrations as high as 100 000 mg/l. These samples are therefore considered the benchmark that we compare our field alloy to, even though it is manufactured differently, it being cast and not hot rolled.

The semi-logarithmic graphs created from our first parallel results on the crevice corrosion potentials seem to adhere to a general trend towards the proposed log-linear relationship. The 904L samples fit very well with the data, with only minor variations from the line. The 316L samples look to have a slight spread of values, but otherwise fit well - especially its average, around the dashed possible line which was placed for reference and was not based on any real values, whilst the 304L samples show a less clear connection and will require more data points for any formal confirmation. In summary, both 316L and 904L have averages that trend around the log-linear line, but 304L does not.

From our exposure tests performed at Statkraft's location we can see that there is a marked increase in the potential for all samples. After 1500 hours the potential is still increasing and on some samples the potential is close to +300 mV vs. Ag/AgCl which is a level that has been measured in other tests (57). Another observation is the difference in potential development between two parallels. Literature gives a direct connection between the temperature of a solution and the corresponding critical pitting corrosion potential (35), which should be coherent with an increase in the related crevice corrosion potential. This increase can be significant as seen in figure 3 in the source, but the level at which our samples' potential has evolved is not explainable solely by the increasing temperature, which is consistent with the literature on the subject (63). As the temperature increases for our field setup, the critical crevice corrosion potential is then expected to fall, which may initiate corrosion on samples that were previously passive.

A source (73) says the temperature of the solution determines the intercept of the breakdown potential-chloride content graph. They give a significant effect of the temperature on the localized corrosion initiation tendency. This is demonstrated by their type 304L samples' average breakdown potentials, at a static 1000 mg/l chloride content, dropping by over a hundred millivolts when increasing the temperature from 10 to 25°C, as well as dropping further with a further increase in temperature. An unfortunate problem with comparing these results with our results is that it is difficult to ascertain the specific onset of crevice corrosion in our case, due to the lack of a remarkable drop in potential in either experiment. To rectify this, further work can explore the dependence of the breakdown potential on the temperature for our samples.

Comparing the results from the field experiment with figure 1 in (77) shows that the increase in potential found on the 316L alloy matches what has been found in previous experiments, see Figure 19 on OCP evolution in the theory section, with the difference that our samples ennobled to about +300 mV vs. Ag | AgCl. and not +300 mV vs. SCE, which is admittedly not a big difference.

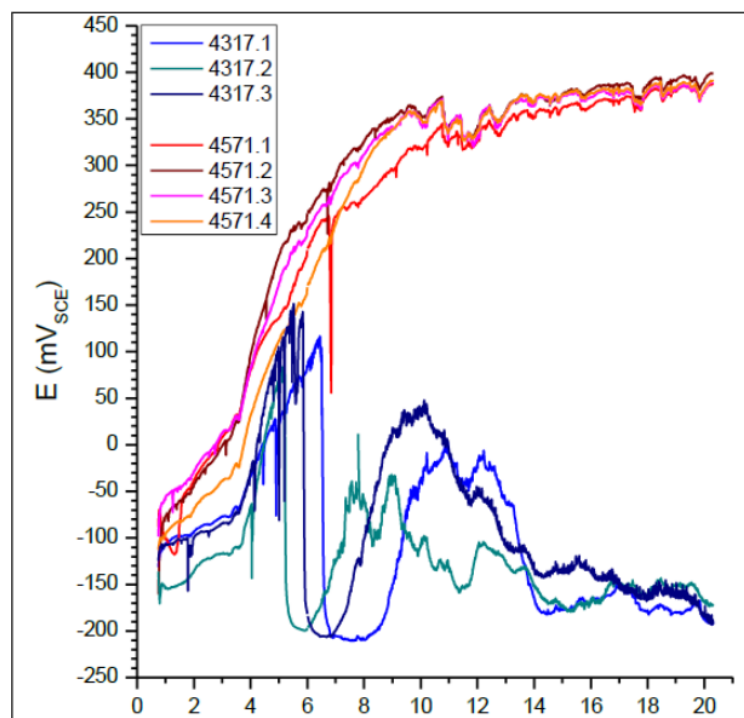


Figure 52: Images of potential development on two different steel grades. Graph provided by supervisor.

One is typically able to observe the onset of corrosion simply through measuring the OCP. It is understood that a drop of several hundred millivolts over a short period of time is

consistent with the initiation of pitting or crevice corrosion. This is by example observed in the image from Figure 52 above, but in our results from both low temperature experiments, the field experiment and the laboratory experiment, corrosion was observed on the samples- see figures Figure 53 and Figure 54 below- without a visible corresponding potential drop. The source (63) also comments on the role of weld scale in the pitting corrosion process, seeing that most of the corrosion attacks happened in the welds throughout the system. It is therefore inferred that if the pipes were cleaned and perhaps pickled, that the corrosion attacks would have been fewer and further between. The impact of heat treatment in the welds is important, as corrosion initiation may not only stem from debris and surface contaminants, but potentially also from segregation of the microconstituents and weakening of for instance the grain boundaries, creating weak spots that both the biofilm and chloride ions can exploit.



Figure 53: Corrosion attack on field-exposed sample of grade EN 1.4317.



Figure 54: Corrosion attack on low-temperature laboratory experiment, grade EN 1.4317.

Two sets of experiments were run on the Wenking potentiostat at a constant potential of +300 mV vs. Ag | AgCl for the purpose of emulating the ennobling effect of a biofilm covering the samples. This was done for a chloride content of 1000 and 250 mg/l, which would be comparable to structures placed in lightly brackish natural waters (78). For our initial experiment, the completion of the setup was not possible the same day, and it was decided that placing the samples into the solution would allow the passive layer to adapt and the OCP to stabilize (14). During this time, the sample of 1.4317 that was placed into the solution initiated quite severe crevice corrosion in a matter of approximately 16 hours at OCP. Due to

this, it was simply disconnected and allowed to evolve for the next week. When removed, it was discovered that the crevice corrosion had corroded the sample quite badly, leaving pits under the crevice formers of several hundred micrometers as measured by the InfiniteFocus microscope, while the 316L was free of corrosion products but had very slight initiation at the outer edge of the crevice formers that was only observed upon closer inspection later. The 1.4470 samples were stained with a hint of corrosion products, but no visible corrosion was observed. These samples were later examined in the Alicona InfiniteFocus 3D optical microscope, and no sign of corrosion initiation was found here either.

The next parallel was set at a chloride content of 250 mg/l. No initiation was observed on the 316L samples in the first parallel at higher chloride contents initially, and as such they were removed from the second parallel. When the experiment was underway and the samples exposed to the potential, it became obvious very quickly that the 1.4317 alloy had initiated. This was to be expected from the PREN value (see Table A - 1 and (79)), having an average value suggesting the critical chloride content for crevice corrosion initiation was approximately somewhere between 0 and 25 mg/l from Figure 15, and the experiment was left to run to completion. From the curves found, it was clear that the samples had initiated during the very first day, and the current was relatively high at about 1 mA. After a week had passed the setup was disassembled and the samples were removed. Upon removal, the entire container was filled with corrosion products, and the samples of 1.4317 looked as if they had been case hardened, showing color gradients from blue to orange around the connection points, see Figure 55 below. The damage was severe, with multiple crevice initiations as well as significant pitting. The potential was measured and controlled throughout the experiment and found to be at the intended potential ± 5 mV at every observation, so the effect of unstable voltage is highly unlikely to have caused the damage. As the biofilm ennoblement evolution reacts to initiation and the total potential over the sample drops, having the potential stay at high values after pitting is rather unrealistic, but the purpose of this experiment was to see whether the samples would initiate under a potential increase similar to that of a biofilm, and this was indeed shown to be the case. Therefore, the state of the sample afterwards is taken to be of little note, only the fact that it initiated is of special interest. This experiment could be repeated under the conditions given by our on-site results in order to more thoroughly characterize the temperature- and chloride concentration-dependencies of this and other alloys.

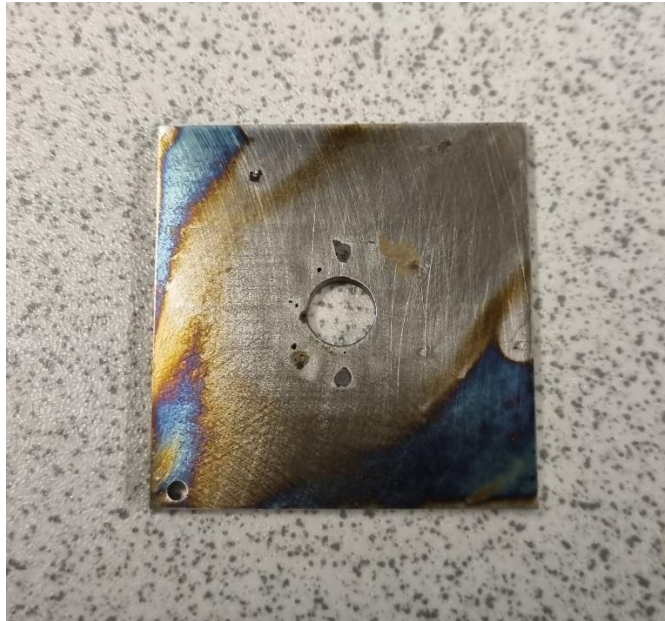


Figure 55: Sample of type EN 1.4317 after one week of potentiostatic polarization to +300 mV vs. Ag / AgCl.

A source from the biofilm section states that biofilm growth is not inhibited by an increase in flow speed, and the (63) source shows a lack of corrosion in the part of the pipe system with the smallest cross-section and therefore the highest flow rate. They imply that this is the case exactly because of the flow speed. The Markov chain source (66) also shows that in the case of chlorides, flow will help clean up and wash away corrosion products and local chloride concentration gradients on the surface. Their model does not consider the biofilm's interaction with the environment, which seems to be an important connection should the attached biofilm be capable of accepting chloride ions that otherwise would have been washed away. (63) seem to imply exactly this, stating that the localized corrosion attacks are "attributed both to the OCP ennoblement of specimens and the chloride ion enrichment in the biofilm". If this is the case, then applying flowing conditions to a system where a biofilm has already attached may not incur the protective capabilities otherwise provided. Should the biofilm be able to adapt to higher flow rates without detaching, this may even increase the influx of chloride ions and render the system more vulnerable. The case might be from these sources that the biofilm cannot initiate adhesion under high flow or extensively turbulent conditions, but once it has latched onto the surface, it can grow and endanger the material regardless, at least under non-extreme conditions of violently turbulent flow. The question remains whether the biofilm would incorporate other particles floating in the water than those strictly necessary to grow. For our field setup, the microbial evolution could have been disturbed or blocked by sediments in the water. See Figure 56 below for reference.



Figure 56: Particulates covering samples in on-site field experiment.

As is visible from the photo, a layer of sediment is covering the samples. When two of the samples were removed after two months of exposure for examination, it was observed in passing that the underside of the sample was remarkably lacking in the substance found on top. A photograph of this comparison is missing, but below in Figure 57 it is possible to see the samples after they had been moved to the laboratory, where the absence of a complete slimy biofilm is noticeable. From our previous work on pitting in the same river water, a biofilm was found to have grown on the side surfaces of the sample, which may suggest that some fraction of the covering layer on top of these samples is comprised not of a biofilm but rather of sand or clay. Rinsing the samples in the laboratory after extraction seems to support this, as when comparing with the previously grown biofilm, there seemed to be little to no organic matter and no uneven thickness change in the sample surface. The sample without the crevice former had no indication of corrosion even beneath the particles covering the surface, which does indicate that the biofilm was either thin, less ennobling than expected or simply did not reach a high enough potential to initiate corrosion. This stands parallel to the fact that since the crevice-covered sample did in fact initiate, the pitting sample should not be far behind. As the decision has been made to allow the remaining samples to stay exposed for the foreseeable future, the results on this issue are yet to come.

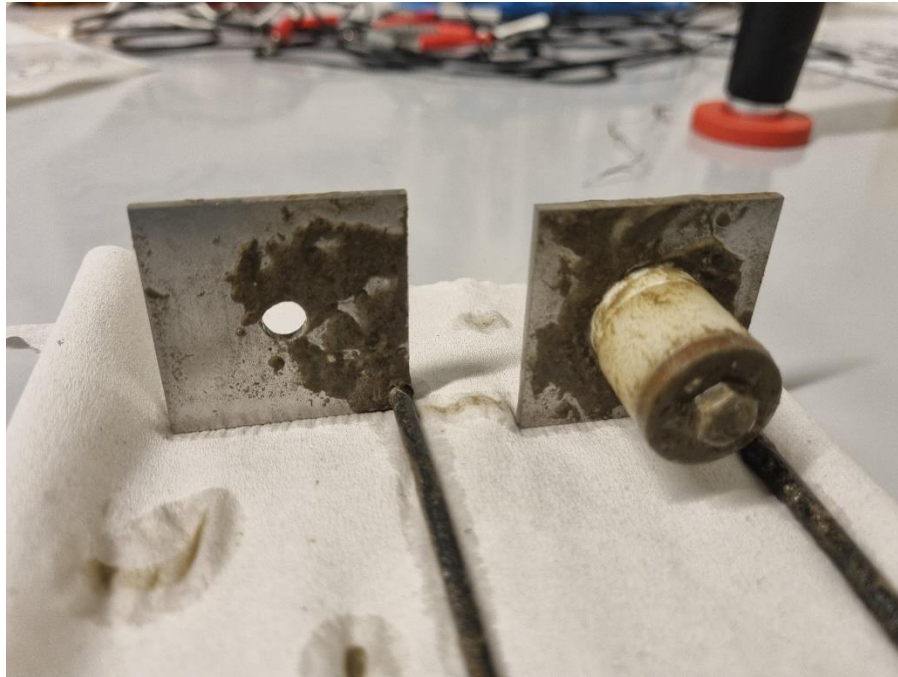


Figure 57: The surface of the freely exposed sample and sample with an artificial crevice taken from the field experiment location, seen from the top of the sample. Samples were not rinsed before the picture was taken.

The surface roughness of the samples we have used is likely not comparable to that of the industrially produced structures that have been examined prior to the project work. A point of interest is therefore to see whether the biofilms that are produced on the likely more mechanically rough surfaces of the power plant components can be correlated with the data we have found from the literature. Bacterial adhesion kinetics in experiments produced in the laboratory may not match real world examples, which is dependent on the surface finish grade, as discussed in the theory.

When performing the potentiodynamic scans on the different alloys, it was prudent to examine the evolution of the OCP as the sample adapted to the electrolyte. On many occasions the preparations were more time-consuming than expected, and when this happened, the sample was allowed to remain in the electrolyte, then when the experiment started the OCP was often observed to have essentially stabilized in the meantime. On alloy 1.4470, however, this was not the case. It was left to stabilize for over half an hour before starting the program on the potentiostat, and when run, the alloy's potential kept increasing. Even after over an hour at OCP, the potential was still climbing by the end of the OCP sampling period. After two unsuccessful runs at lower currents, a set of probing experiments was conducted with a maximum current density of 1 mA/cm^2 , the result of which can be seen in the results section in Figure 32. Following internal discussion, it is still unclear what

causes this behavior, as the general shape of the curve produced seems to imply that the only effect happening is either oxygen evolution or general passivity, but there is no visible transpassive region and corrosion products were still found on the surface of the sample after testing- yet no visible attacks could be found. Given that this behavior has been unique to this specific alloy, it could be that it is a manufacturing issue, seeing as other cast alloys of similar grade seem to have passive currents on an order of magnitude lower than this (80), but the supplier was contacted and no discrepancies in production methods when comparing to other cast products were noted. The other alloys used in this thesis have been rolled except for 1.4317, which is an alloy normally delivered in cast and heat-treated condition. Further examination of the general microstructure and composition of alloy 1.4470 is recommended as a way of probing these anomalous results. No parallel to this behavior could be found in the literature within the timeframe of receiving and applying the alloy during this thesis.

Section 6 Conclusions

In our project work, it was found that the alloy EN 1.4317 of which the components were made of suffered greatly at any chloride content during potentiodynamic experiments and showed neither crevice nor repassivation potentials throughout, indicating that the critical crevice and pitting corrosion potentials were more negative than the OCP in all our experiments. This behavior was reaffirmed in this thesis, during which the experiments were expanded upon with both active biofilm exposure in the field, low temperature open circuit experiments, in addition to simulated biofilm potential ennoblement under potentiostatic conditions. The alloy has initiated corrosion under every experiment, and all these data points combined have shown that the alloy is not resistant to crevice corrosion at any chloride concentration, suffers from crevice corrosion at potable levels, and is susceptible to corrosion initiation from biofilm ennoblement under otherwise remarkably lenient conditions of low temperature and very low chloride contents. The effect of flow as a prevention of adhesion of any biofilm was also discussed, with the conclusion that it was unlikely to provide adequate protection as continuous production is unrealistic, and the alloy cannot withstand biofilm formation that is sure to develop in the case of stagnant water. The alloy is therefore expected to be unfit for use in conditions where a biofilm can develop, and power station facilities are no exception to this.

Experiments were also designed to explore the corrosion resistance of alloys 904L, 22Cr, and 25Cr for comparison. Both duplex alloys, 22Cr and 25Cr, showed high resistance to crevice corrosion, never initiating even under the most aggressive conditions, only succumbing to transpassive dissolution at the absolute highest potentials. The 904L samples did corrode, but this corrosion was initiated at very high potentials as per our definition and as such none of these alloys are expected to corrode under the given conditions of the original problem.

The alloy 1.4470 that was delivered and proposed to substitute the 1.4317 alloy for Statkraft was received late in the process of this thesis. During the preliminary experiments that were done to categorize the attributes of the alloy, it exhibited unusual behavior through very high passive currents, near an order of magnitude higher than was expected of an alloy of this grade. The few experiments that were done to explore the limitations of this alloy were inconclusive, showing more corrosion products on the surface than both the 22Cr and 25Cr samples, yet no clear attacks were found. It may be recommended that a more thorough examination is done of the alloy with OCP measurements in different chloride concentrations,

potentiodynamic experiments with a larger range of parameters including chloride content, temperature and as well as flowing or non-flowing conditions, but this is subject to the wishes of the one taking ownership of the field setup and alloy after the thesis has been finished.

Section 7 Further Work

From examining the alloy 1.4470 provided by Statkraft for this thesis, it is recommended that further analysis be done to fully map its properties. It seems likely through the limited experiments run that the alloy does not actively break down and corrode in waters of higher chloride contents, but it does exhibit a passive current density above that which was considered normal for a steel of this grade at the onset of this thesis. The testing parameters of our modification of the ASTM G61 standard are also deemed insufficient to map the full properties of the alloy due to the test ending prematurely when compared to the last, modified test. The test run at higher maximum potential showed an area of the polarization curve that may be the alloy's passive region, and therefore a new set of parameters fitting the alloy's higher passive current should be constructed for its analysis.

References

1. Keehan E, Karlsson L, Andrén HO. Influence of carbon, manganese and nickel on microstructure and properties of strong steel weld metals: Part 1 – Effect of nickel content. *Sci Technol Weld Join*. 2006 Feb 1;11(1):1–8.
2. Li Z, Raabe D. Strong and Ductile Non-equiatomic High-Entropy Alloys: Design, Processing, Microstructure, and Mechanical Properties. *JOM*. 2017 Nov 1;69(11):2099–106.
3. Callister WD, Rethwisch DG. *Materials Science and Engineering*. Wiley; 2014. 905 p.
4. Devine TM. The mechanism of sensitization of austenitic stainless steel. *Corros Sci*. 1990 Jan 1;30(2):135–51.
5. Sahlaoui H, Makhlouf K, Sidhom H, Philibert J. Effects of ageing conditions on the precipitates evolution, chromium depletion and intergranular corrosion susceptibility of AISI 316L: experimental and modeling results. *Mater Sci Eng A*. 2004 May 15;372(1):98–108.
6. Akgun OV, Inal OT. Desensitization of sensitized 304 stainless steel by laser surface melting. *J Mater Sci*. 1992 Apr 1;27(8):2147–53.
7. Bhadeshia H, Honeycombe R. *Steels: Microstructure and Properties*. Butterworth-Heinemann; 2017. 490 p.
8. Ghosh A. Segregation in cast products. *Sadhana*. 2001 Feb 1;26(1):5–24.
9. do Nascimento AM, Ierardi MCF, Kina AY, Tavares SSM. Pitting corrosion resistance of cast duplex stainless steels in 3.5%NaCl solution. *Mater Charact*. 2008 Dec 1;59(12):1736–40.
10. du Toit M, Steyn HG. Comparing the Formability of AISI 304 and AISI 202 Stainless Steels. *J Mater Eng Perform*. 2012 Jul 1;21(7):1491–5.
11. Wang Z, Paschalidou EM, Seyeux A, Zanna S, Maurice V, Marcus P. Mechanisms of Cr and Mo Enrichments in the Passive Oxide Film on 316L Austenitic Stainless Steel. *Front Mater* [Internet]. 2019 [cited 2023 Jun 1];6. Available from: <https://www.frontiersin.org/articles/10.3389/fmats.2019.00232>
12. Yaniv AE, Lumsden JB, Staehle RW. The Composition of Passive Films on Ferritic Stainless Steels. *J Electrochem Soc*. 1977 Apr 1;124(4):490.
13. Hakiki NE, Belo MDC. Electronic Structure of Passive Films Formed on Molybdenum-Containing Ferritic Stainless Steels. *J Electrochem Soc*. 1996 Oct 1;143(10):3088.
14. Olsson COA, Landolt D. Passive films on stainless steels—chemistry, structure and growth. *Electrochimica Acta*. 2003 Apr 20;48(9):1093–104.
15. Olefjord I, Elfstrom BO. The Composition of the Surface during Passivation of Stainless Steels. *Corrosion*. 1982 Jan 1;38(1):46–52.

16. Wang L, Seyeux A, Marcus P. Thermal stability of the passive film formed on 316L stainless steel surface studied by ToF-SIMS. *Corros Sci*. 2020 Apr 1;165:108395.
17. Abreu CM, Cristóbal MJ, Losada R, Nóvoa XR, Pena G, Pérez MC. The effect of Ni in the electrochemical properties of oxide layers grown on stainless steels. *Electrochimica Acta*. 2006 Apr 1;51(15):2991–3000.
18. Maurice V, Yang WP, Marcus P. X-Ray Photoelectron Spectroscopy and Scanning Tunneling Microscopy Study of Passive Films Formed on (100) Fe-18Cr-13Ni Single-Crystal Surfaces. *J Electrochem Soc*. 1998 Mar 1;145(3):909.
19. Francis R, Byrne G. Duplex Stainless Steels—Alloys for the 21st Century. *Metals*. 2021 May;11(5):836.
20. Martins M, Casteletti LC. Microstructural characteristics and corrosion behavior of a super duplex stainless steel casting. *Mater Charact*. 2009 Feb 1;60(2):150–5.
21. Sieurin H, Sandström R. Sigma phase precipitation in duplex stainless steel 2205. *Mater Sci Eng A*. 2007 Jan 25;444(1):271–6.
22. ISO. Quality requirements for fusion welding of metallic materials — Part 2: Comprehensive quality requirements (ISO 3834-2:2021) [Internet]. International Organization for Standardization; 2021 [cited 2023 Oct 6]. Available from: <https://www.iso.org/obp/ui/fr/#iso:std:iso:3834:-2:ed-3:v1:en>
23. Sánchez-Cabrera VM, Rubio-González C, Ruíz-Vela JI, Ramírez-Baltazar C. Effect of preheating temperature and filler metal type on the microstructure, fracture toughness and fatigue crack growth of stainless steel welded joints. *Mater Sci Eng A*. 2007 Apr 15;452–453:235–43.
24. Nasir NSM, Razab, Mohammad Khairul Azhar Abdul, Mamat, Sarizam, Ahmad, Muhammad Iqbal. REVIEW ON WELDING RESIDUAL STRESS. *SSN*. 2016;11(9).
25. Kiefer JH. Effects of Moisture Contamination and Welding Parameters on Diffusible Hydrogen. 1996;
26. Zhang Z, Wang Z, Jiang Y, Tan H, Han D, Guo Y, et al. Effect of post-weld heat treatment on microstructure evolution and pitting corrosion behavior of UNS S31803 duplex stainless steel welds. *Corros Sci*. 2012 Sep 1;62:42–50.
27. Sundqvist J, Manninen T, Heikkinen HP, Anttila S, Kaplan AFH. Laser surface hardening of 11% Cr ferritic stainless steel and its sensitisation behaviour. *Surf Coat Technol*. 2018 Jun 25;344:673–9.
28. Leif. Welding Duplex Stainless Steels — A Review Of Current Recommendations. *Weld World*. 2012 May 1;56(5):65–76.
29. 茂樹東, 英昭幸, 順一郎村山, 趙夫工藤. ステンレス鋼の耐食性に及ぼす溶接スケールの影響. *防食技術*. 1990;39(11):603–9.

30. Reddy GM, Rao KS, Sekhar T. Microstructure and pitting corrosion of similar and dissimilar stainless steel welds. *Sci Technol Weld Join*. 2008 May 1;13(4):363–77.
31. Zhang Z, Zhao H, Zhang H, Hu J, Jin J. Microstructure evolution and pitting corrosion behavior of UNS S32750 super duplex stainless steel welds after short-time heat treatment. *Corros Sci*. 2017 Jun 1;121:22–31.
32. Xiao K, Li Z, Song J, Bai Z, Xue W, Wu J, et al. Effect of Concentrations of Fe^{2+} and Fe^{3+} on the Corrosion Behavior of Carbon Steel in Cl^- and SO_4^{2-} Aqueous Environments. *Met Mater Int*. 2020 Feb 11;27.
33. Stewart J, Williams DE. The initiation of pitting corrosion on austenitic stainless steel: on the role and importance of sulphide inclusions. *Corros Sci*. 1992 Mar 1;33(3):457–74.
34. Wang MF, Li XG, Du N, Huang YZ, Korsunsky A. Direct evidence of initial pitting corrosion. *Electrochem Commun*. 2008 Jul 1;10(7):1000–4.
35. Leckie HP, Uhlig HH. Environmental Factors Affecting the Critical Potential for Pitting in 18–8 Stainless Steel. *J Electrochem Soc*. 1966 Dec 1;113(12):1262.
36. Burstein GT, Pistorius PC, Mattin SP. The nucleation and growth of corrosion pits on stainless steel. *Corros Sci*. 1993 Jan 1;35(1):57–62.
37. Hong T, Nagumo M. The effect of chloride concentration on early stages of pitting for type 304 stainless steel revealed by the AC impedance method. *Corros Sci*. 1997 Feb 1;39(2):285–93.
38. Xu L, Wu P, Zhu X, Zhao G, Ren X, Wei Q, et al. Structural characteristics and chloride intrusion mechanism of passive film. *Corros Sci*. 2022 Oct 1;207:110563.
39. Oldham K, Myland J, Bond A. *Electrochemical Science and Technology: Fundamentals and Applications*. John Wiley & Sons; 2011. 435 p.
40. Szummer A, Janik-Czachor M. Corrosion behaviour of low-manganese stainless steels. *Corros Sci*. 1993 Jan 1;35(1):317–27.
41. Zhang B, Wei XX, Wu B, Wang J, Shao XH, Yang LX, et al. Chloride attack on the passive film of duplex alloy. *Corros Sci*. 2019 Jul 1;154:123–8.
42. Laycock NJ, Stewart J, Newman RC. The initiation of crevice corrosion in stainless steels. *Corros Sci*. 1997 Oct 1;39(10):1791–809.
43. Hu Q, Zhang G, Qiu Y, Guo X. The crevice corrosion behaviour of stainless steel in sodium chloride solution. *Corros Sci*. 2011 Dec 1;53(12):4065–72.
44. Kennell GF, Evitts RW, Heppner KL. A critical crevice solution and IR drop crevice corrosion model. *Corros Sci*. 2008 Jun 1;50(6):1716–25.
45. Shojaei E, Mirjalili M, Moayed MH. The influence of the crevice induced IR drop on polarization measurement of localized corrosion behavior of 316L stainless steel. *Corros Sci*. 2019 Aug 1;156:96–105.

46. Dickinson WH, Lewandowski Z. Electrochemical concepts and techniques in the study of stainless steel ennoblement. *Biodegradation*. 1998 Jan 1;9(1):11–21.
47. Washizu N, Katada Y, Kodama T. Role of H₂O₂ in microbially influenced ennoblement of open circuit potentials for type 316L stainless steel in seawater. *Corros Sci*. 2004 May 1;46(5):1291–300.
48. Mathiesen T, Frantsen JE. Unusual Corrosion Failures Of Stainless Steel In Low Chloride Waters. In *OnePetro*; 2008 [cited 2023 May 31]. Available from: <https://onepetro.org/NACECORR/proceedings-abstract/CORR08/All-CORR08/118802>
49. Braughton KR, Lafond RL, Lewandowski Z. The influence of environmental factors on the rate and extent of stainless steel ennoblement mediated by manganese-oxidizing biofilms. *Biofouling*. 2001 Nov 1;17(3):241–51.
50. Suleiman MI, Ragault I, Newman RC. The pitting of stainless steel under a rust membrane at very low potentials. *Corros Sci*. 1994 Mar 1;36(3):479–86.
51. El Din AMS, El-Dahshan ME, El Din AMT. Bio-film formation on stainless steels Part 2. The role of seasonal changes, seawater composition and surface roughness. *Desalination*. 2003 May 10;154(3):267–76.
52. Compere C, Le Bozec N. Behaviour of stainless steel in natural seawater. In 1997 [cited 2023 May 31]. Available from: <https://archimer.ifremer.fr/doc/00089/19989/>
53. García S, Trueba A, Vega LM, Madariaga E. Impact of the surface roughness of AISI 316L stainless steel on biofilm adhesion in a seawater-cooled tubular heat exchanger-condenser. *Biofouling*. 2016 Nov 25;32(10):1185–93.
54. Characklis WG. Bioengineering report: Fouling biofilm development: A process analysis. *Biotechnol Bioeng*. 1981;23(9):1923–60.
55. Kwok WK, Picioreanu C, Ong SL, van Loosdrecht MCM, Ng WJ, Heijnen JJ. Influence of biomass production and detachment forces on biofilm structures in a biofilm airlift suspension reactor. *Biotechnol Bioeng*. 1998;58(4):400–7.
56. Melo LF, Vieira MJ. Physical stability and biological activity of biofilms under turbulent flow and low substrate concentration. *Bioprocess Eng*. 1999 Apr 1;20(4):363–8.
57. Hilbert LR, Carpen L, Møller P, Fontenay F, Mathiesen T. Unexpected corrosion of stainless steel in low chloride waters - microbial aspects.
58. Percival SL, Knapp JS, Wales DS, Edyvean RGJ. The effect of turbulent flow and surface roughness on biofilm formation in drinking water. *J Ind Microbiol Biotechnol*. 1999 Mar 1;22(3):152–9.
59. Little BJ, Lee JS, Ray RI. The influence of marine biofilms on corrosion: A concise review. *Electrochimica Acta*. 2008 Dec 1;54(1):2–7.
60. Scotto V, Cintio RD, Marcenaro G. The influence of marine aerobic microbial film on stainless steel corrosion behaviour. *Corros Sci*. 1985 Jan 1;25(3):185–94.

61. Ito K, Matsushashi R, Kato T, Miki O, Kihira H, Watanabe K, et al. Potential Ennoblement of Stainless Steel by Marine Biofilm and Microbial Consortia Analysis. In OnePetro; 2002 [cited 2023 May 31]. Available from: <https://onepetro.org/NACECORR/proceedings-abstract/CORR02/All-CORR02/114881>
62. Dickinson WH, Caccavo F, Lewandowski Z. The ennoblement of stainless steel by manganic oxide biofouling. *Corros Sci*. 1996 Aug 1;38(8):1407–22.
63. Liao J, Fukui H, Urakami T, Morisaki H. Effect of biofilm on ennoblement and localized corrosion of stainless steel in fresh dam-water. *Corros Sci*. 2010 Apr 1;52(4):1393–403.
64. Castle JE, Ke R. Studies by auger spectroscopy of pit initiation at the site of inclusions in stainless steel. *Corros Sci*. 1990 Jan 1;30(4):409–28.
65. Williams DE, Mohiuddin TF, Zhu YY. Elucidation of a Trigger Mechanism for Pitting Corrosion of Stainless Steels Using Submicron Resolution Scanning Electrochemical and Photoelectrochemical Microscopy. *J Electrochem Soc*. 1998 Aug 1;145(8):2664.
66. Brenna A, Ormellese M, Lazzari L. Probabilistic model based on Markov chain for the assessment of localized corrosion of stainless steels. In 2013.
67. Esmailzadeh S, Aliofkhazraei M, Sarlak H. Interpretation of Cyclic Potentiodynamic Polarization Test Results for Study of Corrosion Behavior of Metals: A Review. *Prot Met Phys Chem Surf*. 2018 Sep 1;54(5):976–89.
68. Maier B, Frankel GS. Pitting Corrosion of Bare Stainless Steel 304 under Chloride Solution Droplets. *J Electrochem Soc*. 2010 Aug 9;157(10):C302.
69. Cruz RPV, Nishikata A, Tsuru T. Pitting corrosion mechanism of stainless steels under wet-dry exposure in chloride-containing environments. *Corros Sci*. 1998 Jan 1;40(1):125–39.
70. ASTM G61-86(2018) Standard Test Method for Conducting Cyclic Potentiodynamic Polarization Measurements for Localized Corrosion Susceptibility of Iron-, Nickel-, or Cobalt-Based Alloys [Internet]. American Society for Testing and Materials; 2018 [cited 2023 Jun 12]. Available from: <https://www.astm.org/g0061-86r18.html>
71. Park JO, Matsch S, Böhni H. Effects of Temperature and Chloride Concentration on Pit Initiation and Early Pit Growth of Stainless Steel. *J Electrochem Soc*. 2001 Dec 28;149(2):B34.
72. Akpanyung KV, Loto RT. Pitting corrosion evaluation: a review. *J Phys Conf Ser*. 2019 Dec;1378(2):022088.
73. Dastgerdi AA, Brenna A, Ormellese M, Pedferri M, Bolzoni F. Experimental design to study the influence of temperature, pH, and chloride concentration on the pitting and crevice corrosion of UNS S30403 stainless steel. *Corros Sci*. 2019 Oct 1;159:108160.
74. Xu Y, Pickering HW. The Initial Potential and Current Distributions of the Crevice Corrosion Process. *J Electrochem Soc*. 1993 Mar 1;140(3):658.

75. Moura VS, Lima LD, Pardal JM, Kina AY, Corte RRA, Tavares SSM. Influence of microstructure on the corrosion resistance of the duplex stainless steel UNS S31803. *Mater Charact.* 2008 Aug 1;59(8):1127–32.
76. Peguet L. Localized corrosion resistance of duplex stainless steels: Methodology and properties; A review paper. *Rev Métallurgie.* 2011 Jan 1;108:231–43.
77. Dickinson WH, Lewandowski Z, Geer RD. Evidence for Surface Changes During Ennoblement of Type 316L Stainless Steel: Dissolved Oxidant and Capacitance Measurements. *CORROSION.* 1996 Dec;52(12):910–20.
78. Varjonen O, Hakkarainen T, Nurmaiho-Lassila EL, Salkinoja-Salonen M. The brackish water biofilm on stainless steels: an electrochemical and morphological study. In: *Microbial Corrosion - 1.* Springer Science & Business Media; 1988. p. 164–78.
79. Jung KH, Kim SJ. An Investigation on Application of Experimental Design and Linear Regression Technique to Predict Pitting Potential of Stainless Steel. *Corros Sci Technol.* 2021;20(2):52–61.
80. Wang Y, Li D, Sun L, Li N, Liu M, Shen W, et al. Pitting corrosion of thermally aged cast duplex stainless steel for primary coolant pipes of nuclear power plants. *Corros Eng Sci Technol.* 2017 Aug 18;52(6):447–52.
81. Tekin A, Martin JW, Senior BA. Grain boundary sensitization and desensitization during the ageing of 316L(N) austenitic stainless steels. *J Mater Sci.* 1991 May 1;26(9):2458–66.
82. What is the Heat Affected Zone (HAZ)? - TWI [Internet]. [cited 2023 May 31]. Available from: <https://www.twi-global.com/technical-knowledge/faqs/what-is-the-heat-affected-zone>
83. Udall SL. UNITED STATES DEPARTMENT OF THE INTERIOR.
84. Pickering HW. The significance of the local electrode potential within pits, crevices and cracks. *Corros Sci.* 1989 Jan 1;29(2):325–41.

Appendix A Tables and Graphs

Table A - 1: PREN ranges for the alloys used during the project.

	1.4317	304L	316L	904L	22Cr	25Cr	1.4470
PREN	12 – 15,8	19,6 – 21,6	24,2 – 29,5	32,2 – 39,5	28,7 – 39,8	> 40	31,2 – 37,8

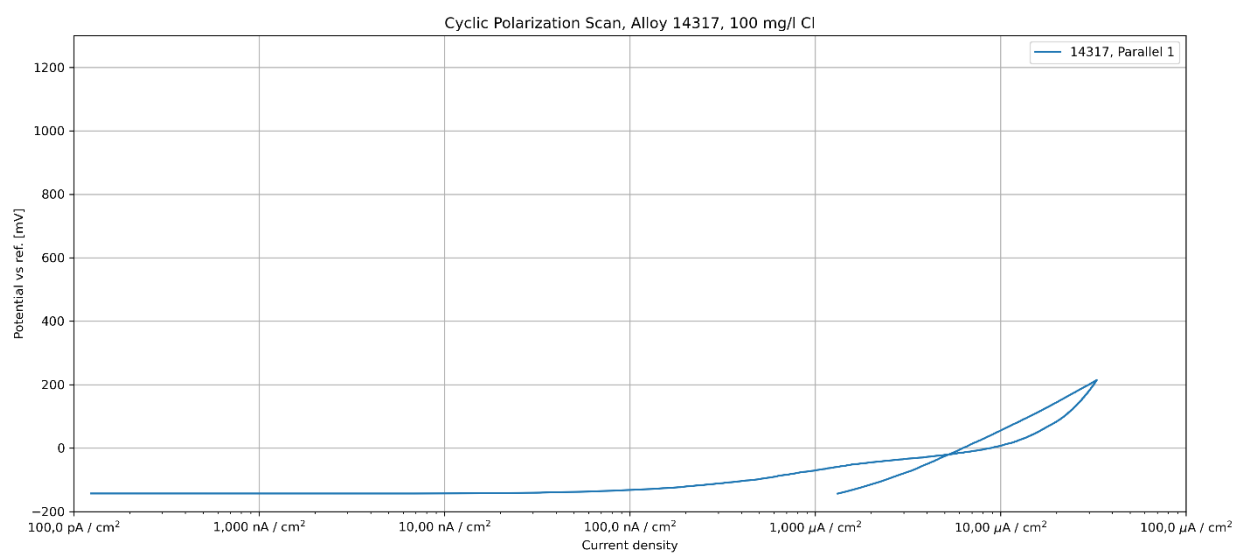


Figure A - 1: Cyclic polarization scan of alloy 1.4317, 100 mg/l chloride content, parallel 1.

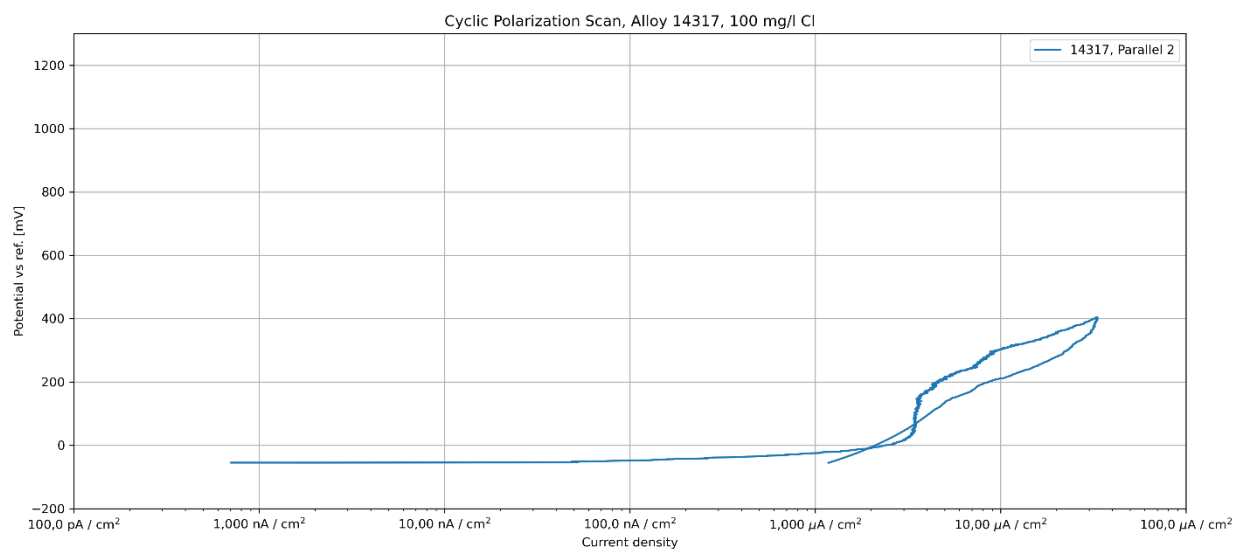


Figure A - 2: Cyclic polarization scan of alloy 1.4317, 100 mg/l chloride content, parallel 2.

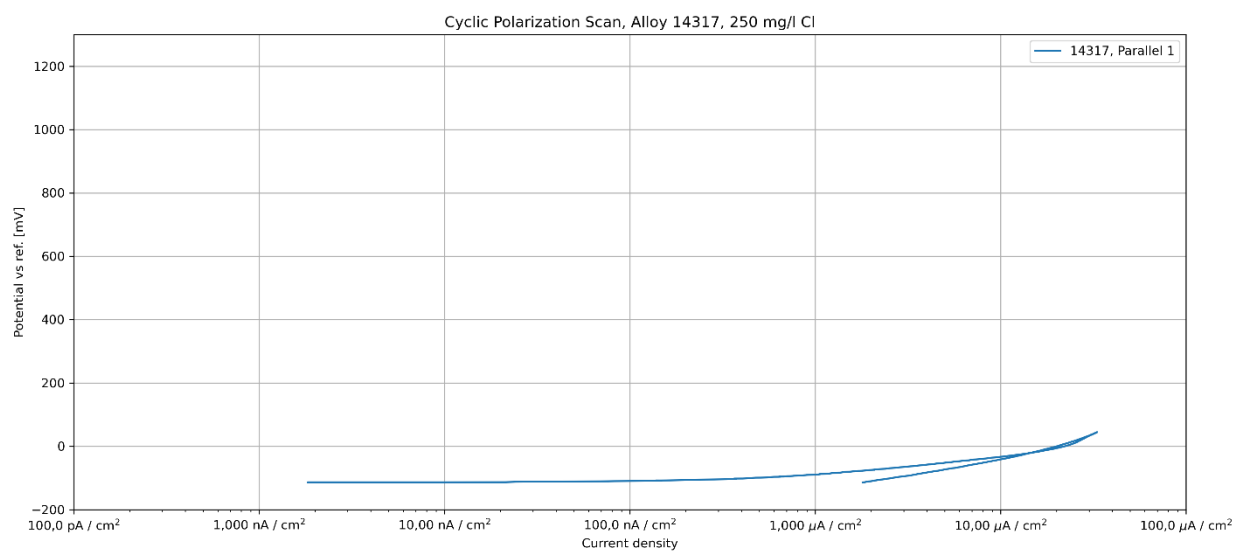


Figure A - 3: Cyclic polarization scan of alloy 1.4317, 250 mg/l chloride content, parallel 1.

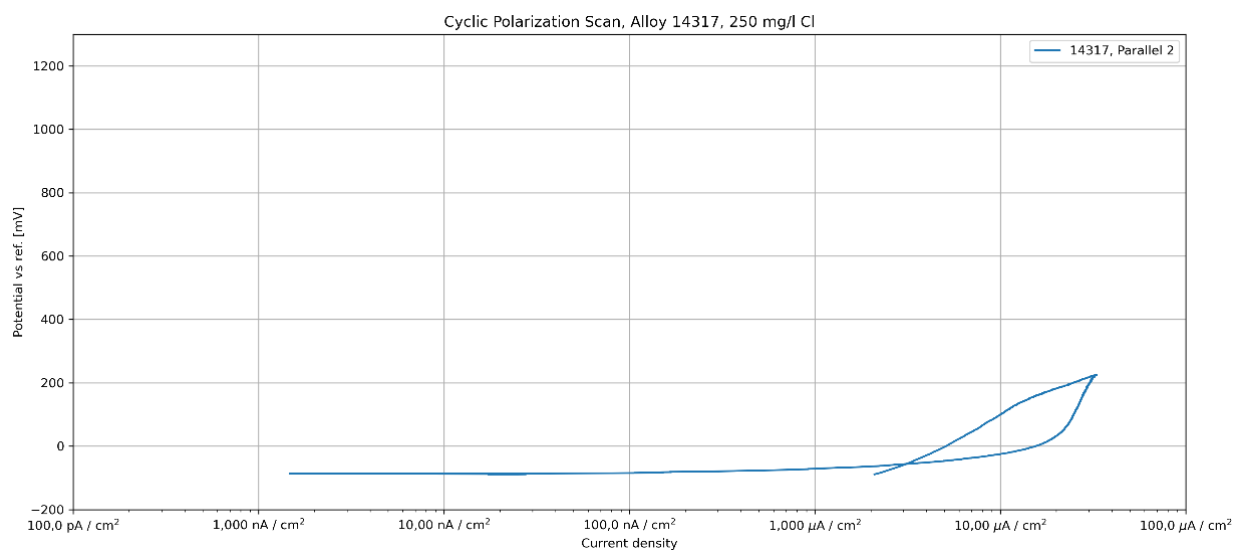


Figure A - 4: Cyclic polarization scan of alloy 1.4317, 250 mg/l chloride content, parallel 2.

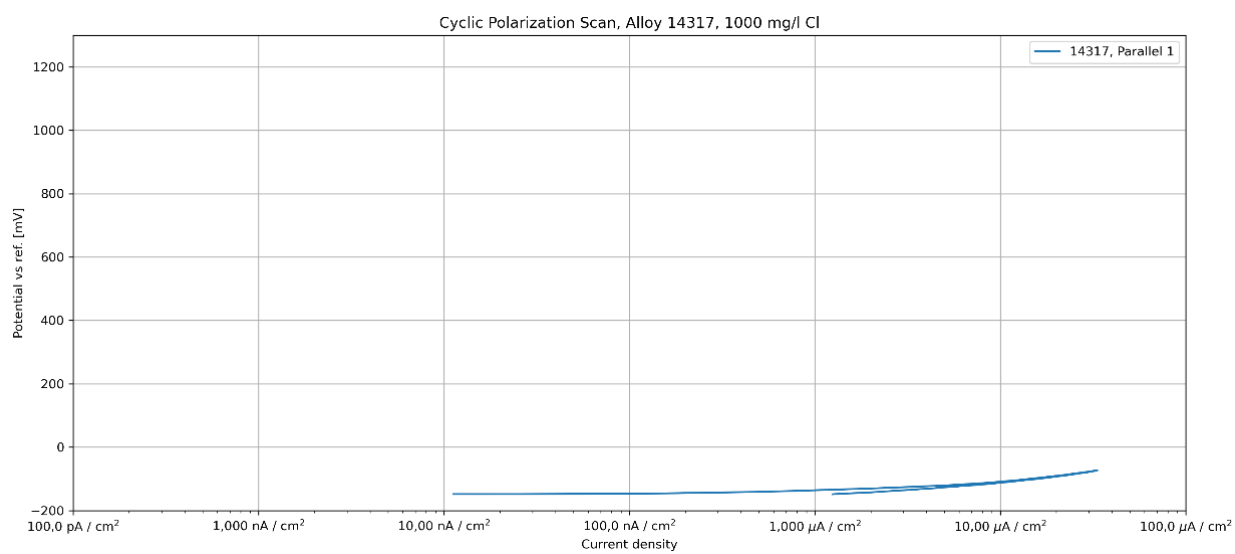


Figure A - 5: Cyclic polarization scan of alloy 1.4317, 1000 mg/l chloride content, parallel 1.

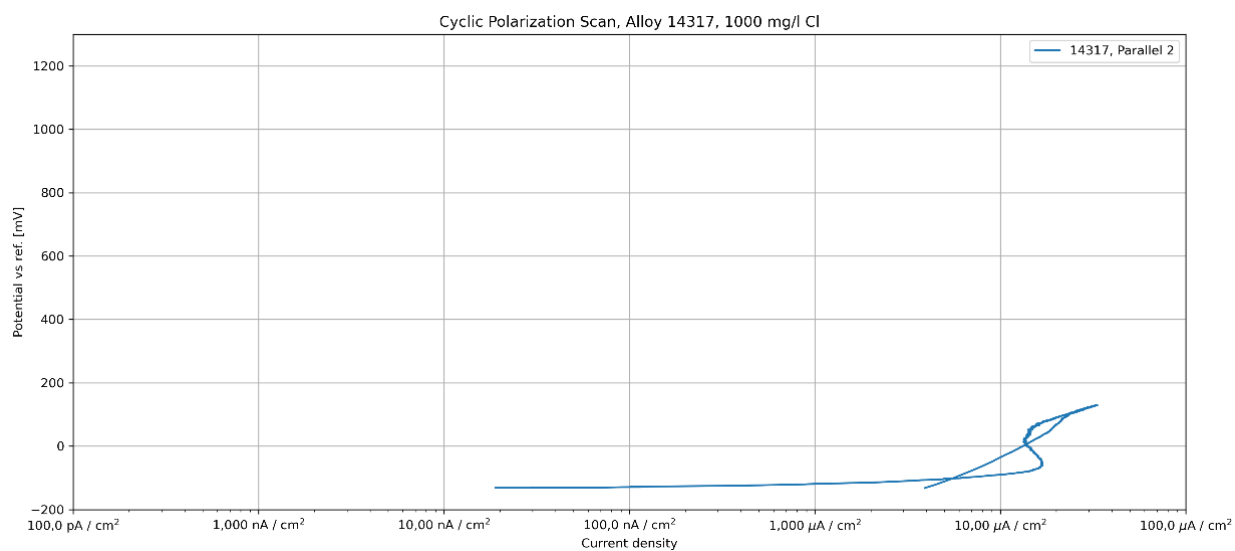


Figure A - 6: Cyclic polarization scan of alloy 1.4317, 1000 mg/l chloride content, parallel 2.

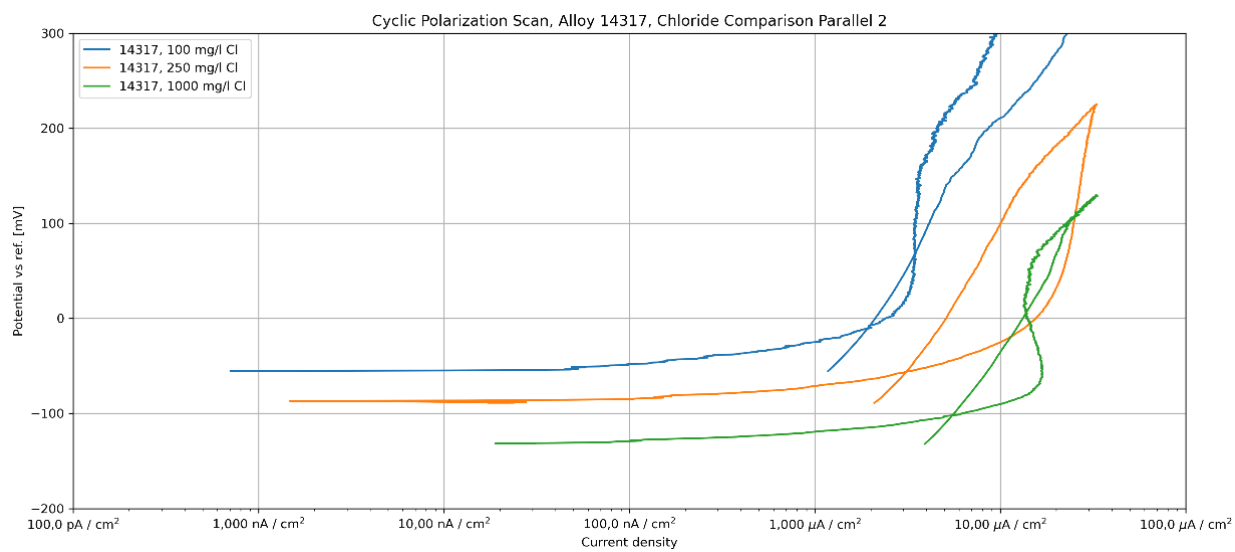


Figure A - 7: Cyclic polarization scan of alloy 1.4317 at various chloride concentrations, parallel 2.

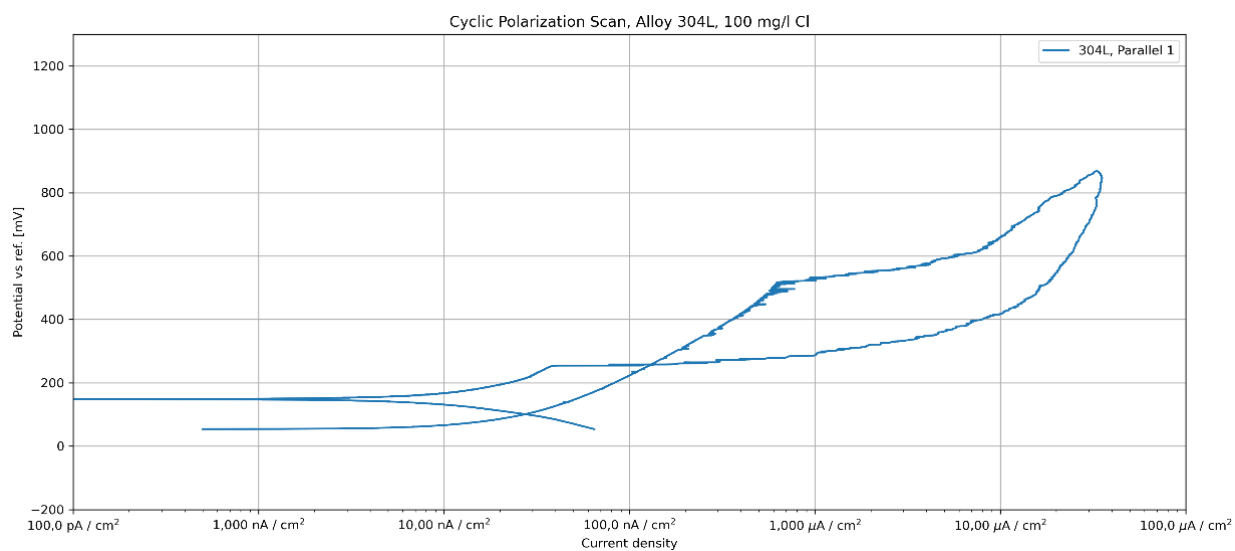


Figure A - 8: Cyclic polarization scan of alloy 304L, 100 mg/l chloride content, parallel 1.

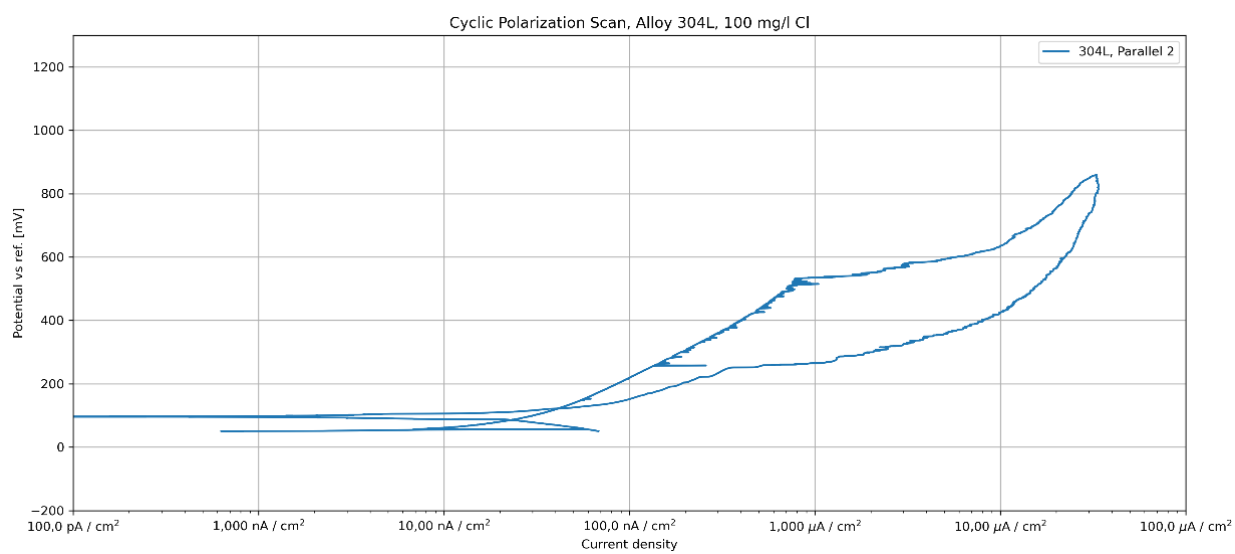


Figure A - 9: Cyclic polarization scan of alloy 304L, 100 mg/l chloride content, parallel 2.

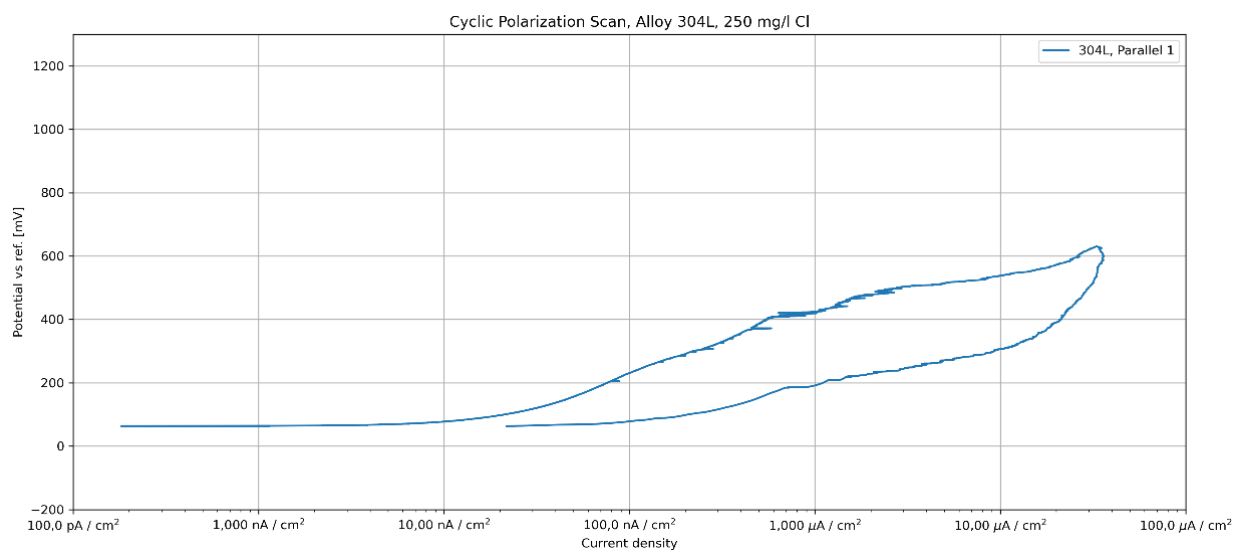


Figure A - 10: Cyclic polarization scan of alloy 304L, 250 mg/l chloride content, parallel 1.

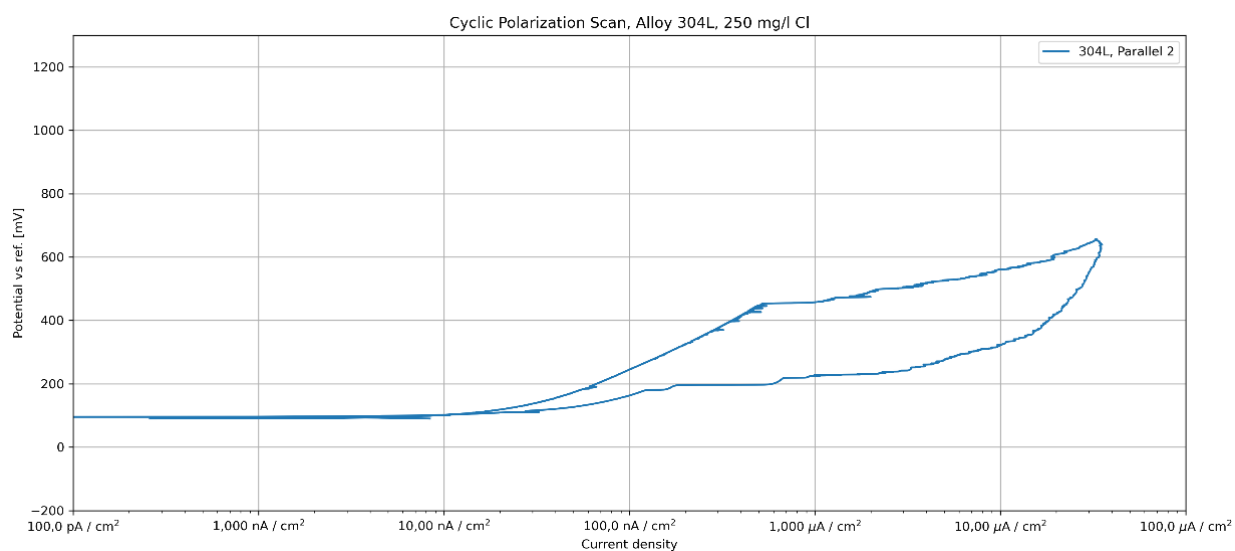


Figure A - 11: Cyclic polarization scan of alloy 304L, 250 mg/l chloride content, parallel 2

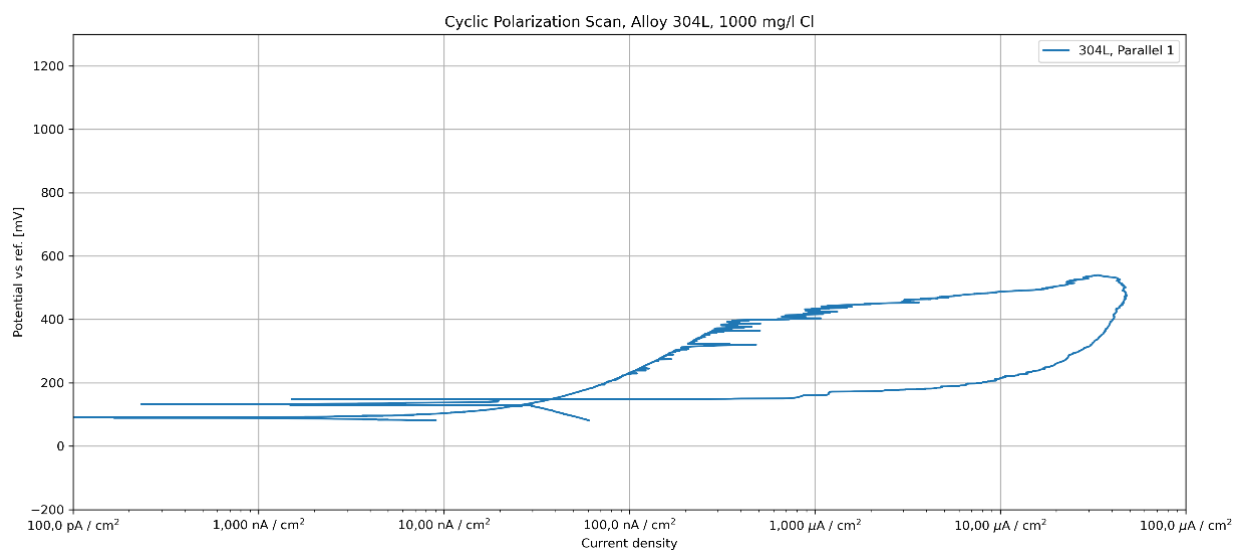


Figure A - 12: Cyclic polarization scan of alloy 304L, 1000 mg/l chloride content, parallel 1.

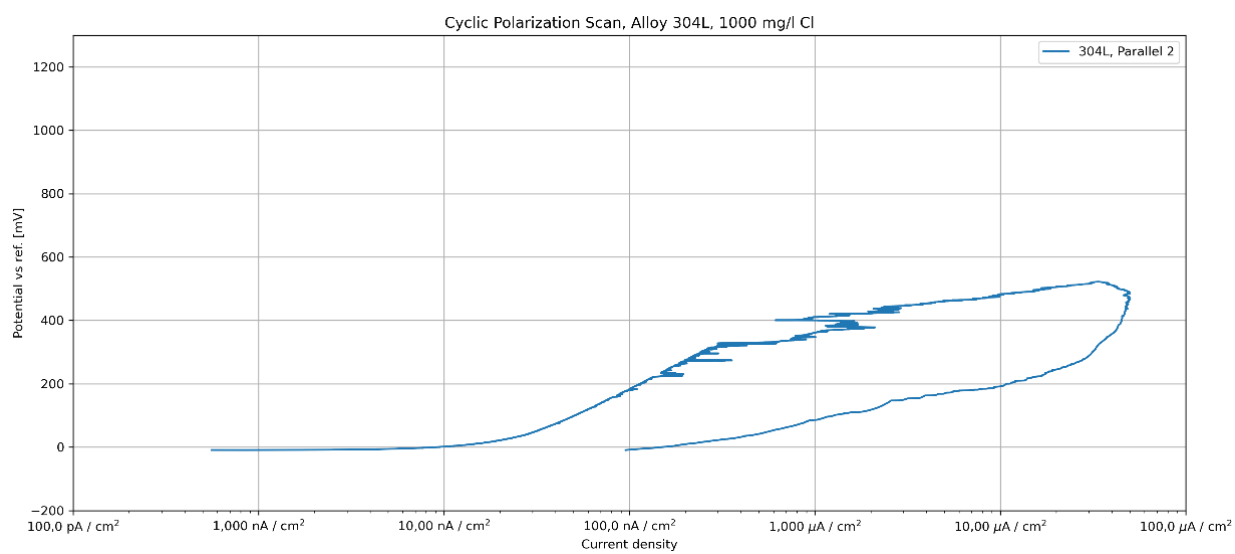


Figure A - 13: Cyclic polarization scan of alloy 304L, 1000 mg/l chloride content, parallel 2.

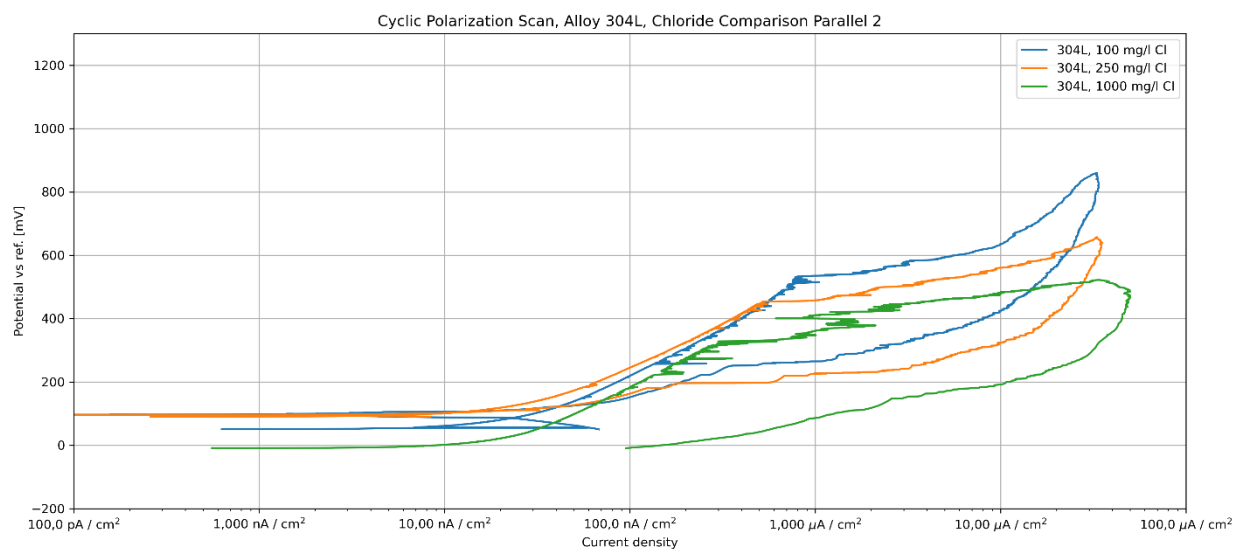


Figure A - 14: Cyclic polarization scan of alloy 304L at various chloride concentrations, parallel 2.

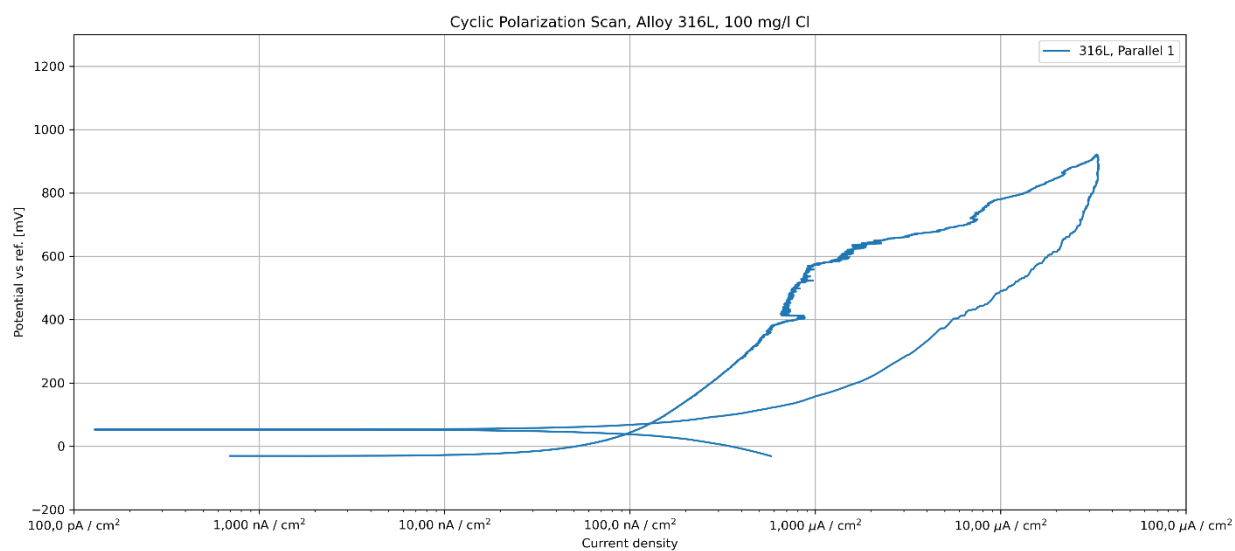


Figure A - 15: Cyclic polarization scan of alloy 316L, 100 mg/l chloride content, parallel 1.

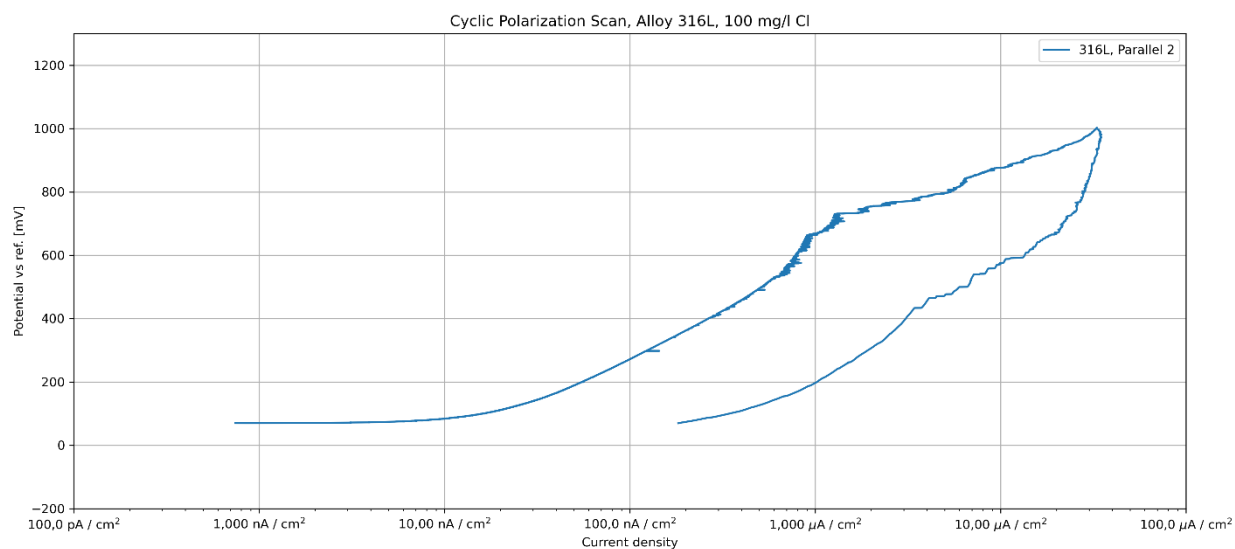


Figure A - 16: Cyclic polarization scan of alloy 316L, 100 mg/l chloride content, parallel 2.

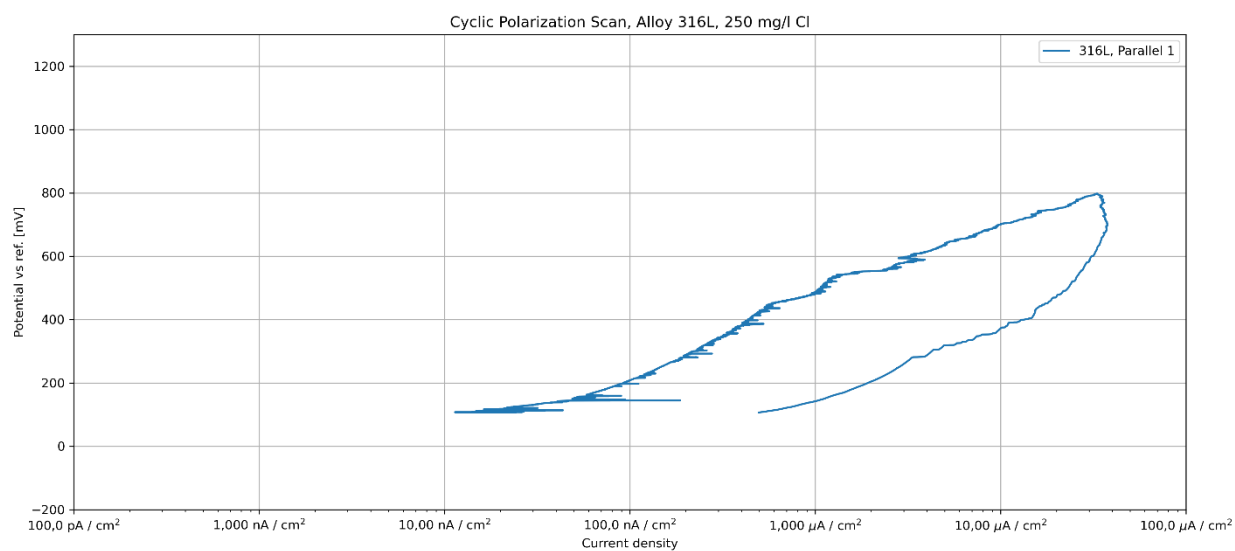


Figure A - 17: Cyclic polarization scan of alloy 316L, 250 mg/l chloride content, parallel 1.

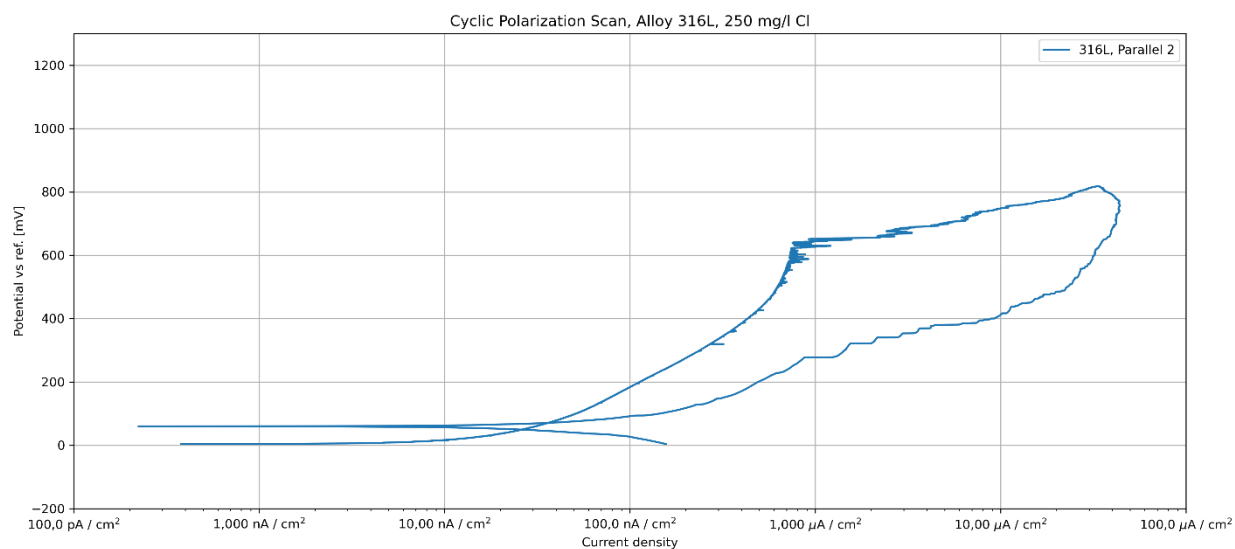


Figure A - 18: Cyclic polarization scan of alloy 316L, 250 mg/l chloride content, parallel 2.

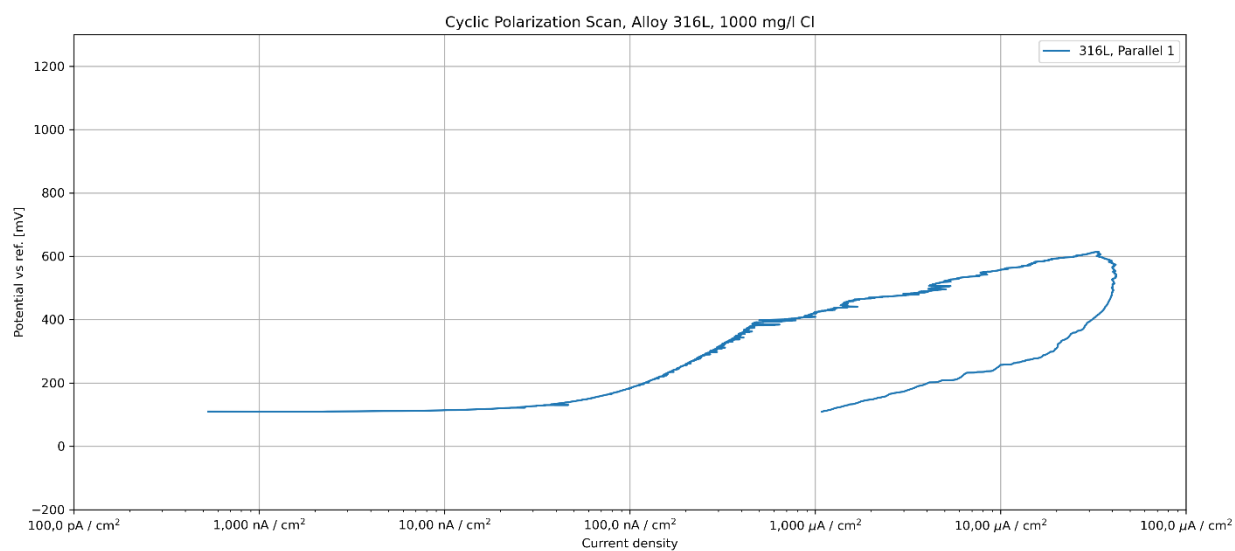


Figure A - 19: Cyclic polarization scan of alloy 316L, 1000 mg/l chloride content, parallel 1.

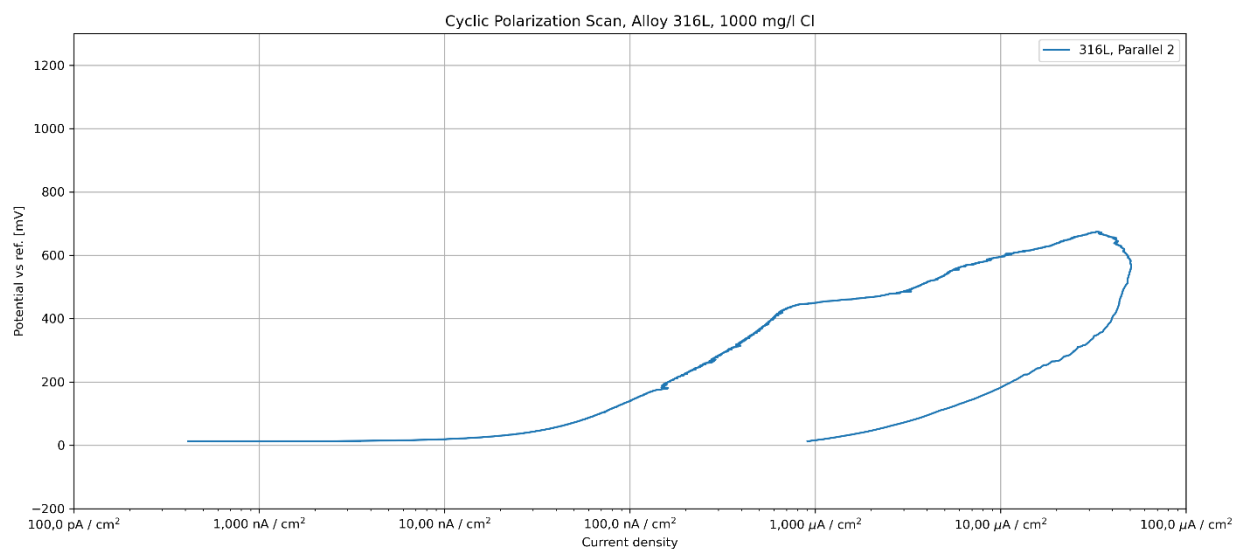


Figure A - 20: Cyclic polarization scan of alloy 316L, 1000 mg/l chloride content, parallel 2.

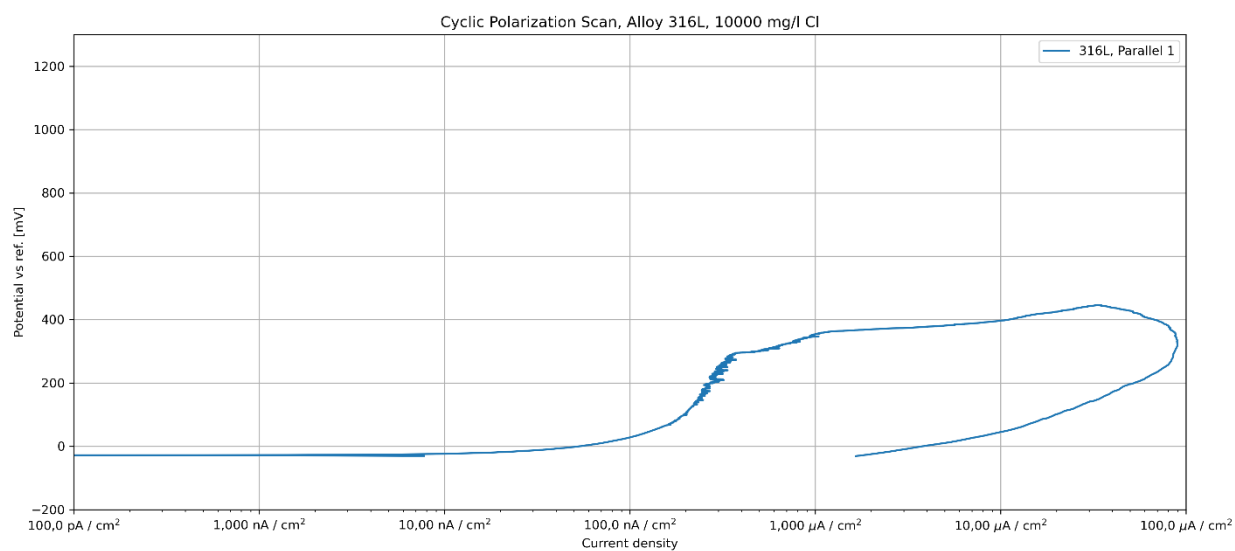


Figure A - 21: Cyclic polarization scan of alloy 316L, 10 000 mg/l chloride content, parallel 1.

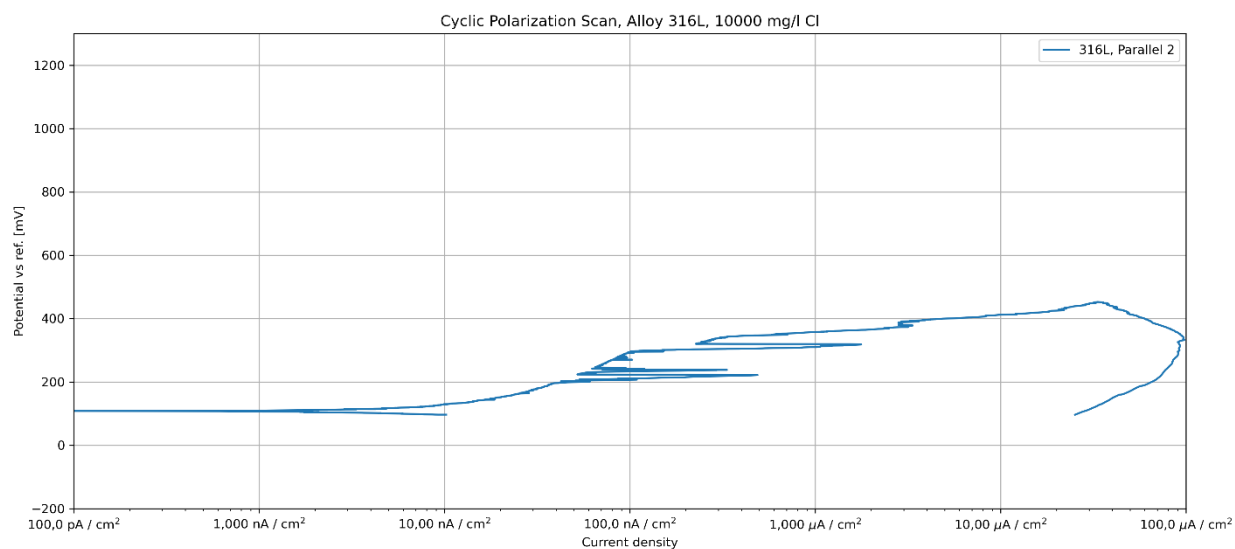


Figure A - 22: Cyclic polarization scan of alloy 316L, 10 000 mg/l chloride content, parallel 2.

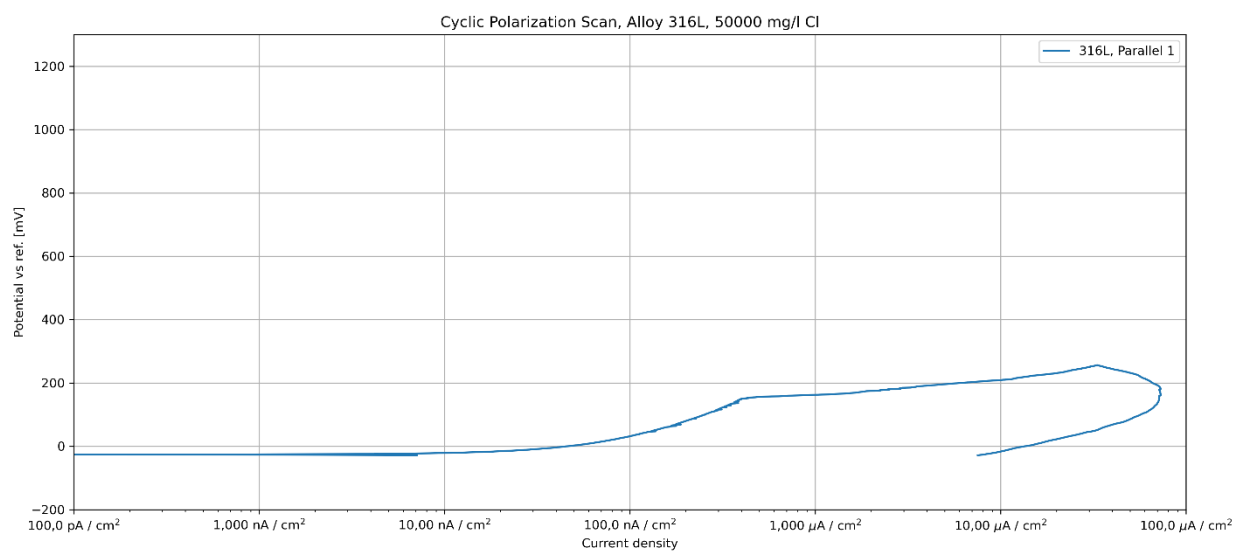


Figure A - 23: Cyclic polarization scan of alloy 316L, 50 000 mg/l chloride content, parallel 1.

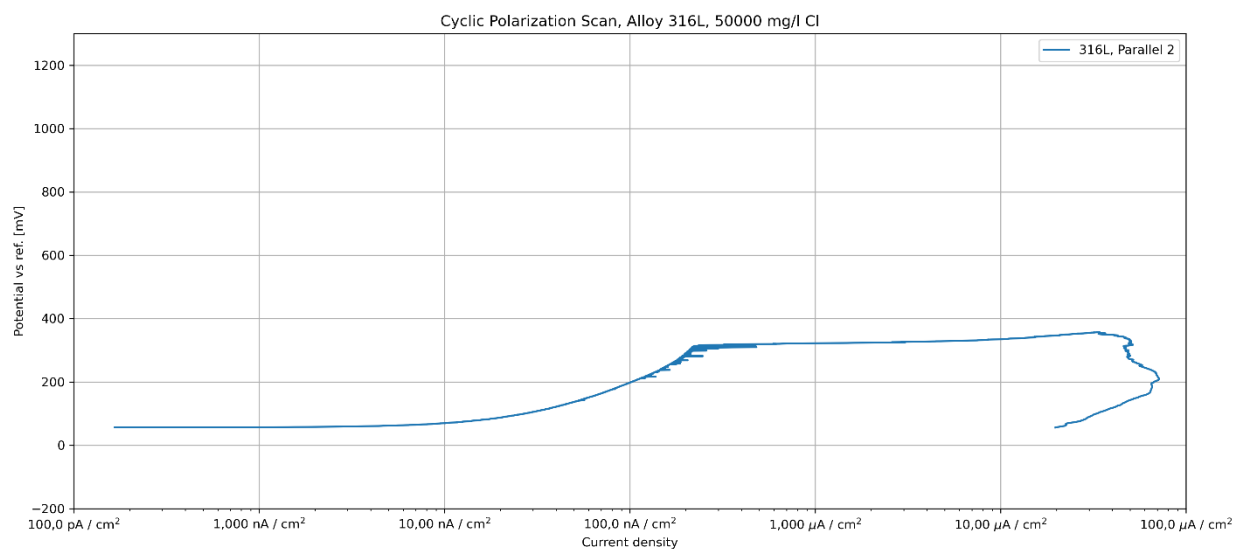


Figure A - 24: Cyclic polarization scan of alloy 316L, 50 000 mg/l chloride content, parallel 2.

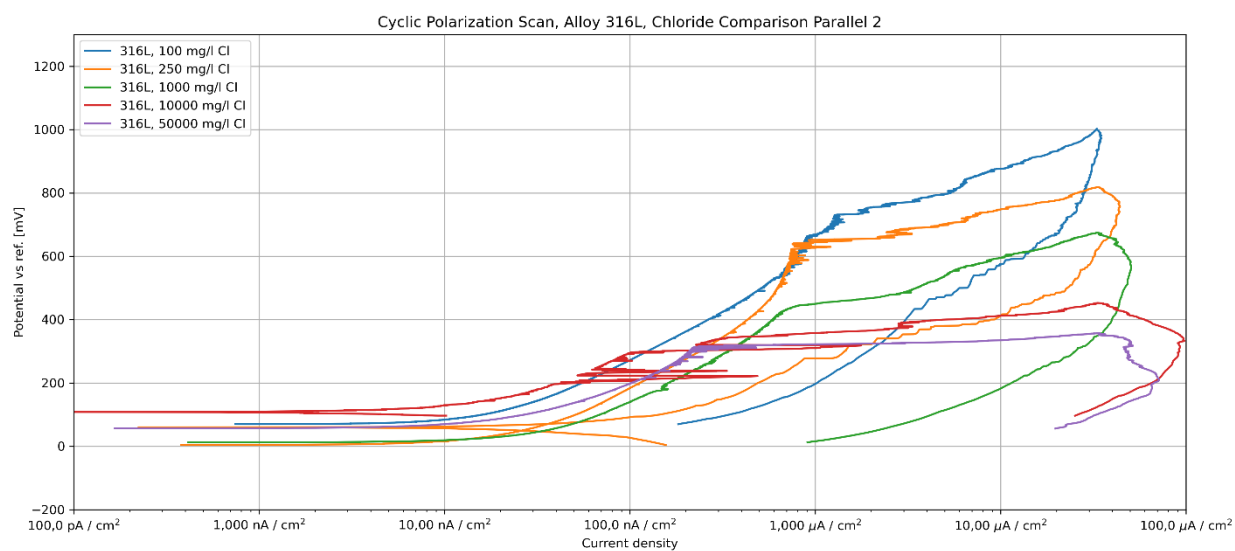


Figure A - 25: Cyclic polarization scan of alloy 316L at various chloride concentrations, parallel 2.

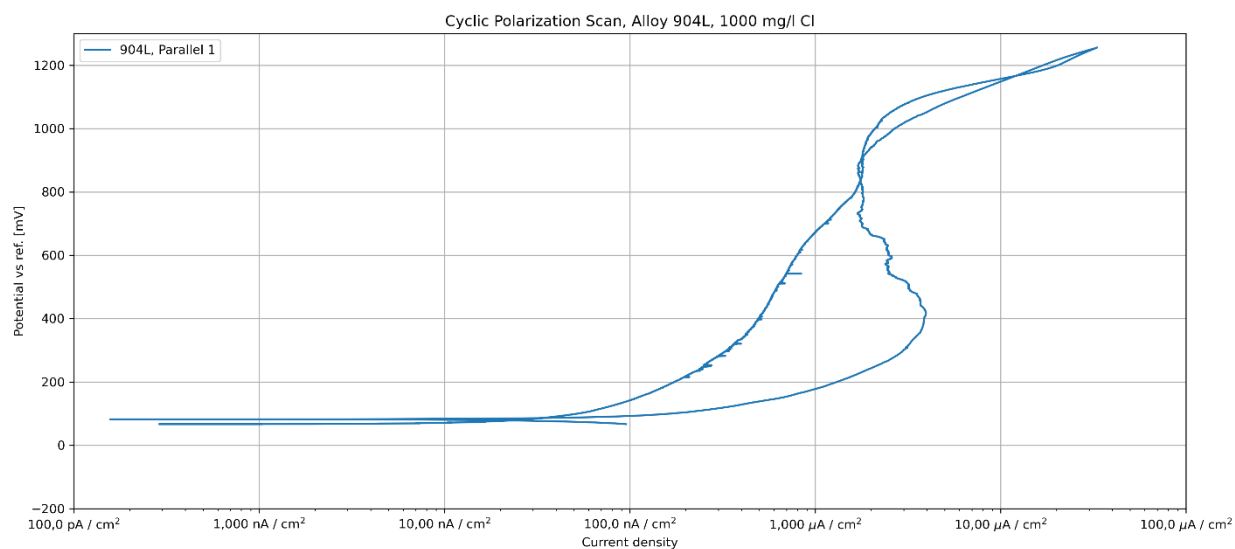


Figure A - 26: Cyclic polarization scan of alloy 904L, 1000 mg/l chloride content, parallel 1.

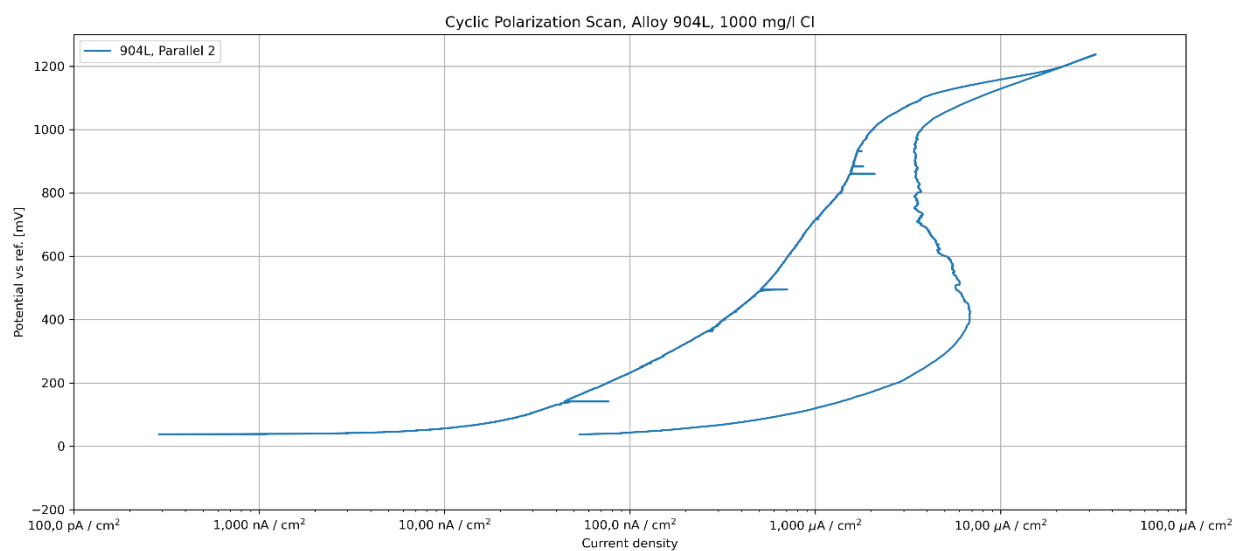


Figure A - 27: Cyclic polarization scan of alloy 904L, 1000 mg/l chloride content, parallel 2.

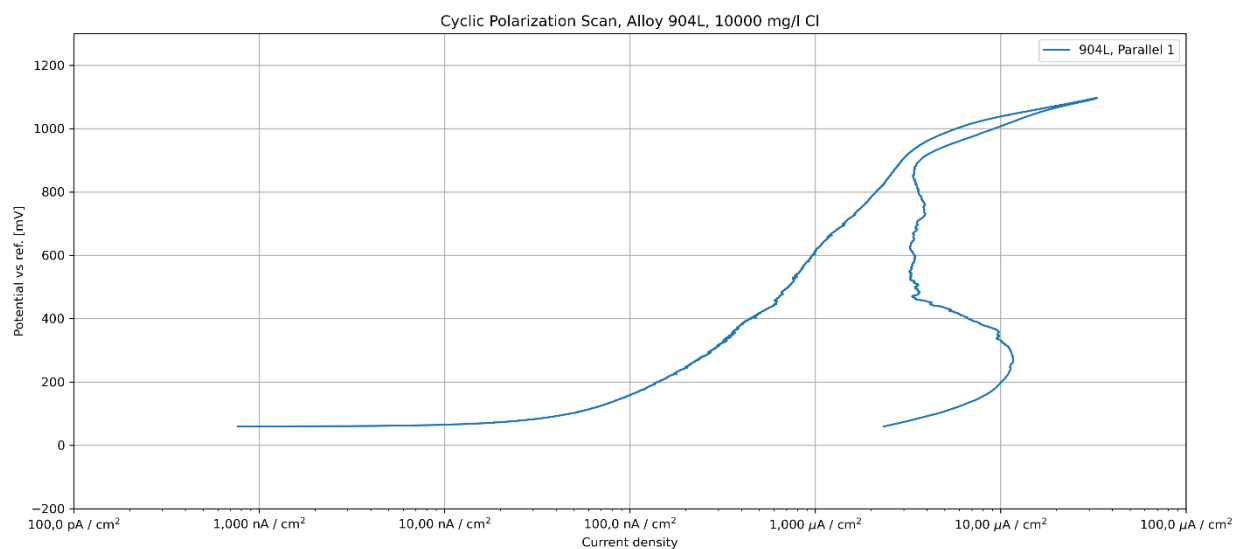


Figure A - 28: Cyclic polarization scan of alloy 904L, 10 000 mg/l chloride content, parallel 1.

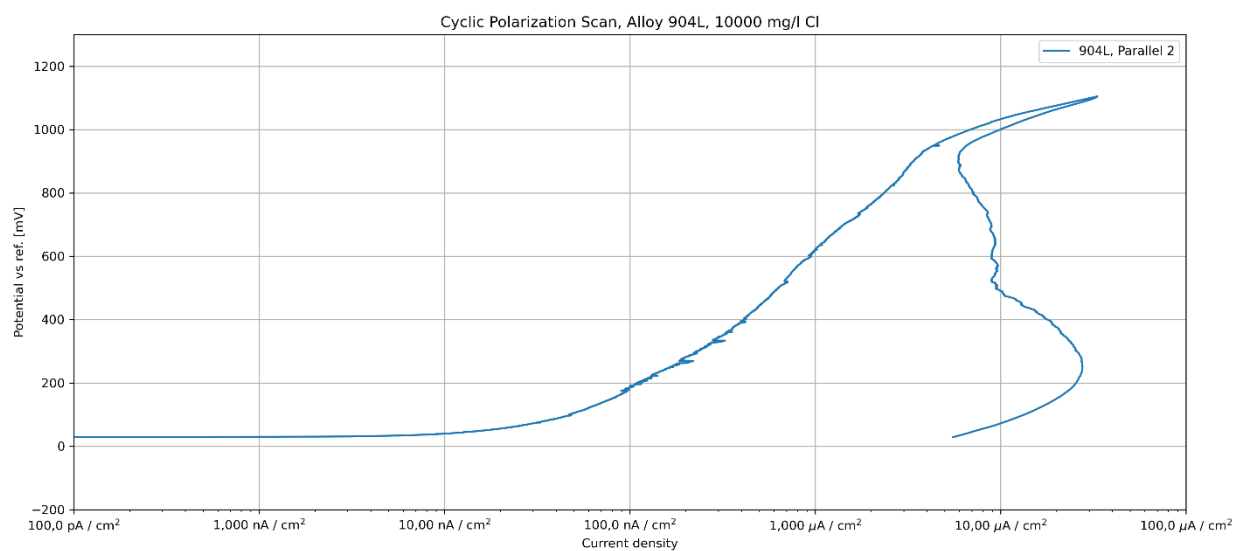


Figure A - 29: Cyclic polarization scan of alloy 904L, 10 000 mg/l chloride content, parallel 2.

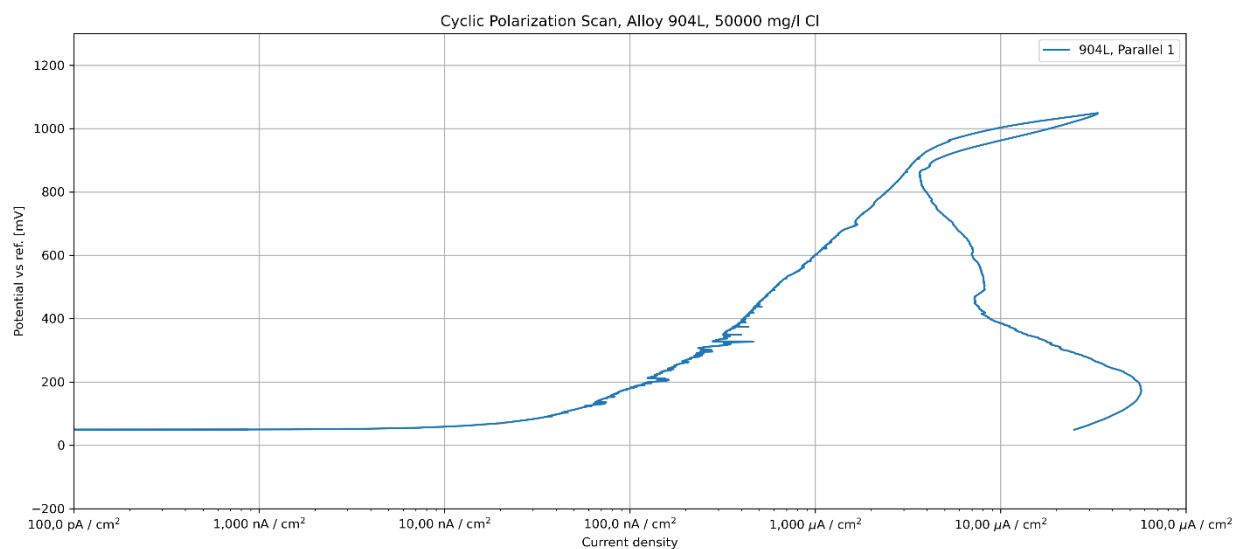


Figure A - 30: Cyclic polarization scan of alloy 904L, 50 000 mg/l chloride content, parallel 1.

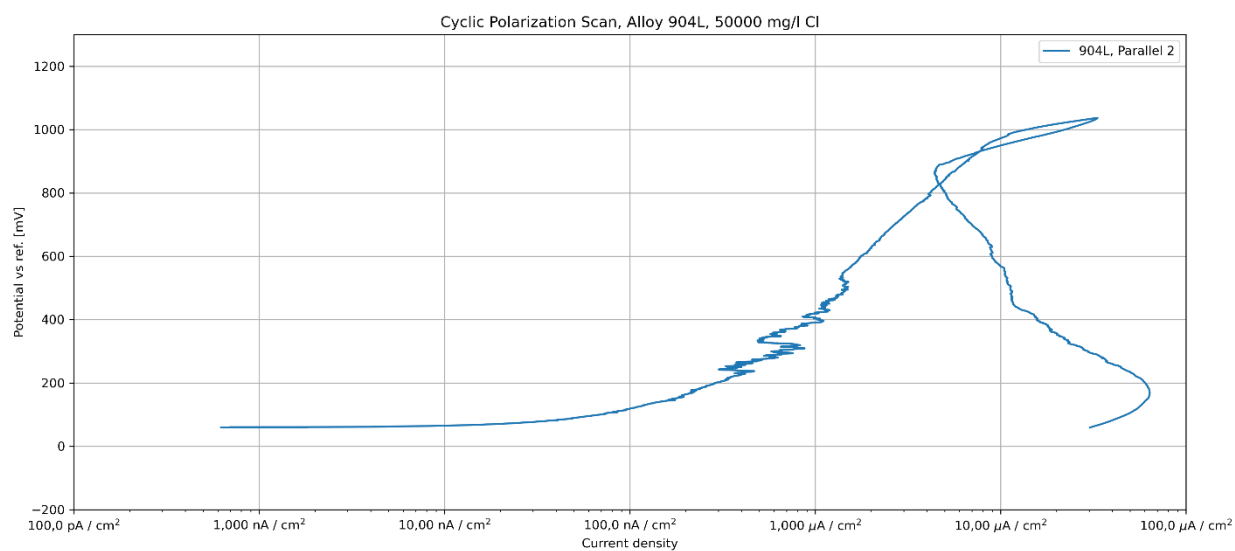


Figure A - 31: Cyclic polarization scan of alloy 904L, 50 000 mg/l chloride content, parallel 2.

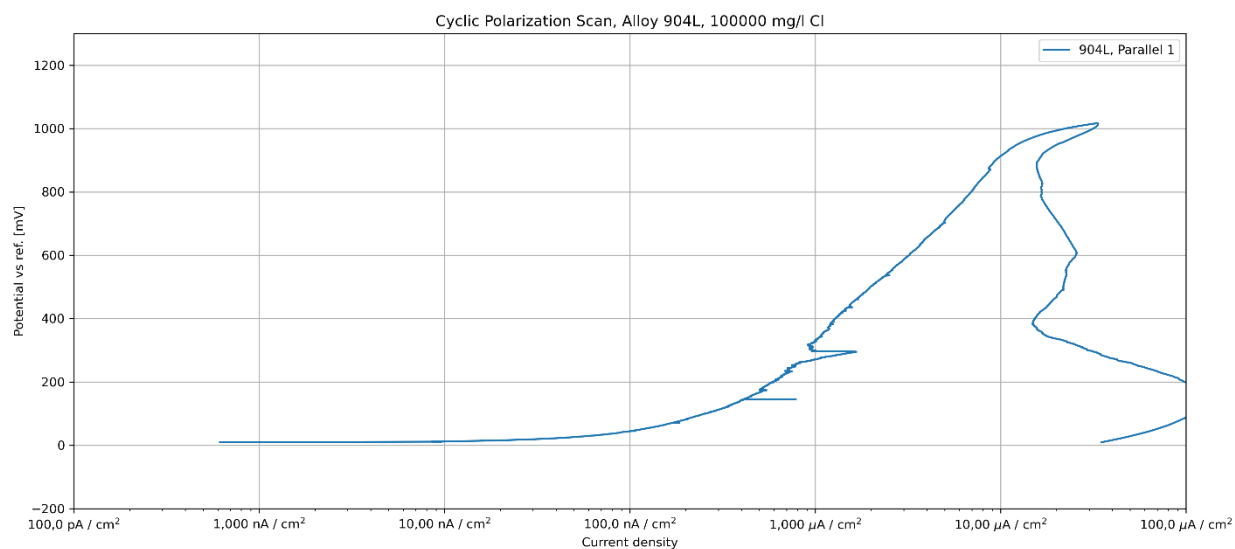


Figure A - 32: Cyclic polarization scan of alloy 904L, 100 000 mg/l chloride content, parallel 1.

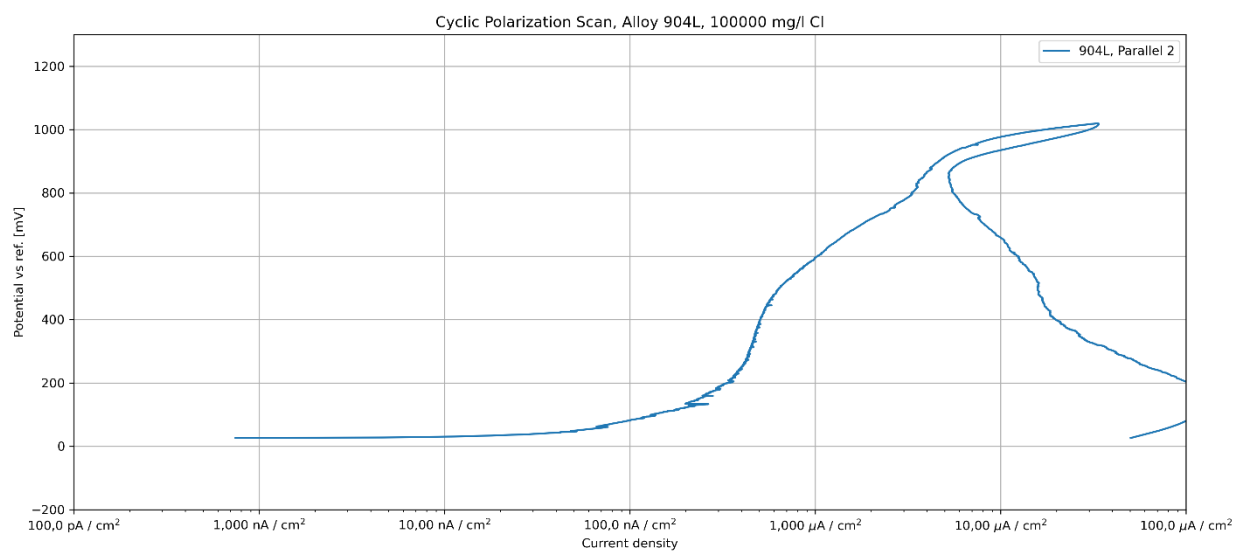


Figure A - 33: Cyclic polarization scan of alloy 904L, 100 000 mg/l chloride content, parallel 2.

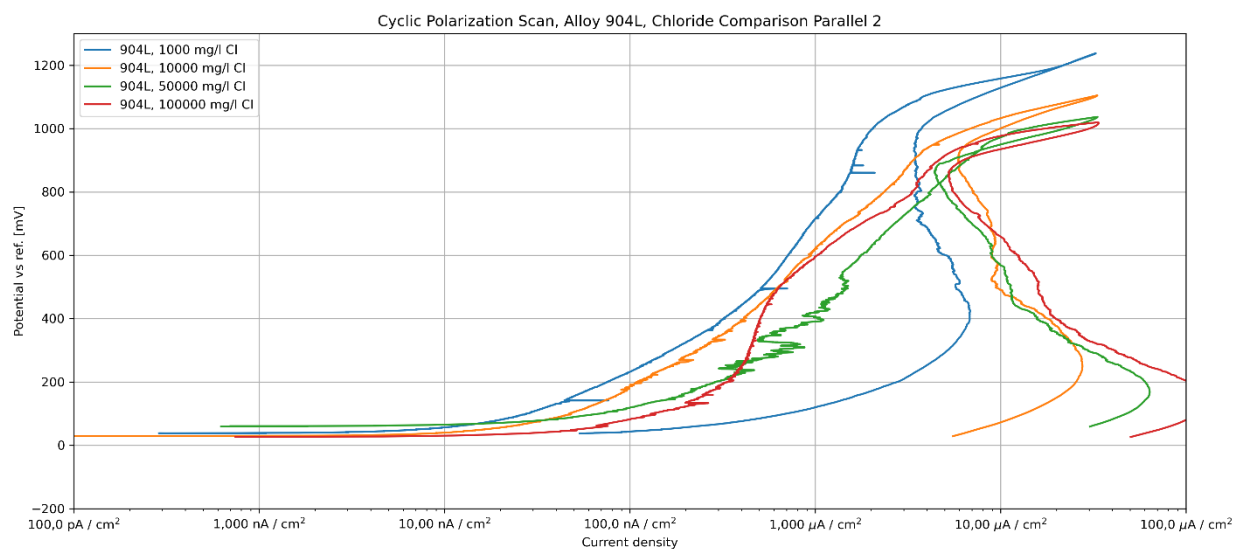


Figure A - 34: Cyclic polarization scan of alloy 904L at various chloride concentrations, parallel 2.

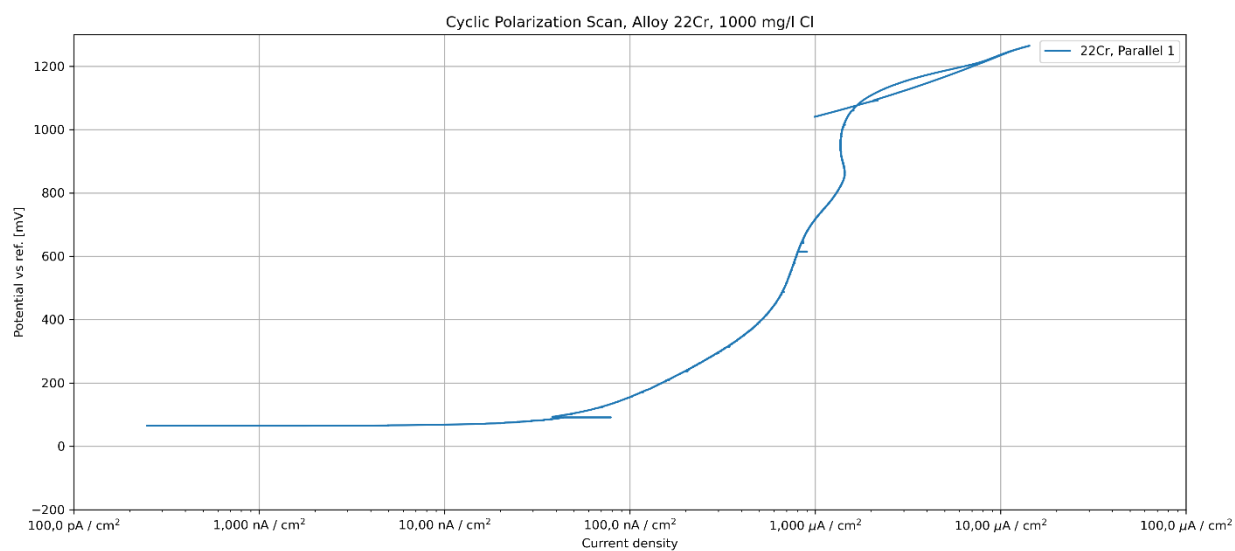


Figure A - 35: Cyclic polarization scan of alloy 22Cr, 1000 mg/l chloride content, parallel 1.

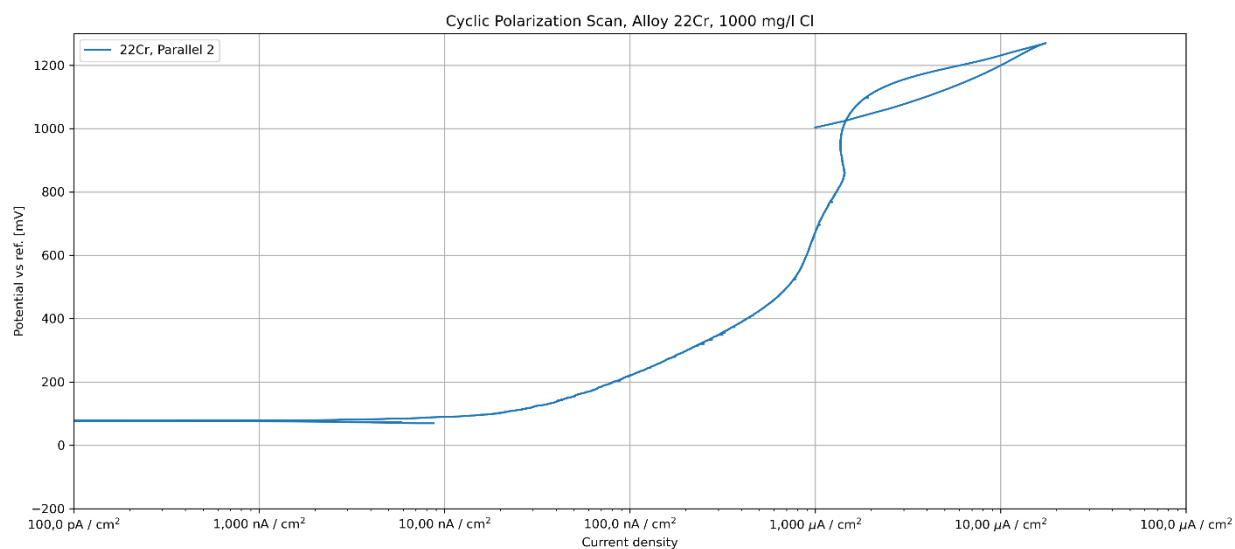


Figure A - 36: Cyclic polarization scan of alloy 22Cr, 1000 mg/l chloride content, parallel 2.

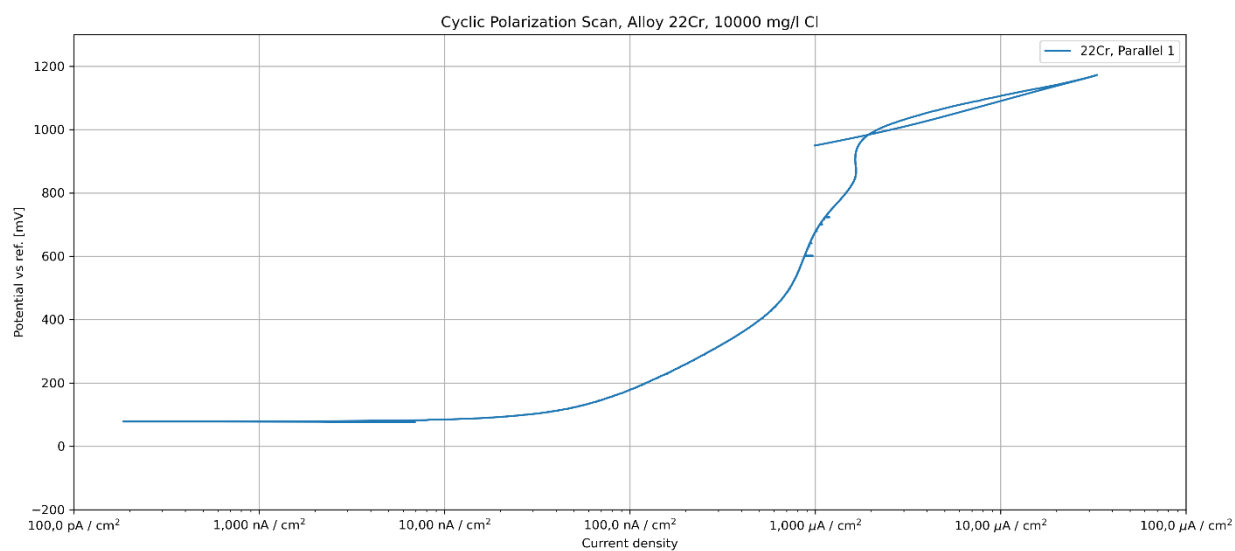


Figure A - 37: Cyclic polarization scan of alloy 22Cr, 10 000 mg/l chloride content, parallel 1.

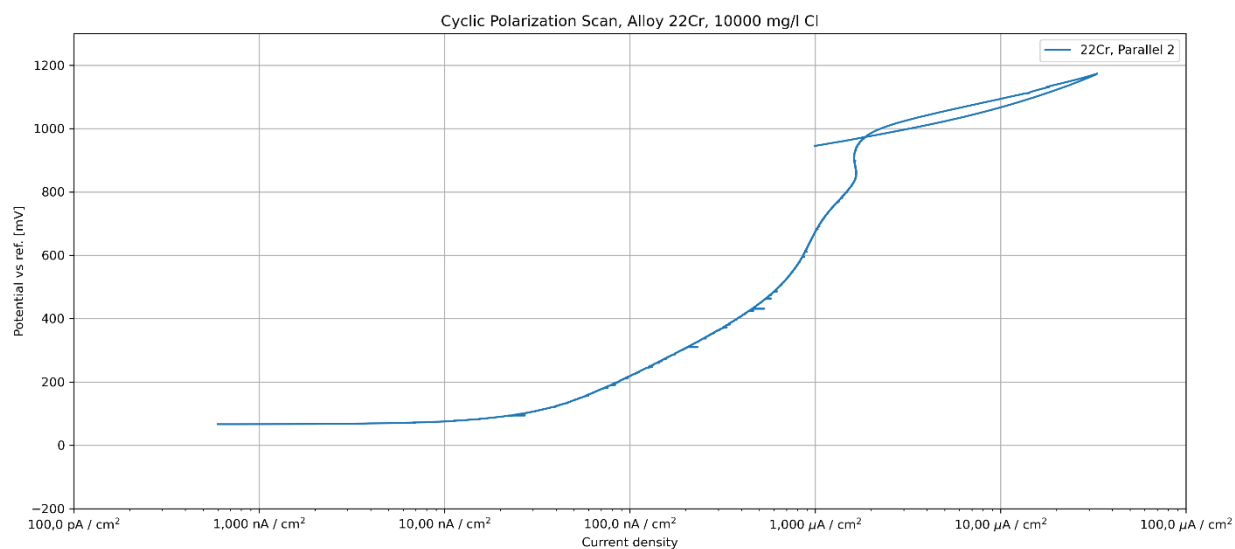


Figure A - 38: Cyclic polarization scan of alloy 22Cr, 10 000 mg/l chloride content, parallel 2.

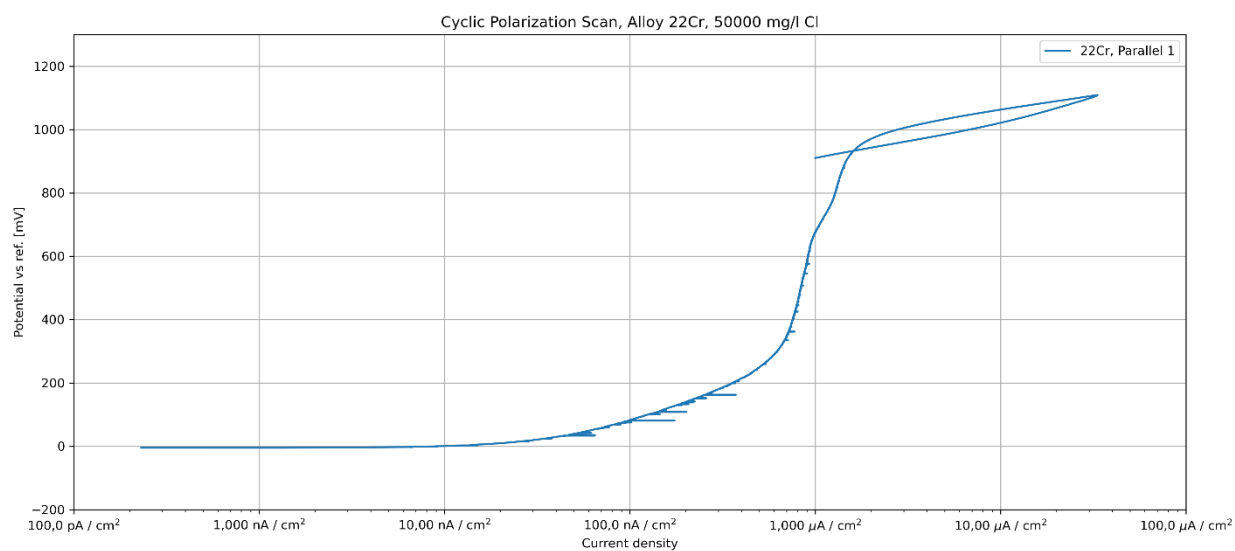


Figure A - 39: Cyclic polarization scan of alloy 22Cr, 50 000 mg/l chloride content, parallel 1.

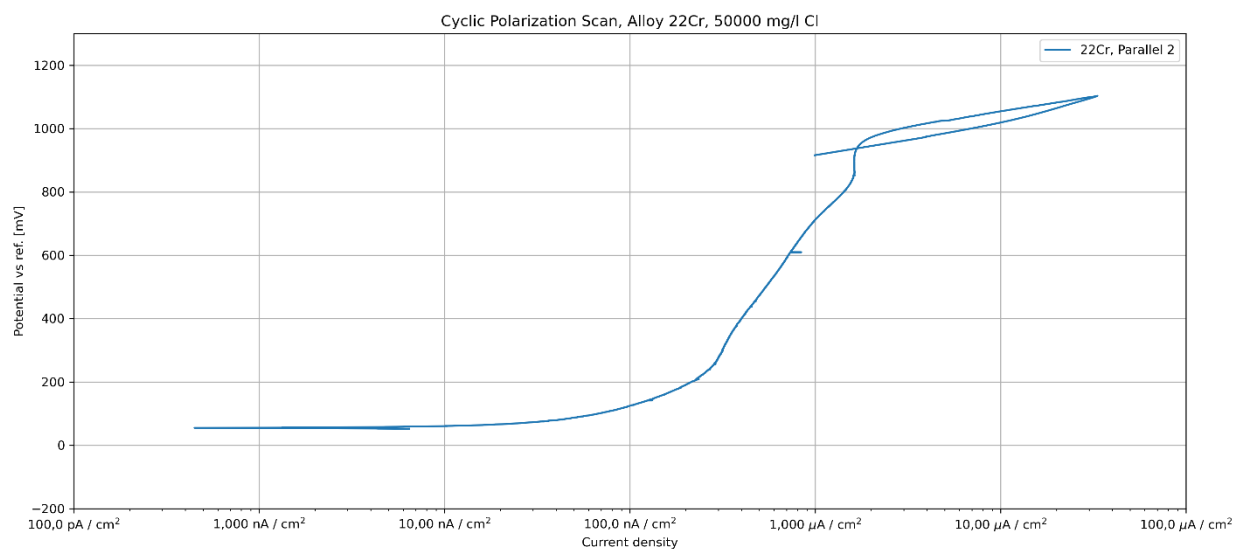


Figure A - 40: Cyclic polarization scan of alloy 22Cr, 50 000 mg/l chloride content, parallel 2.

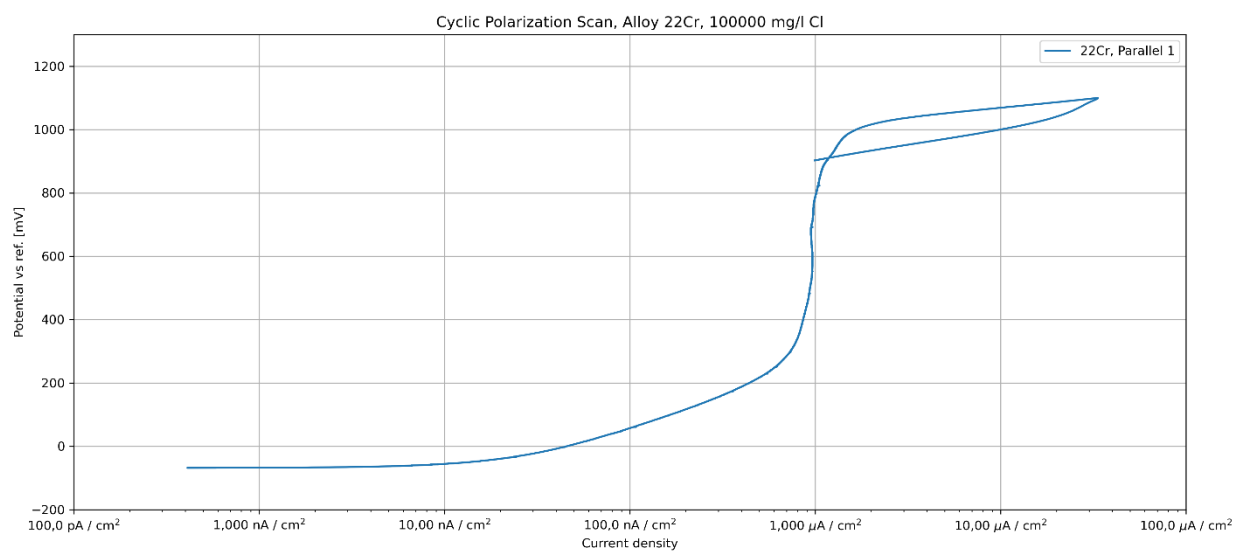


Figure A - 41: Cyclic polarization scan of alloy 22Cr, 100 000 mg/l chloride content, parallel 1.

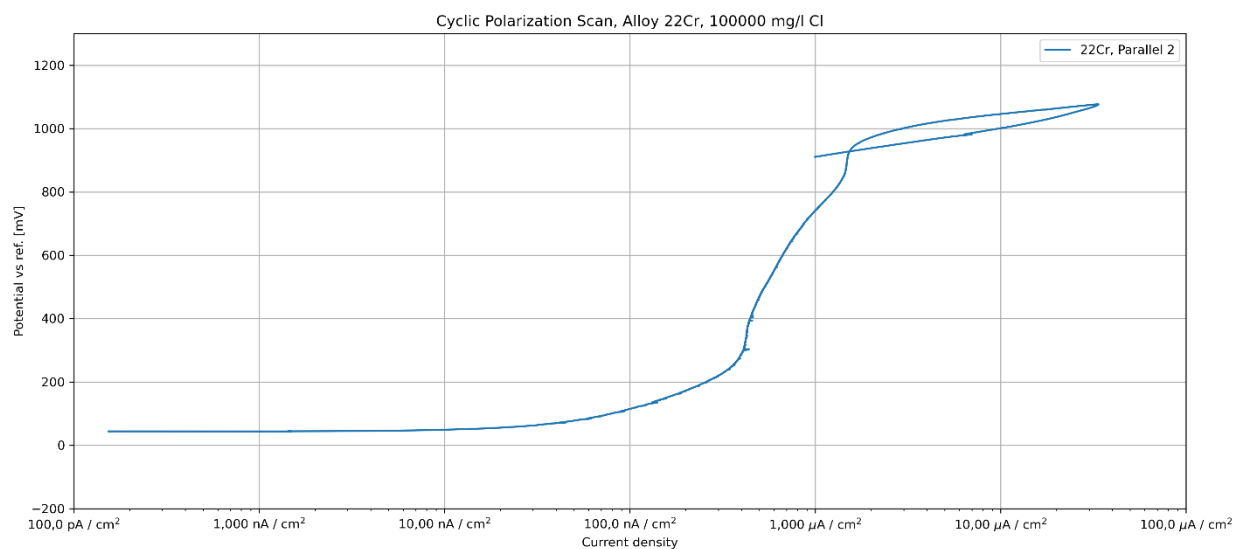


Figure A - 42: Cyclic polarization scan of alloy 22Cr, 100 000 mg/l chloride content, parallel 2.

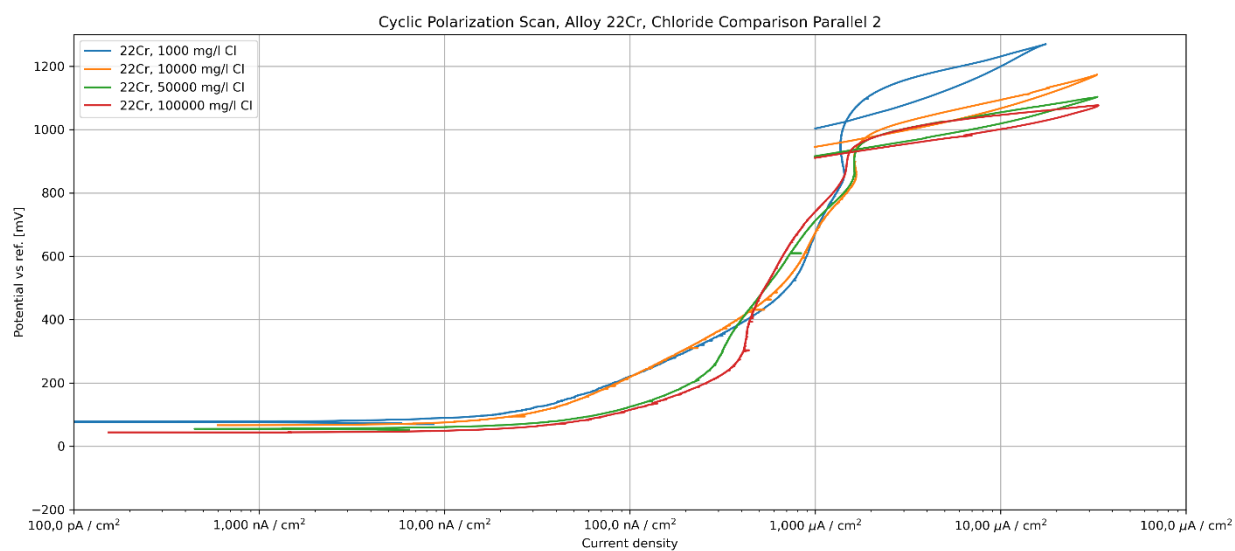


Figure A - 43: Cyclic polarization scan of alloy 22Cr at various chloride concentrations, parallel 2.

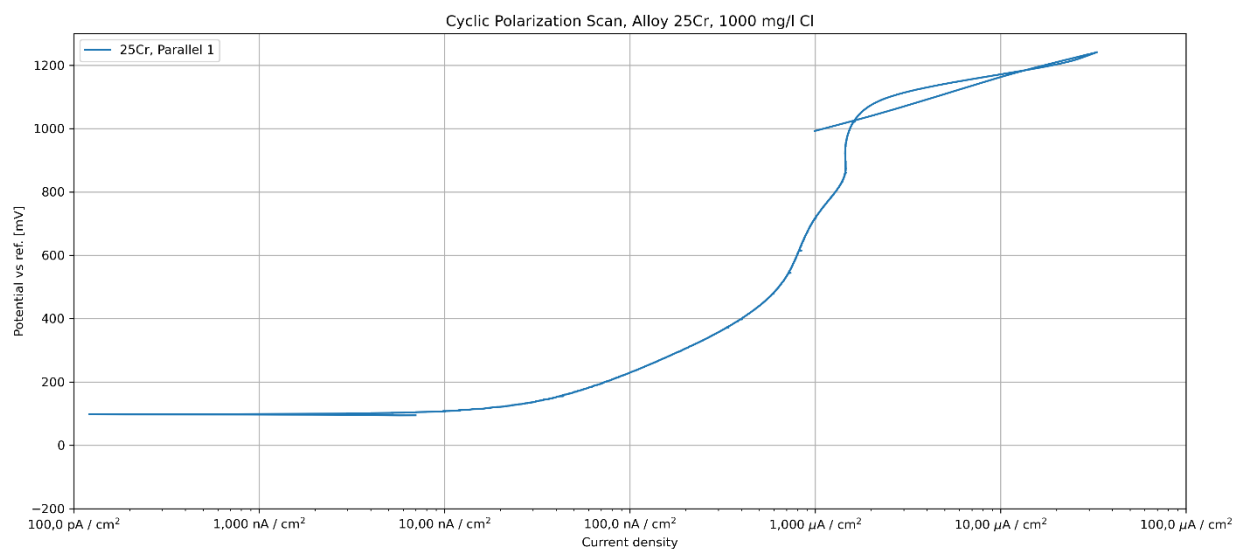


Figure A - 44: Cyclic polarization scan of alloy 25Cr, 1000 mg/l chloride content, parallel 1.

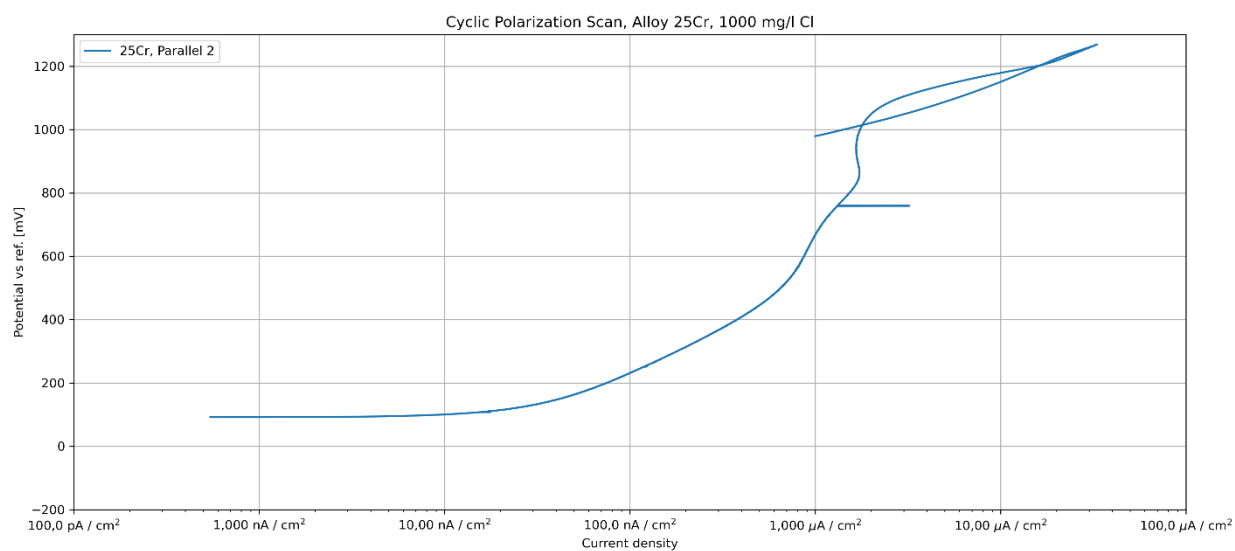


Figure A - 45: Cyclic polarization scan of alloy 25Cr, 1000 mg/l chloride content, parallel 2.

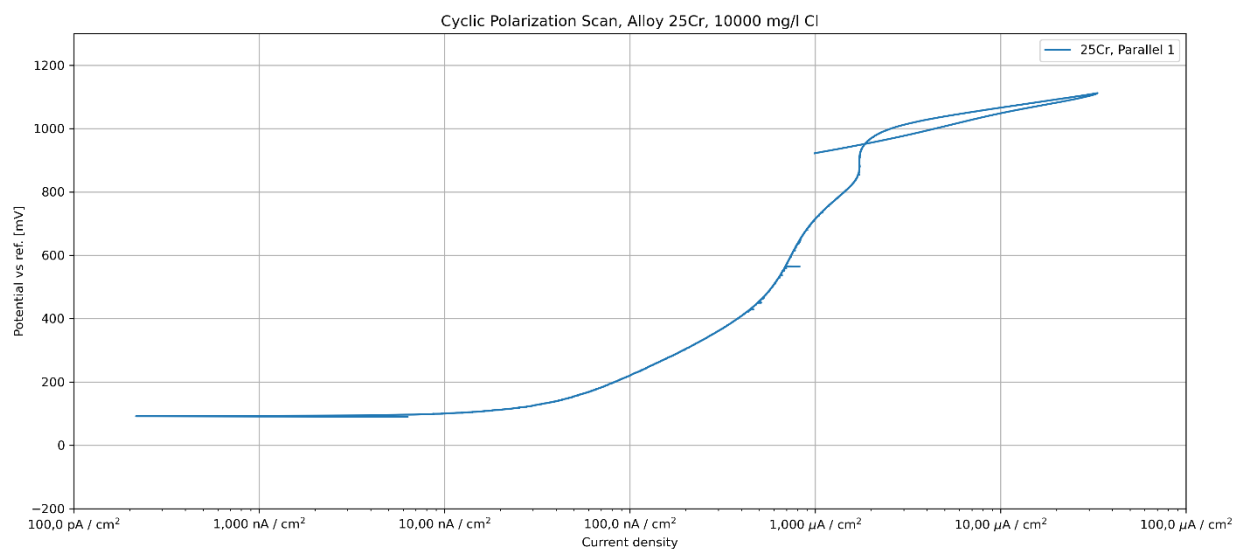


Figure A - 46: Cyclic polarization scan of alloy 25Cr, 10 000 mg/l chloride content, parallel 1.

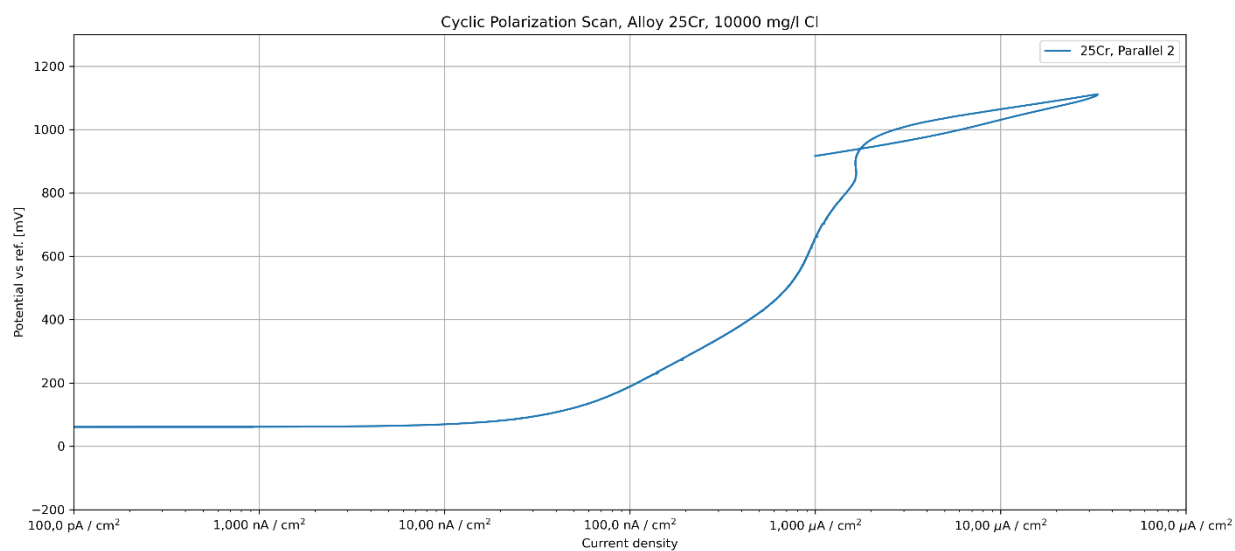


Figure A - 47: Cyclic polarization scan of alloy 25Cr, 10 000 mg/l chloride content, parallel 2.

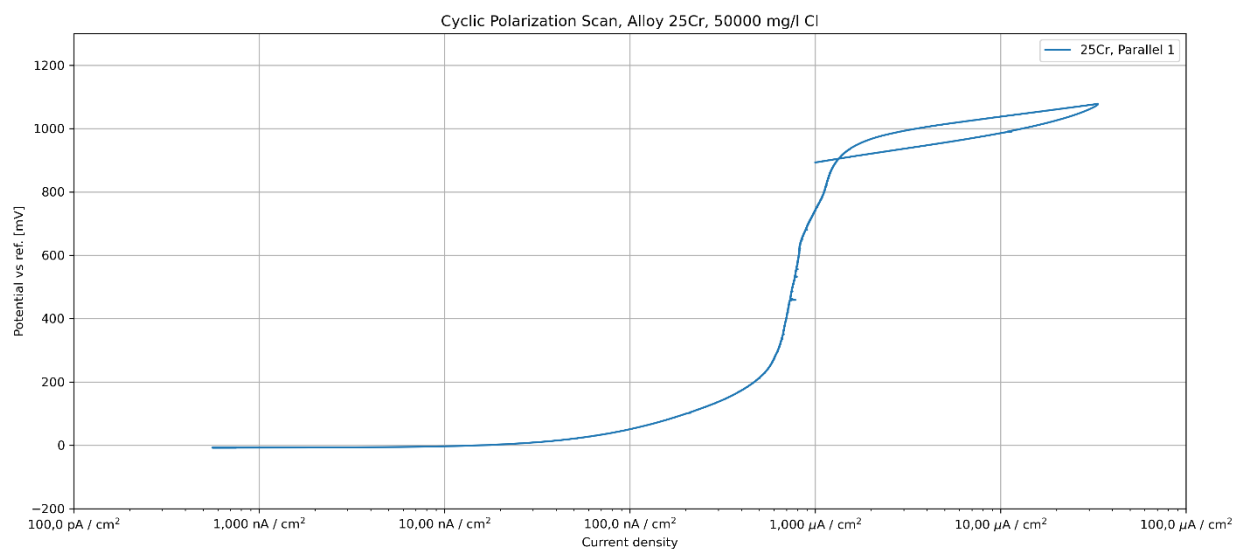


Figure A - 48: Cyclic polarization scan of alloy 25Cr, 50 000 mg/l chloride content, parallel 1.

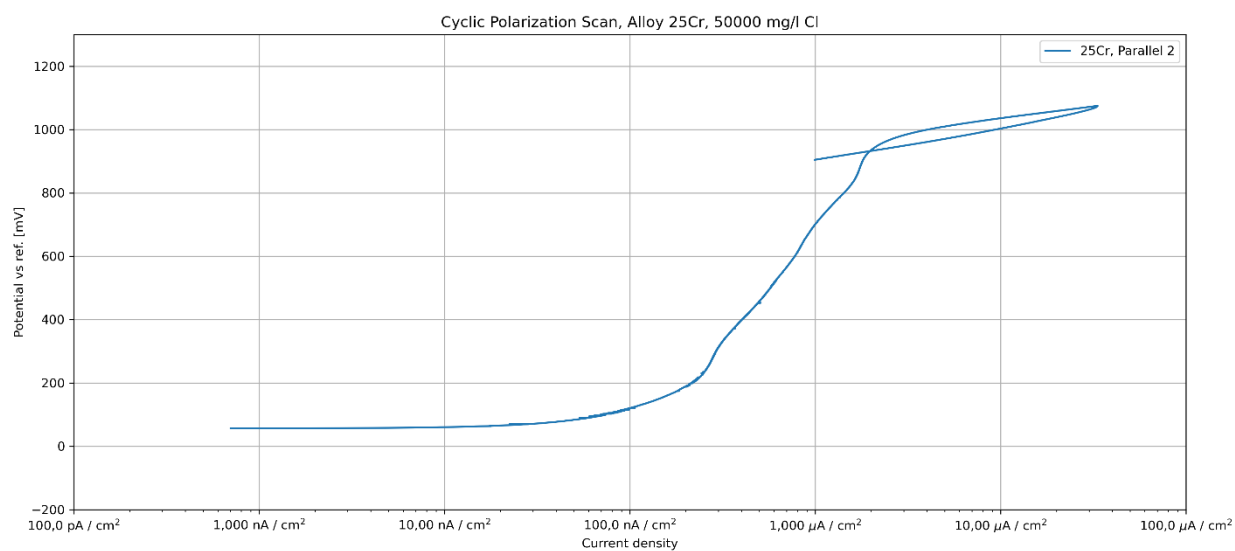


Figure A - 49: Cyclic polarization scan of alloy 25Cr, 50 000 mg/l chloride content, parallel 2.

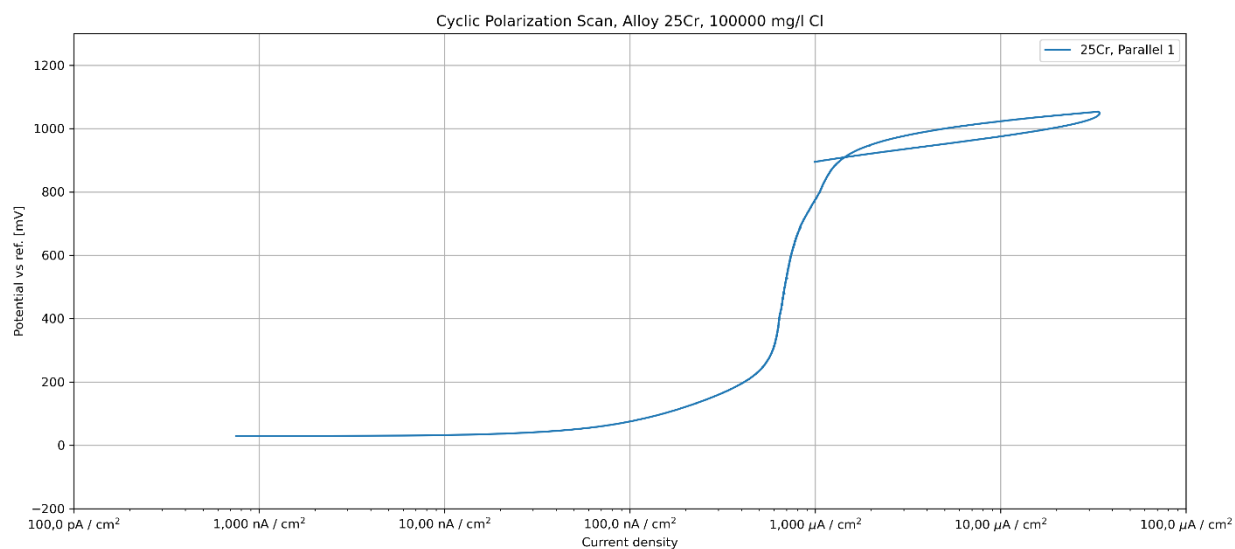


Figure A - 50: Cyclic polarization scan of alloy 25Cr, 100 000 mg/l chloride content, parallel 1.

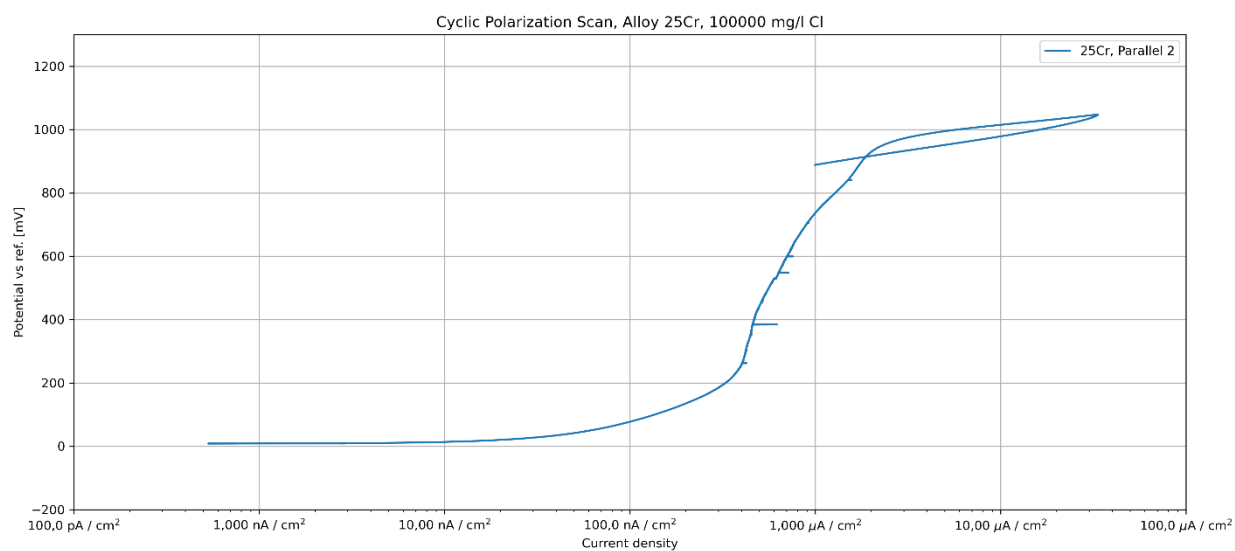


Figure A - 51: Cyclic polarization scan of alloy 25Cr, 100 000 mg/l chloride content, parallel 2.

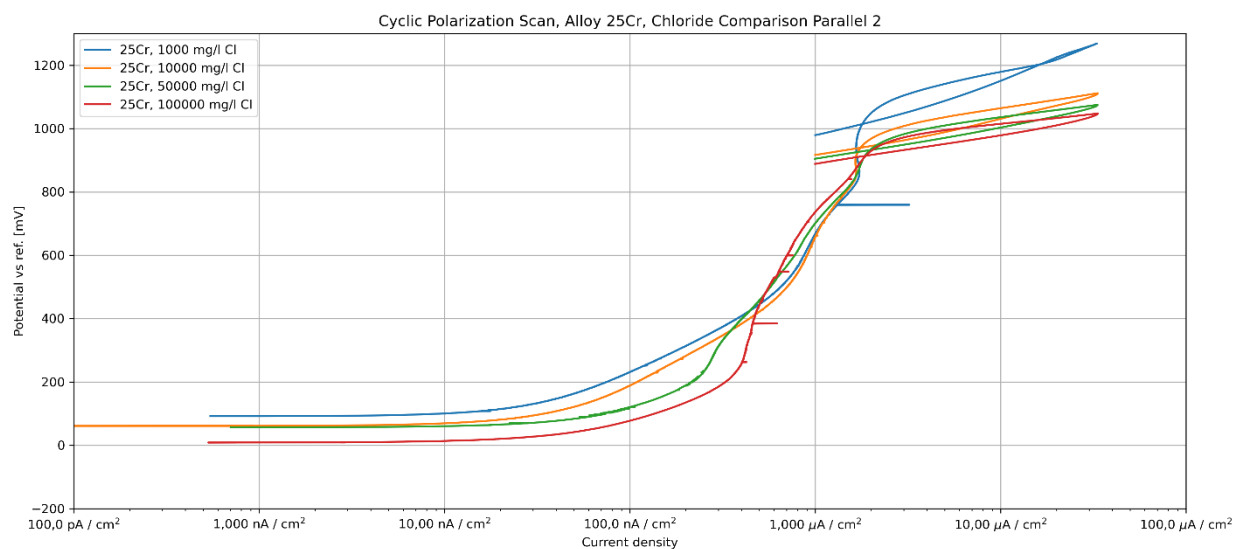


Figure A - 52: Cyclic polarization scan of alloy 25Cr at various chloride concentrations, parallel 2.

Appendix B Risk assessment

RISK ASSESSMENT

ONLY VALID FOR DETAILED ACTIVITIES LISTED IN SECTION 5


1. Identification

Laboratory name: Corrosion lab, metallography lab, tribology lab	Room number: 104, 104A, 161, 162
User's name: David Nilssen	<input checked="" type="checkbox"/> Master <input type="checkbox"/> PhD <input type="checkbox"/> Post-Doc <input type="checkbox"/> SINTEF <input type="checkbox"/> Other:
User's e-mail: davidnil@stud.ntnu.no	User's Phone: 41 48 17 38
Supervisor: Roy Johnsen	Supervisor's phone:
Project number: 70442887	
Period: 21/09/2022 – 11/06/2023	


Description of the project and needs: <p>The project consists of an examination of corrosion on stainless steels in fresh (river) water with some chloride content as well as the effects of chloride content and flow speed on the corrosion rate. This means corrosion testing chambers, distilled and river water, reference electrodes (Ag AgCl KCl) and steel samples of different alloys are needed for the project. Potentiodynamic and potentiostatic scans, as well as other experiments at different temperatures will be done in the corrosion laboratory. Sample preparation, hereunder grinding and polishing, will be done in the metallurgy laboratory, while sample observation will be done in the metallurgy and tribology laboratory, on the optical and infinite focus microscopes respectively.</p>
--

2. Signatures

The user and the supervisor are aware of all the risks involved in the lab activities that are going to be performed. Additionally, the user confirms that they will follow the preventive measures described in this form to minimize all the risks that have been identified.

User's signature	Supervisor's signature
Signature: David Nilssen	Signature: 
Name: David Nilssen	Name: Roy Johnsen
Date: 18/01/2023	Date: 18.01.2023

Approved by:

	Signature:	Name:	Date:
Room responsible:		Ida W. Worum	02.03.2023
Lab manager:			

Note: a pdf copy with all signatures shall be sent to everyone who has signed above.

3. Team (write “NR” if not relevant)

Project manager and organization (Student)	David Nilssen	Responsible for instrumentation	Dong Wang
Laboratory responsible	Ida Wadseng Worum	Operator	David Nilssen
Auditor for safety check	David Nilssen	Responsible for running the experiment	David Nilssen
Responsible for experimental and scientific content (Advisor)	Roy Johnsen	Responsible for logging and storing experimental data	David Nilssen
Responsible for dimensioning load bearing and pressurized components	NR	Responsible for building the rig	NR

4. Administration

Answer: Yes, No or NR (Not relevant)

Is the work order signed? (only for external work)	
Has the operator the required courses/training on the equipment?	Yes
Has the operator followed the safety courses? (Mandatory)	Yes
Can the work be done alone?	Yes
- If not, the work may have to be done under special conditions (evaluated in section 5)	
Does an expert have to check the start of the experiment?	No
- If yes, who?	

5. Description of the Activity

The primary activity is a series of experiments consisting of measuring the crevice, pitting and repassivation potential of six types of stainless steel, alloys 1.4317, AISI 304, AISI 316L, AISI 904L, UNS S32205 and UNS S32750 in distilled water added NaCl following ASTM G61. For this purpose, a container that can hold the sample, counter electrode and reference electrode submerged in the electrolyte for the duration of the experiment is needed, as well as data logging equipment for the measurements of the samples with respect to a silver chloride electrode.

For each activity performed in the lab, health risks affecting the user or others need to be identified. For each risk identified, a preventive measure must be performed, and the final risk value calculated with the “risk matrix”. Explanation of the “risk matrix” can be found in the last page of this form.

This page must be replicated for each different activity performed in the lab. Activities involving the use of chemicals must be filled out in the page titled “Chemical Risk Assessment” in section 5.2.

Corrosion laboratory:

Activity: Crevice, pitting and repassivation potential measurement of stainless steels in distilled water added chlorides, using an Ag | AgCl (sat.) reference electrode.

Risk overview: (mark with X the risk that applies for the activity)

Big loads		Danger of fire	
Heavy lifting		Working at heights	
Hanging load		Hydraulic pressure	
Gas pressure		Water pressure	
High temperature		Low temperature	
Parts at high velocity		Chemicals, if yes; fill in sect. 5.2	X
Sudden acceleration at fracture/failure		Pre-tensioned components	
Dangerous dust		Severe noise	
Danger of pinching		Rotating parts	

Detailed risk evaluation:

Risks
1. The silver chloride electrode could shatter and pollute the electrolyte with silver chloride solution. The electrolyte will then need to be handled as waste dangerous to aquatic life.
2. The potentiostat supplies a small amount of electric potential to the solution, up to a maximum of 12V at once. This experiment will use up to approximately 1.1mA (33 $\mu\text{A}/\text{cm}^2$, samples approximately 34cm ² area) for the sweep from the open circuit potential upwards until E_{crev} is found at a rate of 600mV/h. Upon reaching the maximum current density, a sweep backwards until the OCP is reached again is performed. Maximum voltage applied is 1V in the anodic direction.
3.

Risk matrix of the activity before any safety measures has been applied (Include corresponding color):

Risk	Probability (P) (1-5)	Consequence (C)				Risk value (P x C)			
		Health (1-5)	Material values (1-5)	Environment (1-5)	Reputation (1-5)				
1	2	1	1	2	1	2	2	4	2
2	3	1	1	1	1	3	3	3	3
3									

Required safety equipment (mark with X the risk that applies for the activity):

Glasses	X	Safety shoes	
Helmet		Gloves	X
Screen		Lifting equipment	
Ear protection		Hazard suit	
Harness ropes, other measures to prevent falling		Fume hood	
Lab coat		Fume arm	

Description of other safety measurements: Eg. Safety cap on the instrument prevents the risk of... and/ or the probability of...

Risk after preventative and corrective measures:

Risks	Preventative and corrective measures
1. The silver chloride electrode could shatter and pollute the electrolyte with silver chloride solution. The electrolyte will then need to be handled as waste dangerous to aquatic life.	Care will be taken with respect to the assembly of the experimental setup. This includes the use of rubber equipment for holding the electrode so that it has a smaller possibility of fracturing on assembly.
2. The potentiostat supplies a small amount of electric potential to the solution, up to a maximum of 12V at once. This experiment will use up to approximately 1.1mA (33 μ A/cm ² ,	The solution is not to be touched under any part of the sweep, neither forward nor backward. A lid will be placed and taped shut over the beaker

samples approximately 34cm ² area) for the sweep from the open circuit potential upwards until E _{crev} is found at a rate of 600mV/h. Upon reaching the maximum current density, a sweep backwards until the OCP is reached again is performed. Maximum voltage applied is 1V in the anodic direction.	in order to securely prevent access to the solution while the experiment is running.
3.	

Risk matrix of the activity after safety measures has been applied:

Risk	Probability (P) (1-5)	Consequence (C)				Risk value (P x C)			
		Health (1-5)	Material values (1-5)	Environment (1-5)	Reputation (1-5)				
1	1	1	1	2	1	1	1	2	1
2	1	1	1	1	1	1	1	1	1
3									

Metallographic laboratory:

Activity: Preparation of samples for their measurements in mentioned electrolyte through grinding of samples.

Risk overview: (mark with X the risk that applies for the activity)

Big loads		Danger of fire	
Heavy lifting		Working at heights	
Hanging load		Hydraulic pressure	
Gas pressure		Water pressure	
High temperature		Low temperature	
Parts at high velocity		Chemicals, if yes; fill in sect. 5.2	
Sudden acceleration at fracture/failure		Pre-tensioned components	
Dangerous dust		Severe noise	
Danger of pinching		Rotating parts	

Detailed risk evaluation:

Risks

1. When grinding the samples in the metallography lab, a weak grip on the sample may cause the sample to roll and get carried away with the paper below, causing the paper to grind away at the user's fingers.
2.
3.

Risk matrix of the activity before any safety measures has been applied (Include corresponding color):

Risk	Probability (P) (1-5)	Consequence (C)				Risk value (P x C)			
		Health (1-5)	Material values (1-5)	Environment (1-5)	Reputation (1-5)				
1	3	1	1	1	1	3	3	3	3
2									
3									

Required safety equipment (mark with X the risk that applies for the activity):

Glasses	X	Safety shoes	
Helmet		Gloves	X
Screen		Lifting equipment	
Ear protection		Hazard suit	
Harness ropes, other measures to prevent falling		Fume hood	
Lab coat		Fume arm	

Description of other safety measurements: Eg. Safety cap on the instrument prevents the risk of... and/ or the probability of...

Risk after preventative and corrective measures:

Risks	Preventative and corrective measures
1. When grinding the samples in the metallography lab, a weak grip on the sample	The use of gloves, mental focus, and correct grinding technique, herein keeping the sample

may cause the sample to roll and get carried away with the paper below, causing the paper to grind away at the user's fingers.	as perpendicular to the surface as possible with small angle variations, will sharply reduce the possibility of this injury.
2.	
3.	

Risk matrix of the activity after safety measures has been applied:

Risk	Probability (P) (1-5)	Consequence (C)				Risk value (P x C)
		Health (1-5)	Material values (1-5)	Environment (1-5)	Reputation (1-5)	
1	1	1	1	1	1	1 1 1 1
2						
3						

&

Activity: Observation of corroded samples in light optical microscope.

Risk overview: (mark with X the risk that applies for the activity)

Big loads		Danger of fire	
Heavy lifting		Working at heights	
Hanging load		Hydraulic pressure	
Gas pressure		Water pressure	
High temperature		Low temperature	
Parts at high velocity		Chemicals, if yes; fill in sect. 5.2	
Sudden acceleration at fracture/failure		Pre-tensioned components	
Dangerous dust		Severe noise	
Danger of pinching		Rotating parts	

Detailed risk evaluation:

Risks
1. Carelessness in lowering the microscope may damage the lens from hitting the sample.
2.

3.

Risk matrix of the activity before any safety measures has been applied (Include corresponding color):

Risk	Probability (P) (1-5)	Consequence (C)				Risk value (P x C)			
		Health (1-5)	Material values (1-5)	Environment (1-5)	Reputation (1-5)				
1	2	1	3	1	1	2	6	2	2
2									
3									

Required safety equipment (mark with X the risk that applies for the activity):

Glasses	X	Safety shoes	
Helmet		Gloves	X
Screen		Lifting equipment	
Ear protection		Hazard suit	
Harness ropes, other measures to prevent falling		Fume hood	
Lab coat		Fume arm	

Description of other safety measurements: Eg. Safety cap on the instrument prevents the risk of... and/ or the probability of...

Risk after preventative and corrective measures:

Risks	Preventative and corrective measures
1. Carelessness in lowering the microscope may damage the lens from hitting the sample.	One must always be aware of the distance from the sample to the lens, and never move them closer than necessary (focal point awareness is required).
2.	
3.	

Risk matrix of the activity after safety measures has been applied:

Risk	Probability (P) (1-5)	Consequence (C)				Risk value (P x C)
		Health (1-5)	Material values (1-5)	Environment (1-5)	Reputation (1-5)	
1	1	1	3	1	1	1 3 1 1
2						
3						

Tribology laboratory:

Activity: Observation and analysis of corroded samples with the use of the Infinite Focus Microscope.

Risk overview: (mark with X the risk that applies for the activity)

Big loads		Danger of fire	
Heavy lifting		Working at heights	
Hanging load		Hydraulic pressure	
Gas pressure		Water pressure	
High temperature		Low temperature	
Parts at high velocity		Chemicals, if yes; fill in sect. 5.2	
Sudden acceleration at fracture/failure		Pre-tensioned components	
Dangerous dust		Severe noise	
Danger of pinching		Rotating parts	

Detailed risk evaluation:

Risks
1. If attention is not paid to the sample stage when it is lowered, there is a risk of crushing the lens. This also applies to hardware-induced movement when defining a relative movement in the z-direction.
2.
3.

Risk matrix of the activity before any safety measures has been applied (Include corresponding color):

Risk	Probability (P) (1-5)	Consequence (C)				Risk value (P x C)
		Health (1-5)	Material values (1-5)	Environment (1-5)	Reputation (1-5)	
1	3	1	3	1	1	3 9 3 3
2						
3						

Required safety equipment (mark with X the risk that applies for the activity):

Glasses	X	Safety shoes	
Helmet		Gloves	
Screen		Lifting equipment	
Ear protection		Hazard suit	
Harness ropes, other measures to prevent falling		Fume hood	
Lab coat	X	Fume arm	

Description of other safety measurements: Eg. Safety cap on the instrument prevents the risk of... and/ or the probability of...

Risk after preventative and corrective measures:

Risks	Preventative and corrective measures
1. If attention is not paid to the sample stage when it is lowered, there is a risk of crushing the lens. This also applies to hardware-induced movement when defining a relative movement in the z-direction.	One must always be aware of the distance from the sample to the lens, and never move them closer than necessary (focal point awareness is required). When first calibrating the microscope, the stage must be clear of any objects, which can only be reintroduced after the calibration is finished. The highest point on the sample should always be set as z-level zero in order to keep track of how deep one is

	focusing on the sample surface. When setting the focus, one should always keep track of where the lens is located physically, as the focus plane could be passed already, causing further zooming to only move the lens closer without actually coming into focus.
2.	
3.	

Risk matrix of the activity after safety measures has been applied:

Risk	Probability (P) (1-5)	Consequence (C)				Risk value (P x C)			
		Health (1-5)	Material values (1-5)	Environment (1-5)	Reputation (1-5)				
1	1	1	3	1	1	1	3	1	1
2									
3									

5.2. Chemical Risk Assessment:

Only for activities involving the use of chemicals (except ethanol and acetone for cleaning).

This page **must be replicated** for each different chemical activity performed in the lab. Include all H-sentence and numbers for chemicals used. This can be found in the Safety Data Sheet and the specific chemical (SDS).

Activity: The experiment requires the synthesis of an electrolyte of a certain chloride concentration, which for the primary experiments consists of between 100 mg/l and 10000 mg/l Cl^- using NaCl and distilled water. This will be done on an experiment-by-experiment basis by mixing the two parts. The total volume of each experiment is approximately 1.8 liters, into which the samples will be submerged.

Chemicals used:	Sodium chloride, distilled water
Mixture:	Approx. 297 – 29700 mg NaCl, 1,8L distilled water
Will the mixture be stored in the cabinet for several uses?	No

Risk	Prevention Measures
1.	
2.	
3.	
4.	

Note: All H-sentences must be included as a risk, together with “general” risks when using the specific chemical.

Chemical disposal procedure:
No dangerous waste as both NaCl and distilled water are safe for human consumption in moderate amounts, up to over several grams per day for the salt. We expect trivially little to no dissolution of the stainless steel samples, and therefore negligible amounts of metal ions, as the primary dissolution product will be iron oxides or hydroxides, which are not environmentally dangerous in low amounts. Therefore, for our amounts we consider it safe to handle and dispose down the laboratory drain.

Risk matrix of the chemical activity before safety measures:

Risk	Probability (P) (1-5)	Consequence (C)				Risk value (P x C)
		Health (1-5)	Material values (1-5)	Environment (1-5)	Reputation (1-5)	
1						
2						
3						

Required safety equipment: (mark with X the risk that applies for the activity)

Glasses	X	Safety shoes	
Helmet		Gloves	X
Screen		Lifting equipment	
Ear protection		Hazard suit	
Harness ropes, other measures to prevent falling		Fume hood	
Lab coat			

Description of other safety measurements: Eg. Safety cap on the instrument prevents the risk of... and/ or the probability of...

Risk after preventative and corrective measures:

Risks	Preventative and corrective measures
1.	
2.	
3.	

Risk matrix of the activity after safety measures has been applied:

Risk	Probability (P) (1-5)	Consequence (C)				Risk value (P x C)
		Health (1-5)	Material values (1-5)	Environment (1-5)	Reputation (1-5)	
1						
2						
3						

Comments: Supplementary comments regarding the risk matrixes

6. Sources for mistakes/errors

Is the following considered? Answer: Yes, No or NR (Not relevant)

Loss of electricity	No	Voltage surge	No
Electrical earth failure	No	Insufficient power of the machine	No
Climate control in the room (temperature, humidity, etc...)	No	Water jet	NR
Unstable pressure or hydraulic force	NR	Unintended interruption of power supply	No
Are load and displacement limits established?	NR	Leakage of pipes, hoses, joints, etc...	Yes
Possible interference from other activities	NR	Possible interference towards other activities	NR
Troubles in acquisition and storage	NR	Fire in the laboratory	NR

7. Calibration of equipment

If a calibration of the equipment is performed during the activity, please indicate the date:

Equipment	Date (dd.mm.yy)

8. Traceability

Answer: Yes, No or NR (Not relevant)

Are all experimental materials known and traceable?	Yes
Is there a plan for marking all specimens?	Yes
Is the data acquisition equipment identified?	No
Are the original data stored safely without modification?	Yes
Is there a back-up procedure for the data (hard disk crash)?	No
Is there a plan for storing samples after testing?	Yes
Is there a plan for disposing of old samples?	No

9. Conclusion

Given the experiment parameters and the preventative measures taken, the experiment itself is understood to be safe to run.

Risk matrix explanation

		Health	Material values	Reputation	Environment
Grade	1	Minor injury/strain that requires simple treatment. Reversible injury. Short recovery time.	Operational shutdown, or shutdown of activities <1 day.	Little effect on credibility and respect.	Negligible injury and short recovery time.
	2	Injury/strain that requires medical treatment. Reversible injury/strain. Short recovery time.	Operational shutdown, or shutdown of activities <1 week.	Negative effect on credibility and respect.	Minor injury and short recovery time.
	3	Serious injury/strain that requires medical treatment. Lengthy recovery time.	Operational shutdown, or shutdown of activities <1 month.	Reduced credibility and respect.	Minor injury and lengthy recovery time.
	4	Serious injury/strain that requires medical treatment. Possible disability /permanent disability.	Operational shutdown > 1/2 year. Shutdown of activities up to 1 year.	Credibility and respect considerably reduced.	Long-lasting injury. Lengthy recovery time.
	5	Death or disability / permanent disability.	Operational shutdown, or shutdown of activities >1 year.	Credibility and respect considerably and permanently reduced.	Very long-lasting and irreversible injury.

Consequence (C)	Very serious	5	10	15	20	25
	Serious	4	8	12	16	20
	Moderate	3	6	9	12	15
	Little	2	4	6	8	10
	Very little	1	2	3	4	5
		Very little	Little	Medium	Big	Very big
Probability (P)						

Red	Unacceptable risk. Measures need to be implemented.
Yellow	Medium risk. Measures need to be considered.
Green	Acceptable risk. Measures can be considered.

Add the color of the risk matrix that corresponds with the value you have placed in your personal risk matrix.

